Frequency Noise in Coherent Optical Systems: Impact and Mitigation Methods

ADITYA KAKKAR

Doctoral Thesis in Physics
School of Engineering Sciences
KTH Royal Institute of Technology
Stockholm, Sweden
June 2017

TRITA-FYS 2017:31
ISSN 0280-316X
ISRN KTH/FYS/--17:31—SE
ISBN: 978-91-7729-425-2

KTH Royal Institute of Technology
School of Engineering Sciences
SE-164 40 Stockholm
SWEDEN

Akademisk avhandling som med tillstånd av Kungl Tekniska Högskolan framlägges till offentlig granskning för avläggande av teknologie doktorsexamen i fysik fredagen den 9 juni 2017 klockan 14.00, i Sal C, Electrum, Kungl Tekniska Högskolan Kistagågen 16, Kista.

Tryck: Universitetsservice US-AB

Abstract

The increase in capacity demand along with the advancement in digital signal processing (DSP) have recently revived the interest in coherent optical communications and led to its commercialization. However, design and development of robust DSP algorithms for example for carrier phase recovery (CPR) becomes complex as we opt for high order modulation formats such as 16QAM and beyond. Further, electrical-domain dispersion compensation (EDC), while providing many advantages, makes the system more susceptible to laser frequency noise (FN). For instance, in coherent optical links with post-reception EDC, while the transmitter frequency noise causes only phase impairment, the local oscillator (LO) FN in these systems results in a noise enhancement in both amplitude and phase. This noise is commonly known as equalization enhanced phase noise (EEPN). It results in asymmetric requirements for transmitter laser and LO laser. Further, the system design in the presence of lasers with non-white frequency noise becomes increasingly challenging for increased capacity-distance product.

The main contributions of this thesis are, firstly, an experimentally validated theory of coherent optical links with lasers having general non-white frequency noise spectrum and corresponding system/laser design criteria and mitigation technique. Secondly, low complexity and high phase noise tolerant CPR for high order modulation formats.

The general theory propounded in this thesis elucidates the origin of the laser frequency noise induced noise enhancement in coherent optical links with different DSP configurations. The thesis establishes the existence of multiple frequency noise regimes and shows that each regime results in different set of impairments. The influence of the impairments due to some regimes can ideally be reduced by optimizing the corresponding mitigation algorithms, while other regimes cause irretrievable impairments. Experimentally validated theoretical boundaries of these regimes and corresponding criteria applicable to system/laser design are provided. Further, an EEPN mitigation method and its two possible implementations are proposed and discussed.

The thesis also demonstrates an intrinsic limitation of the conventional Blind Phase Search (BPS) algorithm due to angular quantization and provides methods to overcome it. Finally, this thesis proposes and demonstrates single stage and multi-stage carrier phase recovery algorithms for compensation of phase impairments due to the two lasers for higher order circular and square modulations. The proposed methods outperform the state of art algorithms both in performance and in complexity.

Sammanfattning

Ökningen av kapacitetsbehovet samt framstegen inom digital signalbehandling (DSP) har nyligen återupplivat intresset för koherent optisk kommunikation och lett till dess kommersialisering. Emellertid blir design och utveckling av robusta DSP-algoritmer, till exempel för fasåtervinning (CPR), komplicerade vid avancerade modulationsformat som 16-QAM och därutöver. Vidare gör elektrisk dispersionskompensering (EDC), samtidigt som det har många fördelar, systemet mer mottagligt för laserfrekvensbrus (FN). Medan sändarlaserns frekvensbrus endast orsakar fasbrus i mottagaren för koherenta optiska länkar med EDC, så resulterar frekvensbrus i lokaloscillatorlasern (LO) i både amplitud- och fasbrus i mottagaren. Detta brus är allmänt känt som Equalization Enhanced Phase Noise (EEPN) och resulterar i asymmetriska krav för sändarlasern och LO-lasern. Vidare kompliceras systemdesignen för att maximera kapacitet-avståndsprodukten i system med lasrar med färgat frekvensbrus.

Huvudbidraget i denna avhandling är för det första en experimentellt validerad teori för EEPN samt systemdesignskriterier, laserdesignskriterier och kompenseringsmetoder för koherenta optiska länkar med lasrar som har ett generellt icke-vitt frekvensbrusspektrum. För det andra, en fasåtervinningsmetod för högre ordningens modulationsformat med låg komplexitet och hög fasbrustolerans. Den allmänna teori som presenteras i denna avhandling ger insikt i uppkomsten av EEPN i koherenta optiska länkar med olika DSP-konfigurationer. Frekvensbruset kan indelas i spektrala områden som orsakar olika typer av systemproblem. Systemproblemen på grund av frekvensbrus i vissa områden kan fullständigt kompenseras genom optimering av motsvarande digitala signalbehandlingsalgoritmer, medan frekvensbrus i andra spektrala områden orsakar irreversibla försämringar. Experimentellt validerade kriterier för frekvensbruset i de olika spektrala områdenas tillhandahålls som kan användas för system- och laserdesign. Vidare föreslås en kompenseringsmetod för EEPN och två möjliga implementeringar av denna diskuteras. Avhandlingen visar också att det finns en inneboende begränsning hos den konventionella Blind Phase Search (BPS)-algoritmen på grund av kvantiseringen av fasvinkeln och ger metoder för att övervinna denna. Slutligen föreslår och demonstrerar denna avhandling enstegs- och flerstegs fasåtervinningsalgoritmer för kompensering av fasfel på grund av de två lasrarna för cirkulära och kvadratiska modulationsformat av högre ordning. De föreslagna algoritmerna innebär en förbättring jämfört med de tidigare bästa algoritmerna både när det gäller prestanda och komplexitet.

Acknowledgements

I would like to take this opportunity to acknowledge all those people whose support was key to this very moment. I start with my five supervisors: **Richard Schatz**, my main supervisor, for his unmatched guidance and support throughout my doctoral studies. He has helped me to comprehend the field of laser and fiber optical communication and untangle its complexities. **Sergei Popov**, who trusted on my potential and provided indispensable guidance in achieving the milestones during the studies. **Gunnar Jacobsen,** an eminence in the field under whom I had the honor to work on daily basis. His unparalleled knowledge of the field, farsightedness and the drive to keep things moving ensured that I made a steady progress in my PhD studies. **Xiaodan Pang**, whose technical expertise, eye for details and unwavering support made it an enjoyable and learning experience. **Oskars Ozolins,** another optimist whose technical expertise and vision kept me on track for relevant work. Anders Berntson and the Kista High Speed Transmission Laboratory team members for providing me the opportunity to work with them and benefit from their experience. Honorable mention to Min Yan who kindly agreed to be the advanced reviewer of my PhD. thesis.

I express my gratitude to EU Marie Curie ICONE project and its management for funding my doctoral studies and providing me the opportunity to work closely with leading universities and companies. In this line, I would like to thank Andre Richter and Hadrien Louchet for hosting me at VPIphotonics. Hadrien Louchet provided me valuable guidance and time for brainstorming which lead to ideas that form a crucial part of this thesis. I would also like to thank Darko Zibar for supervising my stay at DTU Fotonik and guiding my research to ensure productive outcome.

I continue with my colleagues that made my day-to-day life simply better. I start with my one of the closest friend and office mate Jaime Rodrigo Navarro with whom I cherish the closest and most productive collaboration and bond. I would also like to thank Aleksejs, Alexander, Sebastian, Elena, Madeleine from KTH, My ICONE friends who are now my friends for life, Ksenia, Auro, Asif, Simone, Giuseppe, Francesca, Tu, Marti, Faruk, Hugo, Hou-man and Noreen.

Most importantly, I would like to thank my father Surendra Kakkar, mother Rachna Kakkar, brother-in-law Himanshu Jain and sister Devika Kakkar Jain for their countless blessings and unwavering support all the time. Without their unconditional love and support, nothing could have been possible. Finally, I thank the Almighty for giving me this opportunity and strength to work on it.

Contents

List of Figures

List of Tables

List of Abbreviations

ADC	Analog to Digital Convertor
AGC	Automatic Gain Control
AM	Amplitude Modulation
ASE	Amplified Spontaneous Emission
ASK	Amplitude Shift Keying
AWG	Arbitrary Waveform Generator
AWGN	Additive White Gaussian Noise
BER	Bit Error Ratio
BPS	Blind Phase Search
BS	Beam Splitter
C-BPS	Conventional Blind Phase Search
CW	Continuous Wave
DAC	Digital to Analog Convertor
DCE	Digital Coherence Enhancement
DP-QPSK	Dual Polarization Quadrature Phase Shift Keying
DSP	Digital Signal Processing
EAM	Electroabsoption Modulator
EDC	Electronic Dispersion Compensation
EDFA	Erbium Doped Fibre Amplifier
EEPN	Equalization Enhanced Phase Noise
ESNR	Electrical Signal to Noise Ratio
F-BPS	Filtered BPS
FEC	Forward Error Correction
FIR	Finite Impulse Response
FM	Frequency Modulation
FN-PSD	Frequency Noise-Power Spectral Density
FO	Frequency Offset
FSK	Frequency Shift Keying
FWM	Four Wave Mixing
GVD	Group Velocity Dispersion
HPF	High Pass Filter
IF	Intermediate Frequency
IFT	Inverse Fourier Transform
IM-DD	Intensity Modulation-Direct Detection
IQ	In-phase and Quadrature Phase
IQM	In-phase and Quadrature Phase Modulator
ISI	Inter symbol Interference

LED	Light Emitting Diode
LO	Local Oscillator
MIMO	Multiple Input Multiple Output
MLE	Maximum Likelihood Estimation
MZI	Mach-Zehnder Interferometer
O/E	Optical to Electrical Conversion
OSNR	Optical Signal to Noise Ratio
OTP	Optical Transmission Path
PBC	Polarization Beam Combiner
PBS	Polarization Beam Splitter
PDF	Probability Density Function
PM	Phase Modulation
PMD	Polarization Mode Dispersion
PSK	Phase Shift Keying
QAM	Quadrature Amplitude Modulation
QPSK	Quadrature Phase Shift Keying
RF	Radio Frequency
SBS	Stimulated Brillouin Scattering
SE	Spectral Efficiency
SLN	Square Law Non-linearity
SMF	Single Mode Fiber
SPM	Self Phase Modulation
SRS	Stimulated Raman Scattering
TIR	Total Internal Reflection
TPE	Timing Phase Estimator
Tx	Transmitter
V&V	Viterbi and Viterib
WDM	Wavelength Division Multiplexing
XPM	Cross Phase Modulation

List of Publications

Publications included in this thesis:

Paper I: **A. Kakkar**, R. Schatz, X. Pang, J. Rodrigo Navarro, H. Louchet, O. Ozolins, G. Jacobsen, S. Popov, "Impact of local oscillator frequency noise on coherent optical systems with electronic dispersion compensation," *Opt. Express* 23(9), 11221-11226 (2015).

Paper II: **A. Kakkar**, X. Pang, O. Ozolins, R. Schatz, J. Rodrigo Navarro, H. Louchet, G. Jacobsen, S. Popov, "A Path to Use Large Linewidth LO in 28 Gbd 16-QAM Metro Links", in *Proc. of ECOC 2015 (OSA/IEEE, 2015)*, paper Tu.3.4.6.

Paper III: **A. Kakkar**, J. Rodrigo Navarro, R. Schatz, H. Louchet, X. Pang, O. Ozolins, G. Jacobsen, S. Popov, "Comprehensive Study of Equalization-Enhanced Phase Noise in Coherent Optical Systems," *IEEE/OSA J. Lightwave Technol.* 33(23), 4834-4841 (2015).

Paper IV: **A. Kakkar**, O. Ozolins, J. Rodrigo Navarro, X. Pang, M. I. Olmedo, R. Schatz, H. Louchet, G. Jacobsen, S. Popov, "Design of Coherent Optical Systems Impaired by EEPN," in *Proc. Of OFC2016 (OSA, 2016)*, paper Tu2A.2.

Paper V: **A. Kakkar**, J. Rodrigo Navarro, R. Schatz, X. Pang, O. Ozolins, A. Udalcovs, H. Louchet, S. Popov, G. Jacobsen, "Laser Frequency Noise in Coherent Optical Systems: Spectral Regimes and Impairments," *Scientific Reports 7, 844 (2017), doi:10.1038/s41598-017-00868-4*

Paper VI: **A. Kakkar**, J. Rodrigo Navarro, R. Schatz, X. Pang, O. Ozolins, F. Nordwall, D. Zibar, G. Jacobsen, S. Popov, "Influence of Lasers with Non-White Frequency Noise on the Design of Coherent Optical Links," in *Proc. Of OFC2017 (OSA, 2017)*, paper Th2A.55

Paper VII: **A. Kakkar**, J. Rodrigo Navarro, R. Schatz, X. Pang, O. Ozolins, H. Louchet, G. Jacobsen, S. Popov, "Equalization Enhanced Phase Noise in Coherent Optical Systems with Digital Pre- and Post-Processing," *MDPI Photonics* 3(2), 12 (2016).

Paper VIII: **A. Kakkar**, J. Rodrigo Navarro, R. Schatz, X. Pang, O. Ozolins, H. Louchet, G. Jacobsen, S. Popov, "Mitigation of EEPN in Coherent Optical Systems With Low-Speed Digital Coherence Enhancement," *IEEE Photonics Technology Letters*, 27(18), 1942-1945 (2015).

Paper IX: **A. Kakkar**, M. Iglesias Olmedo, O. Ozolins, J. Rodrigo Navarro, X. Pang, R. Schatz, H. Louchet, G. Jacobsen, S. Popov, "Overcoming EEPN in Coherent Transmission Systems," in *Proc. of CLEO2016 (OSA, 2016)*, paper SM4F.3.

Paper X: J. Rodrigo Navarro, **A. Kakkar**, R. Schatz, X. Pang, O. Ozolins, A. Udalcovs, S. Popov, G. Jacobsen, "Blind phase search with angular quantization noise mitigation for efficient carrier phase recovery," MDPI Photonics, to appear.

Paper XI: J. Rodrigo Navarro, **A. Kakkar**, R. Schatz, X. Pang, O. Ozolins, F. Nordwall, H. Louchet, S. Popov, G. Jacobsen, "High Performance and Low Complexity

Carrier Phase Recovery Schemes for 64-QAM Coherent Optical Systems," in *Proc. Of OFC2017 (OSA, 2017)*, paper W2A.53

Paper XII: J. Rodrigo Navarro, **A. Kakkar**, X. Pang, O. Ozolins, A. Udalcovs, R. Schatz, S. Popov, G. Jacobsen, "Design of Multi-stage carrier phase recovery schemes for high order coherent optical mQAM Systems," *IEEE/OSA J. Lightwave Technol.*, under preparation.

Paper XIII: J. Rodrigo Navarro, **A. Kakkar**, X. Pang, O. Ozolins, R. Schatz, M. Iglesias Olmedo, G Jacobsen, S. Popov, "Carrier Phase Recovery Algorithms for Coherent Optical Circular mQAM Systems," *IEEE/OSA J. Lightwave Technol.* 34(11), 2717-2723 (2016).

Paper XIV: J. Rodrigo Navarro, **A. Kakkar**, X. Pang, M. Iglesias Olmedo, O. Ozolins, F. Da Ros, M. Piels, R. Schatz, D. Zibar, G. Jacobsen, S. Popov, "Two-Stage n-PSK Partitioning Carrier Phase Recovery Scheme for Circular mQAM Coherent Optical Systems," *MDPI Photonics*. 3(2), 37 (2016).

Paper XV: J. Rodrigo Navarro, X. Pang, **A. Kakkar**, O. Ozolins, R. Schatz, G. Jacobsen, S. Popov, "Adaptive Boundaries Scheme for Cycle-Slip Mitigation in C-mQAM Coherent Systems," *IEEE Photonics Technology Letters*, 27(20), 2154-2157 (2015).

Paper XVI: J. Rodrigo Navarro, M. I. Olmedo, **A. Kakkar**, X. Pang, O. Ozolins, R. Schatz, G. Jacobsen, S. Popov, D. Zibar, "Phase Noise Tolerant Carrier Recovery Scheme for 28 Gbaud Circular 16QAM", in *Proc. of ECOC 2015 (OSA/IEEE, 2015)*, paper Mo.4.3.5.

Publications not included in the thesis:

Paper I: **A. Kakkar**, J. Rodrigo Navarro, X. Pang, O. Ozolins, R. Schatz, U. Westergren, G. Jacobsen, S. Popov, "Low Complexity Timing Recovery Algorithm for PAM-8 in High Speed Direct Detection Short Range Links," in *Proc. Of OFC2017 (OSA, 2017)*, paper W2A.54

Paper II: S. Popov, **A. Kakkar**, J. Rodrigo Navarro, X. Pang, O. Ozolins, R. Schatz, H. Louchet, G. Jacobsen, "Equalization-Enhanced Phase Noise in Coherent Optical Communications Systems", in *Proc. of ICTON 2016*.

Paper III: J. Rodrigo Navarro, **A. Kakkar**, X. Pang, O. Ozolins, A. Udalcovs, R. Schatz, and G. Jacobsen, S. Popov, "64-QAM Coherent Optical Systems with Semiconductor Lasers," Invited talk at *PIERS2017*, St Petersburg, Russia, 22nd – 25th of May, 2017

Paper IV: X. Pang, J. Rodrigo Navarro, **A. Kakkar**, M. Iglesias Olmedo, O. Ozolins, R. Schatz, A. Udalcovs, S. Popov, G. Jacobsen, "Advanced Modulations and DSP enabling High-speed Coherent Communication using Large Linewidth Lasers," in *Proc. of PIERS 2016*, p. 1-1.

Paper V: O. Ozolins, M. Iglesias Olmedo, X. Pang, S. Gaiarin, **A. Kakkar**, J. Rodrigo Navarro, A. Udalcovs, K. M. Engenhardt, T. Asyngier, R. Schatz, J. Li, F. Nordwall, U. Westergren, D. Zibar, S. Popov, G. Jacobsen, "100 GHz

EML for High Speed Optical Interconnect Applications," *IEEE/OSA J. Lightwave Technol.*, Invited paper accepted.

Paper VI: O. Ozolins, M. Iglesias Olmedo, X. Pang, S. Gaiarin, **A. Kakkar**, A. Udalcovs, K. M. Engenhardt, T. Asyngier, R. Schatz, J. Li, F. Nordwall, U. Westergren, D. Zibar, S. Popov, G. Jacobsen, "100 GHz EML for High Speed Optical Interconnect Applications," in *Proc. of ECOC 2016 (OSA/IEEE, 2016)*, Upgraded Invited paper M 2.4.4.

Paper VII: X. Pang, O. Ozolins, S. Gaiarin, **A. Kakkar**, J. Rodrigo Navarro, M. Iglesias Olmedo, R. Schatz, A. Udalcovs, U. Westergren, D. Zibar, S. Popov G. Jacobsen, "Experimental Study of 1.55-μm EML-Based Optical IM/DD PAM-4/8 Short Reach Systems," *IEEE Photonics Technology Letters*, accepted

Paper VIII: O. Ozolins, X. Pang, M. Iglesias Olmedo, A. Udalcovs, **A. Kakkar**, J. Rodrigo Navarro, R. Schatz, U. Westergren, S. Popov, G. Jacobsen, "High-Speed Optical and Wireless Transmission – Challenges and Achievements" in *Proc. of RTUWO2016 (IEEE, 2016)*, p. 1.

Paper IX: S. Popov, X. Pang, O. Ozolins, M. Iglesias Olmedo, **A. Kakkar**, S. Gaiarin, A. Udalcovs, R. Lin, R. Schatz, J. Rodrigo Navarro, A. Djupsjöbacka, D. Zibar, J. Chen, U. Westergren, G. Jacobsen, " Ultra-Broadband High-Linear Integrated Transmitter for Low Complexity Optical Interconnect Applications" in *Proc. of ACP2016 (OSA, 2016)*, p. 1.

Paper X: O. Ozolins, X. Pang, M. Iglesias Olmedo, **A. Kakkar**, A. Udalcovs, J. Rodrigo Navarro, R. Schatz, U. Westergren, G. Jacobsen, S. Popov, "High-speed Optical Interconnects with Integrated Externally Modulated Laser," Invited talk at ICTON 2017, Girona, Spain, 2^{nd} – 6^{th} of July 2017.

Paper XI: X. Hong, O. Ozolins, C. Guo, X. Pang, J. Zhang, J. Rodrigo Navarro, **A. Kakkar**, R. Schatz, U. Westergren, G. Jacobsen, S. Popov, J. Chen, "1.55-μm EML-based DMT Transmission with Nonlinearity-Aware Time Domain Super-Nyquist Image Induced Aliasing," in *Proc. Of OFC2017 (OSA, 2017)*, paper Th3D.3

Paper XII: A. Marinins, O. Ozolins, X. Pang, A. Udalcovs, J. Rodrigo Navarro, **A. Kakkar**, R. Schatz, G. Jacobsen, S. Popov, "Cylindrical Polymer Optical Waveguides with Polarization Independent Performance," in *CLEO2017 (OSA, 2017)*, accepted.

Chapter 1

Introduction

The history of light based communication dates back thousands of years. The attempts to communicate using light, range from the development of 'Smoke signal' based long distance communication to the invention of optical semaphore telegraph in 1790s. Even, Alexander Graham Bell patented an optical telephone system called Photophone in 1880, but it never took a tangible shape as it lost to its more practical earlier invention of Bell, the telephone. The demonstration of TIR (Total Internal Reflection) by Jean-Daniel Colladon in 1841 was a stepping stone in the development of fiber optical communication. However, a host of optical and electronic invention was still awaited. An initial breakthrough was achieved with the development of fiberscope in 1950's. Excessive loss in all glass fiber motivated the scientists towards development of fiber that had an additional coating called 'cladding'. Dr. Charles K. Kao by 1964 had identified the critical theoretical specifications for long-range communication, i.e. 10 or 20 dB of light loss per km. He also showed the need for a purer form of glass to reduce loss. Soon in 1970 a team of researchers in Corning succeeded in developing optical fiber with less than 20 dB/km attenuation, the threshold for making fiber optics a viable technology as proposed by Kao. Dr. Charles K. Kao was later awarded 2009 Noble Prize in Physics for "groundbreaking achievements concerning the transmission of light in fiber for optical communication". During the same period, critical advances in another integral component of the fiber-optic communication, i.e. the light source was taking place. The semiconductor laser, which is widely used in fiber-optic today, was first realized in 1962. The world's first live telephone traffic through a fiber-optic running at 6 Mbps was tested and

deployed in April 1977 by General Telephone and Electronics soon followed by Bell in May, 1977. The growth and demand of fiber optic communication systems, since then has been on rising trajectory. As per Cisco predictions [1] the global IP traffic will see an increase of nearly hundredfold till 2020 compared to 2005 and will reach 2.3 ZB. Coherent fiber optical communication has the potential to meet this global high capacity demands by exploiting multiple dimensions of the lightwave. Therefore, in the following sections we will trace the evolution of coherent fiber optical communication from analog to digital era and discuss the state-of-the-art and challenges.

1.1 Pre-DSP era Coherent Optical Communications

Initial research and development in fiber optical communication was focused on intensity modulation and direct detection (IM-DD) systems. In these systems, the electrical signal was modulated over the lightwave by modulating the output intensity of the semiconductor lasers. This intensity-modulated signal was transmitted over an optical fiber and received with photo detector. The photodetector translated the intensity modulated optical signal into electrical current. These systems provided some distinct advantages in real systems such as, the receiver sensitivity was independent of randomly fluctuating laser phase and state of polarization.

In contrast to direct detection of intensity, the other alternative is to use a local oscillator (LO) laser to interfere with the incoming optical signal. Receivers utilizing LO are called coherent receivers. Coherent receiver can be heterodyne, homodyne and intradyne receivers depending on the intermediate frequency (IF) after optical demodulation. The use of unmodulated local oscillator acts as a local amplifier enhancing receiver sensitivity along with providing the ability to extract phase information. The gain in receiver sensitivity achieved by coherent optical systems in unrepeated links was a major motivation towards coherent systems. Thus, study of the achievable gain in receiver sensitivity for different modulation formats and demodulation scheme was carried out in [2] and [3]. The studies concluded that the utilization of sufficiently high power LO could achieve shot noise limited receiver sensitivity in coherent optical systems. During 1970s, the interest in coherent optical systems with heterodyne detection, first proposed by Delange [4], was overshadowed by the more viable IM-DD systems. The ability to achieve precise frequency stabilization in semiconductor lasers as demonstrated by Okoshi and Kikuchi

[5] and Fabre and LeGuen [6] independently in 1980 reignited the interest in such systems. Following this many demonstrations of coherent optical communication systems were reported until 1990.

Coherent communications also provides the ability to exploit the complex amplitude of the optical field as wells as SOP to enhance the capacity of transmission. However, this in turn makes the system highly susceptible to random variation of phase and SOP making coherent optical system much more complicated compared to their IM-DD counterpart. The utilization of polarization diversity to overcome the dependence of receiver sensitivity on SOP was shown in [7] and [8]. In this scheme, orthogonally polarized LO laser components were used to detect different polarization component of the transmitted signal. Even today the state-of-the-art digital coherent receivers rely on this scheme to solve the SOP dependence. Efforts were also carried out in the direction of stabilizing the SOP of transmitted signal using linear polarization maintaining fiber [9] and circular polarization maintaining fiber [10]. Another critical problem was the random phase fluctuations of the carrier wave due to laser phase noise [5] and [6]. Extensive research was carried out to study the spectral properties of semiconductor laser, its measurement and methods to narrow it down [11], [12], [13] and [14].

Both heterodyne and homodyne based coherent communication systems were investigated and demonstrated around 80s and 90s. The demonstrated heterodyne systems mostly employed frequency shift keying (FSK) modulation of the semiconductor laser frequency and differential detection at the intermediate frequency stage. The utilization of advanced heterodyne technologies, such as use of continuous phase FSK modulation, automatic frequency control of laser, polarization diversity and differential detection was demonstrated using a field trial of undersea transmission at 2.5 Gbps [15]. The homodyne receivers on one hand provided the advantage of directly obtaining a base band signal, but on the other hand required an optical phase-locked loop (OPLL) for the LO to track the carrier phase [16]. The OPLL had some inherent technical difficulties, firstly, limited bandwidth below 1 MHz, making it difficult to maintain system stability for lasers having large phase noise and frequency drift. Secondly, difficulty in the recovery of carrier phase, for instance a phase shift keyed signal which does not have carrier component would require a non-linear signal processing to recover phase.

However, two major technological developments in 1990s led to the interruption, of more than ten years, in further research and development activities of coherent optical communication. The first was the invention of erbium doped fiber amplifier (EDFA) which made the advantage provided by coherent receivers in terms of receiver sensitivity less interesting [17]. Secondly, the increase of transmission capacity over single fiber by exploiting wavelength division multiplexing (WDM) technique for EDFA based IM-DD links. The two technologies together brought about thousand-fold increase transmission capacity along with much-desired features such as simplicity and relatively low cost broad band optical amplifiers for multiple WDM channels. Thus, the advantages provided by coherent optical communication neither were an urgent need nor were the coherent the fiber optical links cost effective in the 1990s.

1.2 DSP era Coherent Optical Communication

The demand for further increase in transmission capacity of the WDM systems triggered the renewed interest in coherent optical communication technologies after 2000. The driving factor was to use multi-level modulation formats based on coherent technology [18]. The first experiment in this line was the demonstration of 40 Gbps differential QPSK system utilizing optical IQ modulation (IQM) and optical delay detection [19].

The major thrust in interest came in 2005 with the demonstration of possibility of digital carrier phase recovery [20]. This was enabled by cooption of architecture and concepts from radio counterparts along with the advances in high speed digital signal processing (DSP). As was widely applied in radio communications one could use digital signal processing either on transmitter side or receiver side or both. The digital data on the transmitter side after digital signal processing is converted into an analog signal using a digital to analog converter (DAC) followed by modulation of in-phase and quadrature components of radio frequency (RF) carrier. Similarly on the receiver side, signal is demodulated to lower frequency by a RF mixed followed by conversion to digital sampled signal for digital processing and decoding in DSP. As stated earlier, inspired by radio technology, DSP based optical transmitter and receivers were demonstrated by replacing RF components with their optical counterpart [20], [21], [22] and [23].

Digital coherent receiver for 20 Gbps QPSK signal with DSP based carrier phase recovery after homodyne detection were demonstrated in [21]. The DSP based carrier phase recovery which can track phase very fast, made the system more stable and practical compared to their low bandwidth optical competitor OPLL. Apart from providing the potential to increase spectral efficiency by using multi-level modulation format [24] and [25], the digital coherent receiver offer important post signal processing functions [26] and [27]. Since the coherent demodulation with an LO can be modeled as a linear process, the optical channel impairments compensation and filtering can be performed in the DSP. Several methods for efficient compensation of fiber dispersion in electrical domain, thus removing the need of optical dispersion compensation, were reported [28] and [29]. Utilization of the polarization-diversity scheme in homodyne detection for polarization alignment was also shown [30] and [31]. Further, DSP based polarization de-multiplexing and polarization mode dispersion (PMD) compensation was reported in [32]. In order to realize a practical DSP based coherent systems high speed ADC and DSP were required. An application specific integrated circuit for dual polarization QPSK (DP-QPSK) was developed [33] and a real time 46 Gbps system was demonstrated [34]. ASIC for the 100 G commercial optical system operating at 32 Gbaud with 127 Gbps single channel transmission capacity and 27% forward error correction (FEC) was realized in [35].

The market demand for 200 G, 400 G links and beyond have now led to intensive research and development into complex high order QAM such as 16, 64-QAM and beyond. The scalability of all DSP algorithms developed for QPSK modulation to high order modulation is not straight forward. For instance, QPSK based systems utilized the feed forward Viterbi & Viterbi (V&V) algorithm [36] for carrier phase recovery, which was borrowed from radio domain. However, as we opt for high order constellations, which are not PSK, such as square 16/64-QAM, the V&V cannot be applied directly and required modifications. Further, as the distance between points in the constellation decreases, the system becomes more sensitive to phase noise, thus requiring a robust and highly phase noise tolerant algorithms. Many modified algorithms such as QPSK partitioning and its multi-stage variants were proposed [37], [38], [39] and [40]. These algorithms aimed at partioning and/or transforming a given constellation to QPSK points and then applying V&V algorithm. On the other hand, Blind Phase Search (BPS) algorithm for high order modulation was proposed in [41]. In this algorithm, the received symbols or constellation

is rotated by discrete number of test phases in order to minimize the cost function which in this case is the distance function. This method is both scalable and phase noise tolerant but has intensive computational complexity requirements. As the future transceivers move towards smaller pluggable packages, the requirements on power consumption and hence computational complexity become critical. Efforts for reducing computational complexity while achieving similar performance were reported in [42], [43], [44], [45], [46] and [47]. As an alternative to square constellation one could use circular constellation which provides two distinct advantages. First, it has inherently high phase noise tolerance and second V&V can be directly applied to these constellations [48].

In 2008, W. Shieh et al. [49] observed that the received signal in coherent optical links even after digital signal processing for dispersion and phase recovery remain impaired by enhanced noise originating from the phase noise of local oscillator. They called this noise equalization enhanced phase noise (EEPN). They also performed theoretical analysis of EEPN assuming white frequency noise laser and concluded that it is difficult to overcome [49] and [50]. T. Xu et al. provided analytical estimate of impact of EEPN on BER for PSK signals [51]. Impact of chromatic dispersion compensation techniques and CPRs on EEPN was studied in [52], [53], [54] and [55]. Experimental demonstration of EEPN on systems was provided in [55] and [56]. All state-of-the-art studies concluded that impairment due to EEPN increases with accumulated dispersion, symbol rate and laser linewidth [49], [50], [51], [52], [54], [53], [55], [56] and [57]. Further, combined laser linewidth symbol duration product was no longer a sufficient figure of merit for characterization and design of coherent optical links. However, questions such as what is a tolerable laser linewidth when utilizing multi-level QAM constellation, what happens when we choose a DSP order other than the most commonly used post-reception DSP, is there a method to mitigate it and what should be requirement of that method and many more, even for widely studied white frequency noise, case remained unanswered. Additionally, the practical consideration that lasers, in general, have non-white frequency noise spectrum remained completely elusive. Thus, warranting a general theory for understanding the origin, exploring possibilities of mitigation and providing criteria assisting efficient system/laser design.

1.3 Overview of the thesis contributions

Original contribution of this thesis is in the following two areas:

1. General theory of influence of laser frequency noise in coherent fiber optical communication systems with electronic domain dispersion compensation.
2. Development of low complexity and high performance carrier phase recovery schemes for multi-level square and circular QAM systems.

In the first area, we have shown with frequency domain analysis that the noise enhancement commonly known as EEPN is mainly caused by the low-frequent frequency noise of the laser. Statistical analysis is carried out for white frequency noise case and experimentally validated closed form expressions for system design parameters, such as tolerable linewidth/penalty and/or mitigation bandwidth for any general system configuration, are provided. The statistical analysis, although helpful in system design for white frequency noise case, becomes insufficient to understand the physical origin, possibilities of DSP optimization amongst others, especially when the frequency noise is non-white. Therefore, we provide an experimentally validated theory for the case of general non-white frequency noise. We demonstrate that the origin of the noise enhancement lies in the frequency noise induced symbol displacement that causes timing jitter and/or inter/intra symbol interference. Different frequency noise spectral regimes cause different set of impairments. Influence of impairments due to some regimes can be reduced by optimizing the corresponding DSP algorithms while other regimes cause irretrievable impairments. We provide the theoretical boundaries of these and criteria for system/laser design. We also provide the study of all eight practicable all-electronic impairment mitigation schemes. The results show that whether the noise enhancement is caused by the transmitter laser or the LO laser depends on the order of pre-and/or post digital signal processing. Although the origin of the noise enhancement depends on order of DSP, the guidelines for system design in presence of this noise enhancement remains same. Mitigation methods for this noise enhancement are also proposed and demonstrated.

In the second area, we demonstrate the basic inherent limitation of the state-of-the-art BPS algorithm due to quantization noise in its phase noise estimator. We show that the mitigation of the out-of-band quantization noise achieved by low pass filtering the BPS phase noise estimator results in higher performance and/or a drastic reduction in its implementation complexity.

Guidelines for design of multi-stage carrier phase recovery for multilevel QAM such as 16/64-QAM and beyond are provided and a CPR algorithm based on this scheme was proposed. In our work we also showed that the direct application of the V&V CPR method to some specific circular constellations resulted in asymmetrical rotations of the constellation also known as cycle slips. This problem is shown to be critical to enhance the phase noise tolerance of circular constellations employing the V&V method for efficient carrier recovery. An adaptive boundaries scheme was proposed for to track these asymmetrical constellation rotations after cycle slip events. However, as this method was still computationally complex, we proposed a low complexity and high performance single and multi-stage n-PSK partitioning methods. These methods outperformed the state of art methods in both performance and reduction in complexity.

1.4 Thesis organization

The remainder of the thesis is organized as follows.

Chapter 2 presents the background of coherent fiber optical communication systems and digital signal processing techniques.

Chapter 3 presents the work included in **Paper I** to **Paper VII.** Theory of influence of laser frequency noise on coherent optical systems is proposed and guidelines applicable for system/laser design are outlined.

Chapter 4 presents the work included in **Paper VIII** to **Paper XVI.** The first section discusses the mitigation methods presented in **Paper VIII** and **Paper IX** for enhanced noise commonly known as EEPN. The second section of the chapter discusses the proposed low complexity and high phase noise tolerant CPR schemes developed in **Paper X** to **Paper XII** for square QAMs. The last section discusses the CPR schemes for non-traditional circular QAM constellations developed and validated in **Paper XIII** to **Paper XVI**.

Chapter 5 provides the conclusion and possible future research related to work presented in the thesis.

Chapter 6 summarizes the original work and author's contribution for each publication included in the thesis.

Chapter 2

Digital Coherent Fiber Optical Communication Systems

A digital telecommunication system, in general, consists of a transmitter, which encodes/modulates the incoming digital message, to be transmitted, on the carrier wave. This modulated carrier wave is then transmitted over the communication medium known as the channel. The signal, due to the degradation in the channel, might require re-amplification and/or regeneration during transmission over the medium. The receiver finally demodulates the message encoded on the carrier wave. The digital signal processing enabled telecommunication provides the advantage to pre-process and post-process the signal in order to enhance the capacity, mitigate channel impairment etc. In coherent fiber optical systems the carrier wave is lightwave and transmission channel is fiber waveguide. In this chapter, we provide the brief background of different components in DSP enabled fiber optical systems. General block diagram of such a system is illustrated in Fig. 2.1.

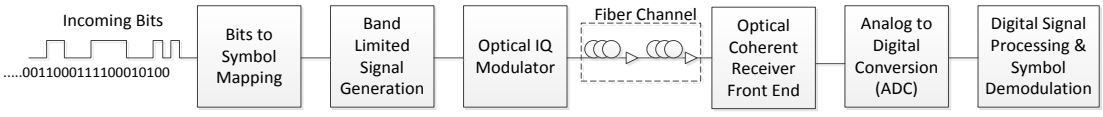

Figure 2.1: Block Diagram of Digital Coherent Fiber Optical Communication System.

2.1 Transmitter

In coherent optical communication, information can be encoded both on the amplitude and phase for each polarization of the light wave carrier. Overall system could employ single carrier configuration or multicarrier configuration. In multicarrier systems, information in also encoded onto the amplitude and phase of the subcarriers which are then multiplexed together using different techniques such that the orthogonality of the signal is maintained [58], [59] and [60]. In this chapter we restrict the scope of discussion to single carrier systems.

2.1.1 Multi-level Modulation Format and Pulse Shaping

Depending on the modulation format, the information is encoded on the amplitude component, phase component, or both of the ideal harmonic signal given by

$$E(t) = A_m \sin(\omega t + \varphi_m) \tag{2.1}$$

where A_m and φ_m, are amplitude and phase of the ideal harmonic signal, which in our case is the laser. The modulation format in which the information is modulated only on the amplitude is known as Amplitude Modulation (AM) or Ampltidue Shift Keying (ASK) for digital modulation. Similarly, if the information is encoded on the phase it is known as Phase Modulation (PM) or Phase Shift Keying (PSK) for digital modulation. In order to increase the amount of transmitted information, it is important to simultaneously encode on both phase and amplitude of the carrier wave. Eq (2.1) can be rewritten, using the identity $\sin(a+b) = \sin(a)\cos(b) + \cos(a)\sin(b)$, as

$$E(t) = A_m \cos(\varphi_m)\sin(\omega t) + A_m \sin(\varphi_m)\cos(\omega t) = a_m \sin(\omega t) + b_m \cos(\omega t) \tag{2.2}$$

where $a_m = A_m \cos(\varphi_m)$ and $b_m = A_m \sin(\varphi_m)$ it can be seen that the AM/PM modulated signal can be written as sum of two AM signals modulated on a carrier with same frequency but in quadrature phase. Thus, the modulation format in which both amplitude and phase is modulated is known as Quadrature Amplitude Modulation (QAM). In digital communication, the incoming bits are encoded onto discrete combination of phase and amplitude or in other words onto discrete combination of amplitude levels on two orthogonal axes. Each combination of phase and amplitude represents a distinct point in the complex plane, known as a symbol. The full set of allowed symbol alphabets in the complex plane is commonly known as a constellation.

Fig. 2.2 shows some examples of QAM constellations. More modulation formats can be found in [61] and [62]. The constellation is chosen such that it minimizes the likelihood of error in the presence of given dominant noise sources. For instance, in coherent detection system where the dominant source of noise is additive white Gaussian in nature, the optimal constellation is the one, which maximizes the minimum distance between the neighboring symbols under the constraint of not exceeding maximum power. The solution is known as Sphere Packing [63]. Similarly, the constellations can be optimized also to minimize the impact of phase noise [48], [64] and [65].

The presence of noise can cause errors in symbol detection. In order to minimize the propagation of symbol error to bit error different coding techniques could be employed. The preferred coding in presence of AWGN is Gray coding in which the adjacent symbol differ only in one bit. Thus in Gray coded systems one symbol error translates in general to one bit error [66]. However, in presence of phase noise it might be beneficial to differentially encode in order to reduce the impact of cycle slips due to symmetry in the constellation. This restricts the use of direct Gray coding of constellation. However, a method to Gray code the quadrants and differentially Gray encode between quadrants for square constellation was proposed in [41]. A differential encoding and bit mapping scheme for circular QAM is also proposed in [67] and [68].

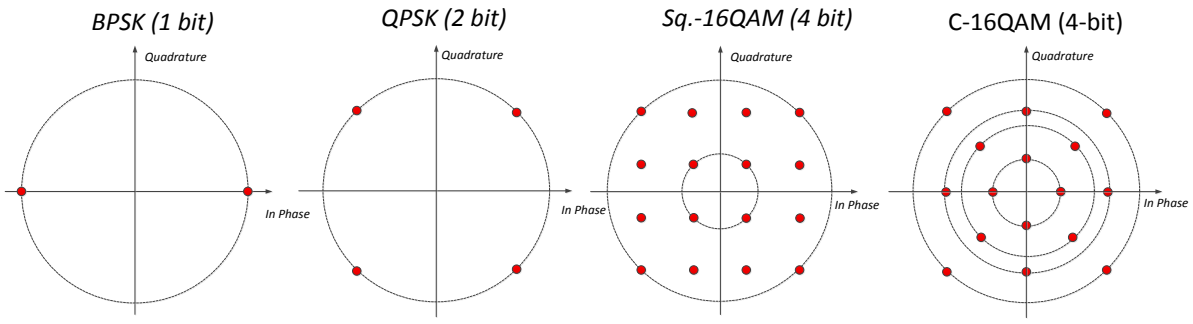

Figure 2.2: Example Quadrature Amplitude Moulation (QAM) Constellations.

Further, band-limited pulse shaping filter may be required to minimize the bandwidth required to transmit symbols/information over a channel. This requirement might arise due to limited available channel bandwidth and/or the desire to transmit more information per unit spectrum [69] and [70]. Limiting the signal in bandwidth results in broadening of signal in time which can

cause inter-symbol interference (ISI). The method of constructing a band limited filter to overcome the effects of ISI is given by Nyquist ISI criterion. Family of raised cosine filters provide an implementation of low-pass Nyquist Filter with a general frequency domain description as follows.

$$H(f)=\begin{cases} T, & |f|\le \dfrac{1-\beta}{2T} \\ \dfrac{T}{2}\left[1+\cos\left(\dfrac{\pi T}{\beta}\left[|f|-\dfrac{1-\beta}{2T}\right]\right)\right], & \dfrac{1-\beta}{2T}<|f|<\dfrac{1+\beta}{2T} \\ 0, & \textit{otherwise} \end{cases} \tag{2.3}$$

in the above equation β is the roll off factor, R_s is the baudrate of the signal and the required bandwidth is equal to $(1+\beta)R_s$. The ideal Nyquist Filter is a subset of the raised cosine filter with β=0.

2.1.2 Laser Source and Frequency Noise

Lasers and light emitting diodes (LED) are used as light sources to achieve communication in optical-base communication systems. The LEDs are cheap but have drawbacks such as small modulation bandwidth and spatially and spectrally incoherent emission resulting in broad spectrum and only suitability to multimode fiber, which limits the performance due to the large multimode and chromatic dispersion. On the other hand, lasers can be made monochromatic, can be coupled to single mode fiber, have high output power and can be phase modulated. Thus, a laser is the preferred light source in high speed coherent optical communication systems with single mode fiber. Inherent uncertainty in generation and absorption processes due to the particle nature of photons and electrons results in noise in the laser output resulting in non-pure finite spectral width. The most critical laser noise for coherent optical communication is the frequency noise of the laser. It could be modeled as the random phase fluctuation of the CW laser. The output of the laser emitting at nominal angular frequency, ω_0, having phase noise φ(t) and amplitude A assuming no intensity noise, can be modelled as

$$E_{Laser}(t) = Ae^{j(\omega_0 t+\varphi(t))} \tag{2.4}$$

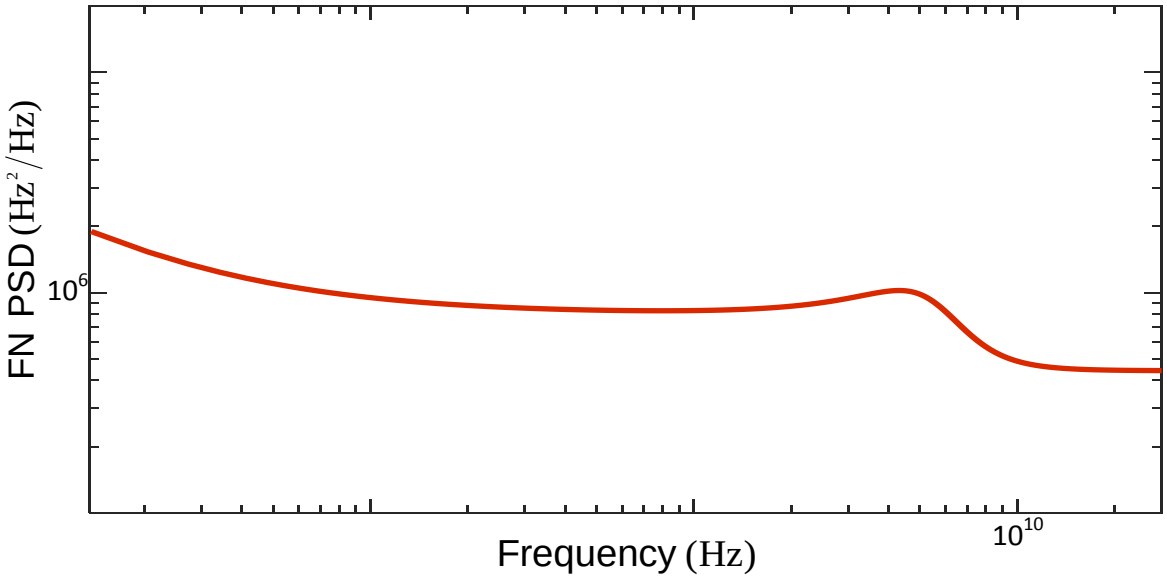

Figure 2.3: General Frequency Noise Spectrum (FN-PSD) of a semiconductor laser.

In frequency domain it is represented by frequency or phase noise spectrum. A general frequency noise (FN) power spectral density (PSD) is illustrated in Fig. 2.3. The single sided frequency noise spectrum can be written as [71]

$$S_\upsilon(f) = \frac{10^9\zeta}{\pi f} + \frac{\Delta\upsilon_{int}}{\pi(1+\alpha^2)}\left(1+\frac{\alpha^2\upsilon_{RF}^4}{\left(\upsilon_{RF}^2-f^2\right)^2+\left(\frac{K\upsilon_{RF}^2}{2\pi}\right)^2 f^2}\right) \tag{2.5}$$

where ζ is the measure of the magnitude of 1/f flicker noise at 1 GHz level, $\Delta\upsilon_{int}$ is the linewidth given by Schawlow Townes formula, υ_{RF} is the resonance frequency, α is Henry's linewidth enhancement factor and K provides the change of damping rate with the squared resonance frequency of the laser. The spontaneous emission in the laser mode generates white frequency noise resulting in intrinsic linewidth $\Delta\upsilon_{int}$. The carrier density fluctuations induces variation of refractive index of the medium which in turn causes white linewidth enhancement along with causing a peak at the photon-carrier resonance frequency and commonly known as carrier

induced frequency noise. Finally, the first term in eq. (2.5) corresponds to the flicker noise in the low frequency range. Mechanical coupling, coupling of electromagnetic fields from the surrounding, power supply and electrical circuits are some of the sources of flicker noise.

In high speed coherent systems, the performance of carrier phase recovery is generally evaluated for tolerance to white frequency noise, which can be modelled as Wiener Process, as the phase fluctuations due 1/f noise is very small over symbol period and carrier induced noise is assumed to negligible [72] and [73]. Impact of carrier induced frequency noise on system performance was evaluated in [74]. Furthermore, frequency noise in coherent optical links can cause additional impairments than only phase impairments, both due to FM to AM conversion in wavelength selective components and, equalization enhanced phase noise (EEPN) in links with electronic dispersion compensation.

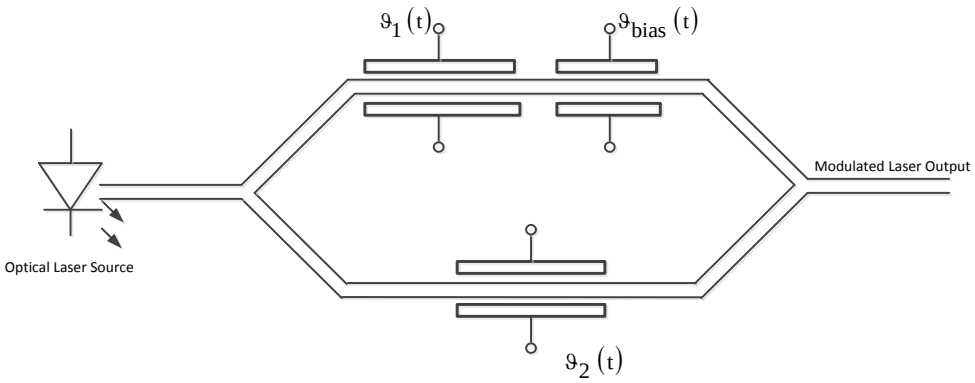

Figure 2.4: Lithium Niobate based Mach-Zehnder Modulator Architecture.

2.1.3 Optical Modulator

Directly modulated lasers [75], electro absorption modulators (EAM) [76] and Lithium Niobate based Mach-Zehnder modulators are the most commonly used for light modulation. Since in coherent systems, in general, both phase and amplitude of the lightwave are modulated, we focus on Lithium Niobate modulator in Mach-Zehnder Interferometer (MZI) configuration. The operating principle of Lithium Niobate based MZI modulator is depicted in Figure 2.4. In these devices the continuous wave (CW) laser is split into two arms and the modulating voltage is applied on either one or both arms. The temporal transfer function of the device can be derived from

$$E_{out}(t)=\begin{bmatrix}\frac{1}{\sqrt{2}} & \frac{1}{\sqrt{2}}\end{bmatrix}\begin{pmatrix} e^{\{j[\vartheta_1(t)+\vartheta_{bias}(t)]\}} & 0 \\ 0 & e^{\{j[\vartheta_2(t)]\}}\end{pmatrix}\begin{bmatrix}\frac{1}{\sqrt{2}} \\ \frac{1}{\sqrt{2}}\end{bmatrix}E_{in}(t) \tag{2.6}$$

In eq. (2.6) $E_{in}(t)$ is the input CW laser signal split into two arms using a 1:2 power splitter followed by phase shift induction on the two arms of the MZI represented by square matrix, finally the signal in two arms are combined using a 2:1 power combiner to give the output signal $E_{out}(t)$. The temporal transfer function can be written as

$$T_{MZI}(t)=\frac{E_{out}(t)}{E_{in}(t)}=\frac{1}{2}e^{\{j[\vartheta_1(t)+\vartheta_{bias}(t)]\}}+\frac{1}{2}e^{\{j[\vartheta_2(t)]\}} \tag{2.7}$$

Eq. (2.7) after rearrangement of terms can be written as

$$T_{MZI}(t)=e^{\left\{\frac{j}{2}[\vartheta_1(t)+\vartheta_2(t)+\vartheta_{bias}(t)]\right\}}\cdot cos\left(\frac{1}{2}\left[\vartheta_1(t)-\vartheta_2(t)+\vartheta_{bias}(t)\right]\right) \tag{2.8}$$

Thus the MZI modulator can be operated both as phase modulator and amplitude modulator by choosing $\vartheta_1=\vartheta_2$ or $\vartheta_1=-\vartheta_2$. When $\vartheta_1=\vartheta_2$ the MZI is said to operate as a pure phase modulator in push-push mode. The MZI can also be operated as amplitude modulator by choosing $\vartheta_1=-\vartheta_2$, this mode is known as push-pull mode. There are two interesting operating points of the push-pull mode depending on the bias ϑ_{bias}. When operated around the null point of the cosine function, the normalized transfer function is given by

$$T_{MZI}(t)=sin\left(\frac{1}{2}\Delta\vartheta(t)\right) \tag{2.9}$$

While, when operated around the quadrature point the transfer function the modulator works as intensity modulator with transfer function.

$$T_{MZI}(t)=1+cos\left(\Delta\vartheta(t)\right) \tag{2.10}$$

In coherent optical communication, it is desirable to access any point in the constellation. The general configuration to encode the in-phase and quadrature component of the complex signal directly onto the optical carrier is given by Fig. 2.5. This configuration is known as optical IQ-modulator. This scheme utilizes two MZI modulators one for the upper arm and other for the lower arm. The two arms have a relative phase shift of $\pi/2$. The two MZI are operated in push-pull mode. In case of polarization multiplexed system the laser source is split using polarization beam splitter (PBS) into two orthogonal polarization and fed into two IQ modulation followed by polarization beam combiner (PBC).

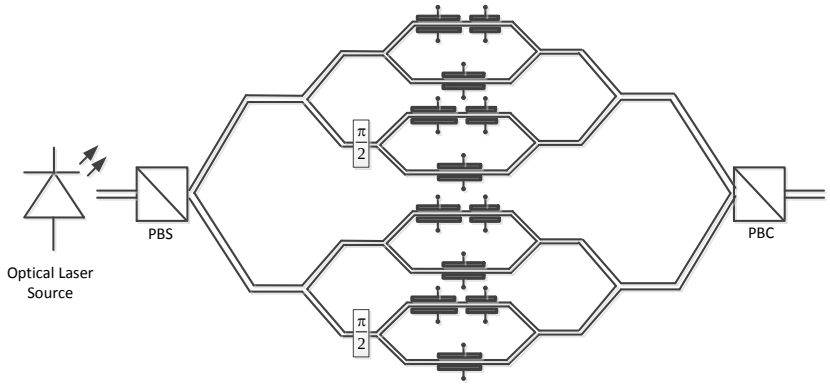

Figure 2.5: Polarization Diverse MZM based IQ Modulator.

2.2 Fiber Channel

The fiber channel could be single mode or multimode. Single mode fiber (SMF) has the least pulse broadening and lowest power loss and since long distance coherent systems employ SMF, we will limit our focus to it. The main sources of the degradation of signal quality while transmission through a fiber are additive white Gaussian noise (AWGN) caused by optical amplifiers to compensate for the fiber attenuation, chromatic dispersion, polarization mode dispersion and fiber nonlinearities.

2.2.1 Attenuation and Amplification

Rayleigh scattering, material absorption and physical deformations such as micro bending, macro bending and splices & connector are important contributors to the loss mechanism in the fiber transmission [77]. The fluctuation in the refractive index over distances smaller compared to lightwave wavelength, due to the inhomogeneities of the refractive index in the silica glass

results in Rayleigh scattering. The material absorption is composed of the intrinsic absorption in the silica and external absorption due to the impurities in the silica. The losses in the fiber are wavelength dependent. The relation of the average output and input optical power, after the signal propagates through a fiber of length L [77]

$$P_{out} = P_{in} e^{-\alpha L} \tag{2.11}$$

In eq. (2.11), Pin is the input power, Pout is the output power and α is the attenuation coefficient in neper per meter. Attenuation is generally expressed in dB/km.

The losses in the fiber can be compensated by using in-line amplifiers [77]. Erbium doped fiber amplifier (EDFA) and Raman amplifiers are two popular in-line amplifiers. In the EDFA the gain medium is erbium doped fiber, while the latter is based on the Raman scattering phenomenon. EDFAs are most generally used for lumped amplification after each fiber span while the Raman amplifier can use the same transmission fiber and thus provide distributed amplification. The signal is impaired by independent and identically distributed (i.i.d.) additive white Gaussian noise due to the amplified spontaneous from the optical amplifiers.

2.2.2 Chromatic Dispersion

Different parts of the spectral content of the modulated wave travel at different speed in the fiber due to two effects. Firstly, the group index of the glass is wavelength dependent, even for plane waves. This is known as material dispersion. Secondly, the propagation constant changes in a non-linear way, thus making the bounce angle of the confined wave wavelength dependent. This is known as waveguide dispersion. Together these effects are known as group velocity dispersion (GVD). In fiber systems, GVD causes temporal spreading of the information pulse. The shorter wavelengths travel faster than the longer wavelength components around 1.55 μm wavelength. This is called anomalous dispersion or negative dispersion as it is in contrast to the dispersion in visible range. The transfer function of the fiber dispersion can be written in terms of central frequency ω_0, frequency dependent propagation constant β, attenuation α and fiber length L as [77]

$$H(\Delta\omega) = e^{\left(-\frac{\alpha(\omega_0+\Delta\omega)}{2}L\right)} e^{\left(-j\beta(\omega_0+\Delta\omega)L\right)} \tag{2.12}$$

Taylor Expanding the propagation constant β in terms of $\Delta\omega$ around ω_0 and putting in eq. (2.12) we get

$$H(\Delta\omega) = e^{\left(-\frac{\alpha_0}{2}L\right)} e^{(-j\beta_0 L)} e^{(-j\beta_1 \Delta\omega L)} e^{\left(-j\beta_2 L(\Delta\omega)^2 + \ldots\right)} \tag{2.13}$$

In eq. (2.13), the frequency dependence of the attenuation coefficient is neglected. The first two terms represent the loss and the constant phase delay, respectively. The next term is the constant group delay seen by the signal. The pulse broadening is caused by the last part in which β_2 is the group velocity dispersion parameter. Fig. 2.6 illustrates the pulse broadening phenomenon of a train of Nyquist pulses after to transmission over a dispersive fiber due to second order dispersion. Higher order dispersion such as third order dispersion also causes pulse broadening but has normally much less impact than β_2 and is neglected in the analysis presented in this thesis. The relation between GVD and commonly known dispersion parameter, where c_0 is the speed of light, is given by

$$D = -\frac{2\pi}{\lambda^2} c_0 \beta_2 \left[\frac{ps}{nm \cdot km}\right] \tag{2.14}$$

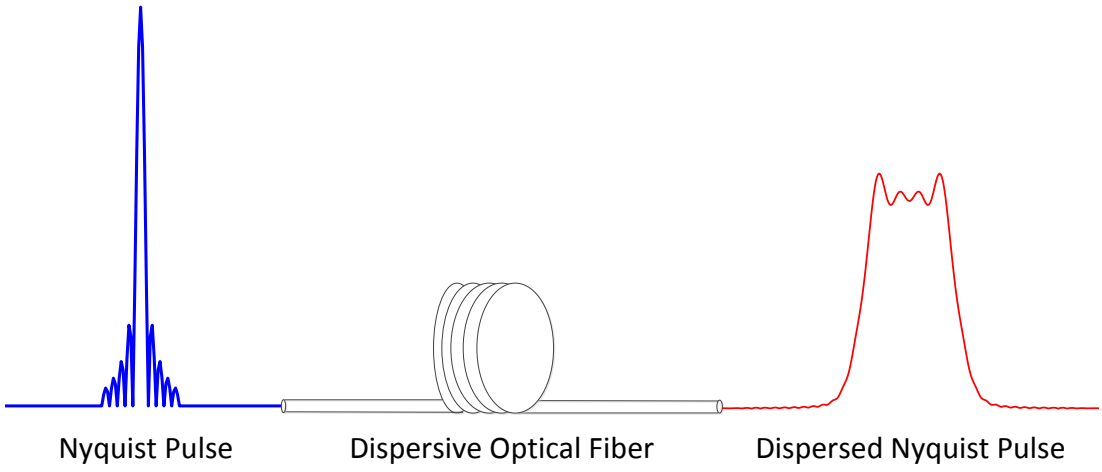

Figure 2.6: Illustration of pulse broadening of a Nyquist pulse after transmission through a dispersive fiber channel.

2.2.3 Polarization Mode Dispersion

Polarization mode dispersion (PMD) is caused by birefringence in the fiber so that the orthogonal polarizations travel with different phase and group velocity. A periodical change in polarization

is caused due to difference in phase velocity. However, pulse broadening is caused by the difference in group velocity. PMD is a stochastic and time varying phenomenon and hence requires an adaptive filter to mitigate the effect. The PMD parameter is measured in units $\text{ps}/\sqrt{\text{km}}$.

2.2.4 Fiber Non-linearity

The polarization **P** can be written as a nonlinear function the electrical field **E** as [78]

$$P = \varepsilon_0 \left(\chi^{(1)} \cdot E + \chi^{(2)} EE + \chi^{(3)} EEE + ... \right) \tag{2.15}$$

where ε_0 is the vacuum permittivity, and $\chi^{(i)}$ is the i^{th} order susceptibility. This results in a non-linear refraction. $X^{(1)}$ is included in the angular frequency ω_0 dependent linear refractive index $n(\omega_0)$. Due to symmetry in molecules like silica, second order susceptibility $\chi^{(2)}$ is negligible. The nonlinear refraction is mainly due to the third order susceptibility $\chi^{(3)}$. This makes the refractive index dependent on the intensity of light. The nonlinear refractive including the influence of third order susceptibility can be written as

$$\tilde{n}\left(\omega_0, |E|^2 \right) = n\left(\omega_0 \right) + n_2 |E|^2 \tag{2.16}$$

in the above equation, optical intensity is given by $|E|^2$, n_2 is the nonlinear index coefficient [116].

Non-linear effects such as self-phase modulation (SPM), cross-phase modulation (XPM) and four wave mixing (FWM) can be mathematically described as a real part of third order susceptibility $\chi^{(3)}$. Self-phase modulation (SPM) is when the intensity of signal modulates the refractive index and in turn its own phase. When the phase modulation occurs due to the intensity of other signal coexisting in the fiber with different wavelength, polarization, or direction of propagation, it is known as XPM. FWM is the nonlinear phenomenon when three waves at different frequencies, say ω_1, ω_2 and ω_3, but phase matched interact to generate a fourth wave $\omega_4 = \omega_4 + \omega_2 - \omega_3$. The phenomenon occurs when the chromatic dispersion is nearly zero, e.g. dispersion shifted fiber.

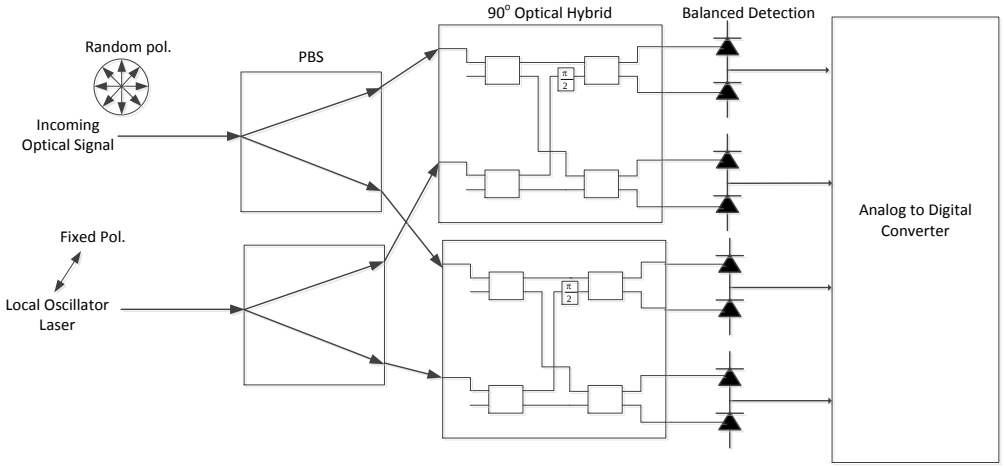

Figure 2.7: *Polarization and Phase Diversity Coherent Optical Receiver Front End.*

Stimulated Ramam Scattering (SRS) and Stimulated Brillouin Scattering (SBS) are stimulated inelastic scattering and are described by the imaginary part of the third order susceptibility $\chi^{(3)}$. In these stimulated scattering, the pump photon is absorbed to create a lower frequency photon and a phonon. In SRS an optical phonon is involved and it occurs in both backward and forward directions. While in SBS, acoustic phonon is involved and it occurs only in backward direction.

2.3 Receiver

The receiver of a coherent optical fiber communication system consist of an coherent detection front end, analog to digital convertor (ADC) followed by digital signal processing (DSP) and decoding.

2.3.1 Coherent Detection Front-end

The general configuration of the most commonly used coherent detection front end is the phase and polarization diversity homodyne [79] and [80] or intradyne receiver [81] as shown in Fig. 2.7. The phase diversity ensures simultaneous measurement of in-phase and quadrature components while so called intra-dyne measurement means that the intermediate frequency is not necessarily zero, the only requirement is that intermediate frequency (IF) needs to be less than the 1/symbol period.

The incoming signal with random polarization and the LO (with fixed polarization) are split into orthogonal x- and y-polarizations using two polarization beam splitter. The x-polarization components are then fed into the phase diversity receiver for x-polarization, and similar process is followed for the y-polarization. The phase diversity receiver consists of a 90^o degree optical hybrid followed by two balanced detectors. In the optical 90^o hybrid, both the signal and the LO are first split using a 180^o hybride, which is basically a 1:2 power splitter, which provides two signals with inverted amplitudes. One of the outputs from the LO power splitter is then phase shifted by 90^o. The two quadrature outputs of the LO is combined with the signal again using two 180^o hybrids which are 2:1 power combiners. The 180^o hybrids provide the sum and difference of the signals. The outputs of the entire 90^o hybrid are fed into balanced detectors. Each balanced detector consists of two square law photodetectors. The balanced detector cancels the common DC component. The output of one balanced detector provides the current proportional to the in-phase component of the signal into the receiver and the other provides the quadrature phase component. Detailed mathematical derivations for the coherent detection could be found in [82]. The retrieval of the original signal requires further signal processing such as correction of hybrid imperfections, de-multiplexing of polarizations, carrier phase recovery which are briefly described later in this chapter.

2.3.2 Analog to Digital Converter (ADC)

The ADC converts the electrical signal obtained after the coherent detection of the optical signal into a digital signal. The ADC is composed of two subsystems, i.e. a sampler and a quantizer. The sampler converts the time continuous analog signal to a time discrete analog signal while the quantizer discretize the amplitude of the signal into a finite number of levels, determined by the bit resolution of the ADC. Sampling in time domain results in repetition of the spectrum in frequency domain. Hence, according to Nyquist sampling theorem, the minimum sampling rate required to reconstruct a band-limited baseband signal to avoid aliasing is twice the maximum frequency of the signal [61]. In practical systems, there is a tradeoff between signal processing requirements, such as equalization, digital timing recovery etc., and the difficulty to design high speed ADCs for data rates used in such optical systems [61] and [83]. Sampling rate of $2/T_s$ for symbol duration of T_s is normally used [83].

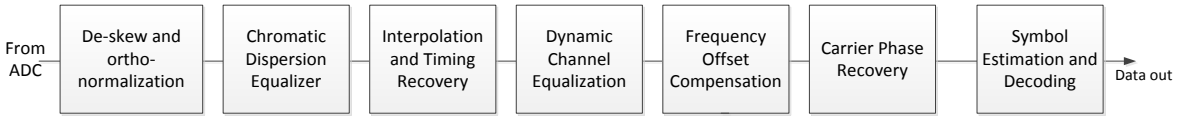

Figure 2.8: *Post Processing Digital Signal Processing Blocks.*

Quantization noise and the clipping of large signals are two signal degradation sources from the ADC. The amount of tolerable clipping is determined by the modulation format and pulse shaping filter used in the system. Quantization noise should be much lower than the front-end noise in a well-designed system. Automatic gain control (AGC) is used to maintain the signal levels so that it neither suffers from severe clipping, nor excessive quantization noise.

2.3.3 Digital Signal Processing

The digital signal processing blocks for a typical post-processing architecture are shown in Fig. 2.8. However, different configurations for performing the digital signal processing have been proposed and studied [84]. All proposed architectures are a subset of the 8 practicable DSP processing architectures analyzed in [84]. In this section we provide a brief overview of the purpose and functionality of the algorithms utilized in the DSP for a fiber channel without nonlinearities.

2.3.3.1 Deskew Algorithms

The digital signal might not be synchronized in time. One can either measure the timing mismatch or estimate it by cross correlating the signal. The skew is then compensated by the deskew algorithm [85]. The delay can be written as combination of sample delays and subsample delays. The integer sample delay is just a delayed version of the signal hence straightforward to implement while, in order to correct for subsample delay, interpolation is required.

2.3.3.2 Orthonormalization Algorithms

The orthonormalization algorithm is applied to recover the original signal after reception with a suboptimal hybrid. Gram-Schmidt and Löwdin orthogonalization are two different algorithms generally used for this purpose. Let the angle between the two received components due to hybrid imperfection be $\pi/2\text{-}2\theta$. In Gram-Schmidt method, the mutually orthogonal vectors are obtained by taking the first vector as reference and leaving it unchanged while rotating the second one by angle 2θ with respect to it [86]. The signal after orthogonalization is normalized to unity power

by multiplying the second vector by $\alpha = \sqrt{\langle r_2^2 \rangle - \langle r_1 r_2 \rangle / \langle r_1^2 \rangle}$ where $\langle r_i^2 \rangle$ is the mean power and i[th] vector and $\langle r_1 r_2 \rangle$ is mean cross power.

The Löwdin method achieves orthogonalization by creating a set of orthogonal vectors which are closest to the original vector in a least mean square sense [87]. The optimal choice of transformation matrix L for given correlation matrix R is $L=R^{-1/2}$ [88]. The Löwdin method rotates both vectors in opposite direction by θ, in contrast to the Gram-Schmidt process, which reduces the quantization noise and distributes the noise equally in both components.

2.3.3.3 Chromatic Dispersion Equalizer

Owing to the coherent nature of the optical system, there is a linear translation of the optical signal to the electric domain. Thus both amplitude and phase information is preserved and the pulse broadening due to the chromatic dispersion of the fiber can be compensated in the digital domain. In frequency domain the all-pass dispersion transfer function can be modelled as [89]

$$H_{fiber}(f) = e^{jkf^2} \tag{2.17}$$

In this equation, k is the accumulated dispersion given by $k = \pi \cdot D \cdot l \cdot c / f_0^2$ where, D is the dispersion coefficient, l is the fiber length, c is the speed of light and f_0 is the central optical frequency. Different time domain and frequency domain implementations of dispersion equalization have been studied in [28], [29] and [90].

2.3.3.4 Dynamic Channel Equalizer

After compensating for the static pulse broadening due to the fiber chromatic dispersion remaining inter-symbol interference (ISI) due to e.g. limited channel bandwidth can be equalized either by employing a static equalizer or a dynamic adaptive equalizer. The main target of the dynamic adaptive equalizer is to compensate for time varying linear impairments such as polarization mode dispersion (PMD) and State of Polarization (SOP). The adaptive equalizer may be realized using a multi input multi output (MIMO) equalizer using four finite impulse response (FIR) filters [91]. The MIMO filter performs the inverse Jones matrix of dynamic channel and the outputs are given by

$$x_{out}[k] = h_{xx}^{H}[k]\,x_{in}[k] + h_{xy}^{H}[k]\,y_{in}[k]$$
$$y_{out}[k] = h_{yy}^{H}[k]\,y_{in}[k] + h_{yx}^{H}[k]\,x_{in}[k] \quad (2.18)$$

Here, h_{xx}, h_{yy}, h_{xy}, h_{yy} are N tap filter with x_{in} and y_{in} represents the sliding block of N samples.

The algorithm could be training based or blind equalization. Blind equalization methods such as constant modulus algorithm (CMA) proposed by Godard [92] can be employed for single amplitude level constellations such as QPSK. In presence of phase noise, CMA enables equalization before carrier phase recovery since the cost function is based on the distance to the unity circle. Similarly, radially directed equalizer can be used for higher order constellations. The experimental demonstration of radially directed equalizer using CMA for pre-convergence was shown by Winzer et al. [93].

2.3.3.5 Interpolation and Timing Recovery

In order to achieve samples with optimal signal to noise ratio and phase representation, the timing error needs to be estimated and corrected by using a digital interpolator and a timing phase estimator (TPE). Interpolation could be based on approximation theory [94] using Lagrange polynomials or utilize spline based interpolation of the sampled signal [95]. Interpolation in DSP can be achieved through a two-step process. The first step is to up-sample the signal by stuffing it with zero valued samples to attain an increased sampling rate followed by low pass filtering. An ideal (Shannon) interpolation function [96] is a spline of infinite order. The efficient approximations to this ideal band-limited interpolation function are finite order splines such as linear and cubic splines. These splines can be implemented using FIR filters [97] and [98].

The various algorithms for both th non-data-aided [99] and data-aided [100] algorithms have been studied extensively for digital timing recovery [101]. The common non-data aided algorithms are square law of nonlinearity (SLN) method proposed by Oeder & Meyr [102], the Gardner method [99], the Godard method [103] and the Lee method [104]. The SLN requires at least three samples per symbol compared to others which require two samples per symbol. The performance of various blind timing phase estimators for digital coherent receivers was studied in [105].

2.3.3.6 Frequency Offset Compensation

After recovering the timing phase of the signal, the frequency offset between the transmitter laser and the LO laser needs to be compensated before carrier phase recovery. This can be achieved by either sending a training signal or performing blind frequency recovery. The former is less preferred as it reduces the achievable spectral efficiency (SE). A challenge of the blind frequency estimation is to find a method that works for an arbitrary modulation format. A considerable amount of efforts have been made to develop efficient frequency offset (FO) estimation for parallel high speed systems. These algorithms could be broadly classified into three categories. The first class of algorithms are based on the well-known M^{th} power algorithm to remove modulation [36] followed by FO estimation through time domain differential phase method or frequency domain FFT method. These algorithms are less efficient in higher order non-circular QAM modulation. Second set of methods which are scalable for higher order QAM are based on the Blind Frequency Search are proposed in [106]. In this method the carrier offset frequency is scanned over a given range and the FO which minimizes the Euclidean distance/ minimum phase cost function is chosen. The third category relies on training sequence for initial estimate and then uses the phase from the following a phase recovery unit to track FO change blindly [107].

2.3.3.7 Carrier Phase Recovery

After the frequency offset compensation, residual phase due to phase noise of the two lasers is estimated and compensated. The feedback phase recovery is not suitable for high speed coherent optical systems with parallel processing architecture. Thus, the most promising architecture is the feed forward carrier phase estimation and compensation. As the coherent optical communication moves towards higher order modulation formats, the tolerance to phase noise decreases. Hence, robust phase noise tolerant and yet low complexity CPR methods that are scalable to higher order modulation formats, are needed. As discussed in the introduction, the feed forward Viterbi & Viterbi (V&V) algorithm for carrier phase recovery, is a well known for n-PSK modulation formats such as QPSK. In this method, the received symbols are raised to the n^{th} power to remove the modulation information in order to obtain a phase noise estimate [36]. However, the V&V cannot be applied directly to higher order modulation such as square 16/64-QAM. Many modified algorithms such as QPSK partitioning and its multi-stage variants based

on V&V are proposed in [37], [38], [39] and [40]. These algorithms aimed at partioning and/or transforming a given constellation to QPSK points and then applying V&V algorithm. On the other hand, Blind Phase Search (BPS) algorithm for high order modulation was proposed in [41]. In this algorithm, the received symbols or constellation is rotated by discrete number of test phases in order to minimize the cost function such as the distance function. This method is both scalable and phase noise tolerant but has intensive computational complexity requirements. Since the CPR is one of the area of contributions of the thesis, more details are discussed in Chapter IV. Finally after carrier phase recovery, symbol estimation and decoding is performed.

Chapter 3

General Theory of Influence of Laser Frequency Noise in Coherent Optical Systems

As have been discussed in the previous chapters, coherent fiber optical communication systems together with high speed DSP provides the possibility to use multiple dimension of light wave together with electrical domain compensation of transmission impairments. Specifically, employing EDC provides many advantages such as enhanced tolerance to fiber nonlinearity and network flexibility. But it has been observed that this makes the system more susceptible to laser frequency noise, for instance, to LO frequency noise in systems with post reception DSP. This is because, even after post reception impairment processing, systems remain influenced by an enhanced noise commonly known as EEPN [49]. Impulse response method was utilized in the previous analyses to theoretically evaluate the problem and it was concluded that LO phase noise passing through the dispersion equalization was the origin of the EEPN. It is important to note that, apart from linear components, coherent optical systems consists of, non-linear components which works as multipliers such as photodetectors. This necessitates a stringent non-linear and time variant analysis due to the non-associative relation between multiplication and convolution operations.

In this chapter, we present and discuss the non-linear and time variant analysis of coherent optical systems for all practicable system configurations based on the findings in **Paper I** to

Paper VII. Section 3.1 describes the general system model used in the analysis and summarizes the practicable schemes for all electronic impairment mitigation. Section 3.2 provides the time and frequency domain analysis of these scheme for the Lorentzian line shape lasers i.e. lasers with white frequency noise. Parameters essential for system design are provided and discussed. Finally, the general theory of laser frequency noise in coherent fiber optical system applicable for lasers with any general frequency noise spectrum is presented in section 3.3. The theory provides criteria useful for system/laser design.

3.1 General System Model and Practicable Schemes Employing All-Electronic Impairment Mitigation

In this section, we discuss the general system configuration for coherent optical system and summarize the possible implementations of these systems with all-electronic impairment mitigation. A generalized system model is shown in Fig. 3.1. We consider, without loss of generality, a baseband equivalent representation of the system with power normalized representation of the components so that the net system gain remains unity independent of the transmitted constellation.

In general, in the electrical transmitter the incoming bit stream is translated into a band-limited complex electrical signal represented by Fourier transform pair $r_{elec}(t)\left|R_{elec}(f)\right.$. In some system configurations, in order to *a priori* compensate for the impairments such as channel chromatic dispersion and/or laser phase noise, the band-limited signal is pre-processed. This signal after pre-processing is modulated on the transmitting laser to generate the modulated optical signal. The stochastic base band equivalent representation of the transmitting laser *Tx* in terms of Fourier transform pair can be written as $e^{j\phi_{Tx}(t)}\left|X_{Tx}(f)\right.$. The output signal is then transmitted over an all-pass dispersive fiber with the response $h_f(t)\left|e^{jkf^2}\right.$ considering only the second order dispersion and neglecting higher order dispersion terms. The accumulated dispersion factor is given by $k = 2\cdot\pi^2\cdot\beta_2\cdot l = \pi\cdot D\cdot l\cdot c\cdot f_0^{-2}$. The signal at the receiver end is then coherently detected with a local oscillator (LO) laser represented by a stochastic base band equivalent response $e^{j\phi_{LO}(t)}\left|X_{LO}(f)\right.$.

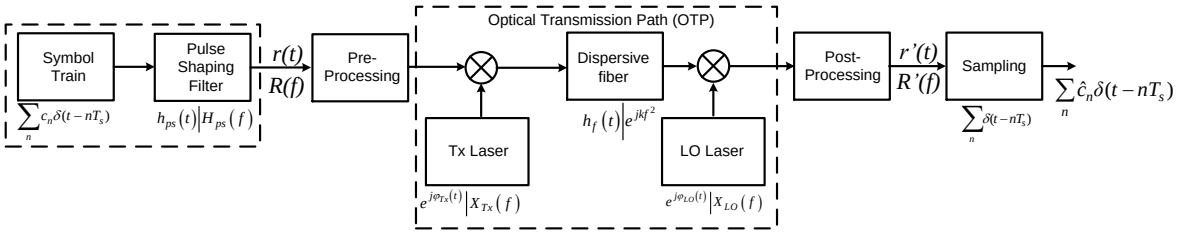

Figure 3.1: *Generalized system model of coherent optical system with electronic dispersion compensation. The Fourier transform pairs of the signal and the response of components are indicated.*

The modulation on the Tx laser, transmission over the fiber link and coherent detection with LO laser together make up the Optical Transmission Path (OTP). The residual impairments, which are not pre-mitigated on the transmitter side, are mitigated by post processing the coherently detected signal. The post-processed signal is given by the Fourier transform pair $r'(t)\left|R'(f)\right.$. A post-processing module might also involve the matched filtering operation to improve the signal quality in the presence AWGN noise. However, linear filtering has negligible impact on laser frequency noise induced EEPN which is the main focus of this analysis, as shown in [50], [84] and [108]. The reason of negligible impact is that EEPN has a spectrum almost identical to the signal spectrum which will also be shown in the course of this analysis. Hence we will omit the match filtering operation, without compromising stringency of the analysis. Furthermore, ideally, sampling and then performing CPR is equivalent to performing CPR followed by sampling operation as sampling is a memory less operation. Under the assumption of ideal compensation, the mitigation operations are modeled as the inverse of the impairment source. Thus, the Fourier transform pairs for EDC and CPR can be written as $h_f^{inv}(t)\left|e^{-jkf^2}\right.$ and $e^{j\phi_{Laser}^{CPR}(t)}\left|X_{Laser}^{CPR}(f)\right.$ respectively. "Laser" here represents Tx, LO or a combined recovery for both Tx and LO represented by *Tx+LO*.

In the case of systems utilizing complex high order QAM modulation formats, a symbol train at the rate of R_b/m, by mapping the incoming bits at rate R_b onto a symmetrically distributed symbols with m bits per symbol, is generated. This is followed by pulse shaping in order to generate a band-limited continuous signal given by $r_{elec}(t)=\sum_n c_n h_{ps}(t-nT_s)$ where

$h_{ps}(t) \Big| H_{ps}(f)$ is the Fourier transform pair of the pulse-shaping filter as in the system model illustrated in Fig. 3.1.

More than one system configuration can be a viable option due to the possibility of performing both pre- and post-processing of the signal. A large number of possibilities can be conceptualized by permuting the order and position (pre and/or post) of three mitigation operations which are equalization of the fiber CD, CPR for Tx and CPR for LO. Thus making it imperative to ascertain the practically implementable configurations out of these large number of possibilities. All the possible configuration schemes for all impairment mitigation together with a detailed analysis for each of the schemes and its influence on the EEPN phenomena can be found in **Paper VII** [84] and the summary of the results is provided Table 3.1 below.

Table 3.1: All Practicable Schemes for Electronic Impairment Mitigation in Coherent Optical Systems

Scheme	Processing Order Relative to OTP	References
Scheme 1	OTP→EDC→CPR_{LO+Tx}	[83]
Scheme 2	OTP→CPR_{LO+Tx}→EDC	[53], [54]
Scheme 3	OTP→CPR_{LO}→EDC→CPR_{Tx}	[109], [110] and [111]
Scheme 4	CPR_{Tx}→ OTP→EDC→CPR_{LO}	[109], [110] and [111]
Scheme 5	CPR_{Tx}→ OTP→CPR_{LO}→EDC	[109], [110] and [111]
Scheme 6	EDC→ OTP→CPR_{LO+Tx}	[52]
Scheme 7	EDC→CPR_{Tx}→ OTP→CPR_{LO}	[109], [110] and [111]
Scheme 8	CPR_{Tx}→EDC→ OTP→CPR_{LO}	[109], [110] and [111]

Note: OTP: Optical Transmission Path, CPR: Carrier Phase Recovery, EDC: Electronic Dispersion Compensation

3.2 Analysis and Design of Systems utilizing Lasers with White Frequency Noise Spectrum

In semiconductor lasers, neglecting the internal laser dynamics, the intrinsic frequency noise of the laser can be attributed to the spontaneous emission induced perturbation of the optical signal phase. This intrinsic frequency noise is white, proportional to the spontaneous emission and yields a Lorentzian linewidth. This linewidth is independent of the time of observation. The stochastic baseband equivalent response then can be written in terms of stochastic baseband equivalent transform of the spontaneous emission $\hat{e}_{sp}(f)$ as

$$X(f)=\frac{\hat{e}_{sp}(f)}{j(2\pi f)+\frac{\Delta\gamma}{2}} \tag{3.1}$$

The assumption that the laser just has intrinsic white frequency noise reduces the complexity of the system analysis, as the white noise is a wide sense stationary process. In this case, the interaction between the signal and the laser with the white frequency noise can be modeled in the frequency domain as the convolution of the stochastic Fourier transform train of symbol pulses with the stochastic Fourier transform the laser output assuming a given realization. The statistical properties can then be derived by calculating the required statistical moment over different realization. Next in this section, we discuss briefly the analysis, statistical properties and the parameters essential for system design detailed in **Paper I** to **Paper IV** and **Paper VII** using the most common system configuration. The analysis for other configurations is provided in [84] and is summarized in Table 3.2. Scheme 1 in Table 3.1 corresponds to the most commonly used realization of Fig. 3.1 in which impairment mitigation is performed post processing. The post processing block consists of EDC followed by combined CPR for Tx and LO. In this case, the frequency domain response of the received signal can be written as

$$R'(f)=\left[\int_{-\infty}^{\infty}\hat{R}(f-f_1)\cdot e^{jk\left(f_1^2-2ff_1\right)}\cdot X_{LO}(f_1)\cdot df_1\right]\otimes \hat{X}_{Tx+LO}^{CPE}(f). \tag{3.2}$$

The compensation of the linear accumulated dispersion e^{jkf^2} by the linear channel equalizer e^{-jkf^2} is revealed by the frequency domain analysis. The analysis also indicates that the intermixing, in the intensity sensitive photodetector, of the side bands of the dispersed signal and the LO output are not compensated by the linear equalizer resulting in a noise enhancement. Replacing $X_{LO}(f)$ by its frequency response given by eq. (3.1) in eq. (3.2) can be rewritten as

$$R'(f)=\left[\int_{-f_{cutoff}}^{f_{cutoff}}\hat{R}(f-f_1)\cdot e^{jk\left(f_1^2-2ff_1\right)}\cdot\left(\frac{\hat{e}_{sp}(f_1)}{j2\pi f_1+\frac{\Delta\gamma}{2}}\right)\cdot df_1\right]\otimes \hat{X}_{Tx+LO}^{CPE}(f). \tag{3.3}$$

The influence of nearby signal frequencies on a given frequency within the integral in eq. (3.3) is weighted by a factor $\left(j(2\pi f_1)+\Delta\gamma/2\right)^{-1}$. The contribution to EEPN is governed by

this factor for systems in which symbol rate and the integration limit f_{cutoff} are much larger than the linewidth. Based on the certain criterion, such as tolerable system penalty, the cutoff frequency can be defined as the frequency beyond which the contribution from the spontaneous emission to EEPN, and therefore LO frequency noise, can be neglected. Thus suppressing frequencies below this frequency cutoff can efficiently mitigate the impact of EEPN. The above analysis also indicates that the cutoff frequency depends on the laser linewidth and is virtually independent of the symbol rate or accumulated dispersion. The validation of this analysis through numerical simulations using 28 Gbaud QPSK and 16-QAM transmissions was carried out in **Paper I** [112]. The experimental validation of the outcome of the analysis was carried out in **Paper II** employing a 28 Gbaud 16-QAM signal transmission over 523 km SSMF fiber and is shown in Fig. 3.2.

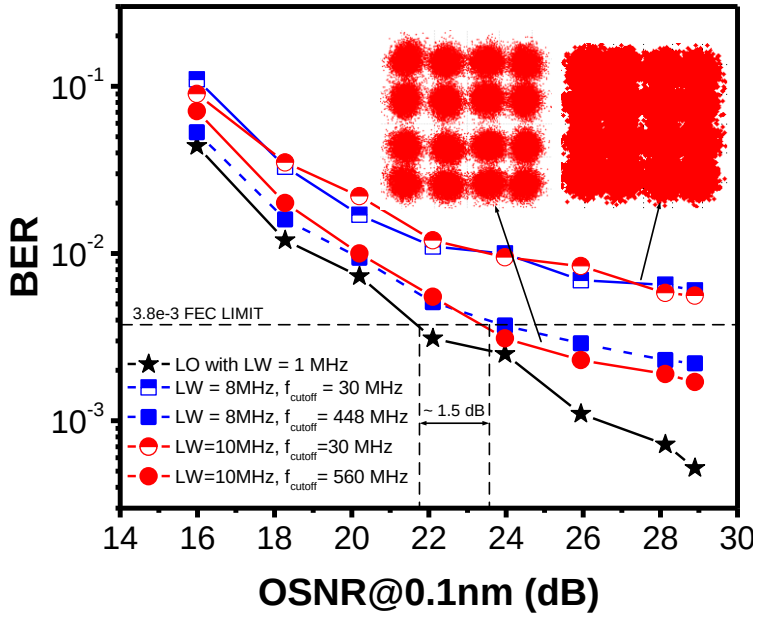

Figure 3.2: *BER versus OSNR performance for different laser linewidth for transmission over 523 km of fiber link.*

The time domain response of the received signal is given by the inverse Fourier transform (IFT) of eq. (3.2) as,

$$r'(t)=\left[\int_{-\infty}^{\infty} X_{LO}(f_1)\cdot e^{-jkf_1^2}\cdot e^{j2\pi f_1 t}\cdot r_{elec}\left(t-\frac{kf_1}{\pi}\right)\cdot e^{j\varphi_{Tx}\left(t-\frac{kf_1}{\pi}\right)}df_1\right]\cdot e^{j\varphi_{Tx+LO}^{CPR}(t)}. \qquad (3.4)$$

The term $X_{LO}(f_1)\cdot e^{-jkf_1^2}$ in eq. (3.4) shows that the LO laser is indeed dispersed by the equalizer. But this phenomenon, i.e. phase to amplitude conversion due to the LO passing through the equalizer is not the main cause of the noise enhancement known as EEPN. This is because it is theoretically possible to compensate for this dispersion of LO by equalizer, by pre-dispersing the LO before combining it with the received signal, but it does not compensate for EEPN. Also in a statistical view, each component of the LO sideband demodulates a delayed version of the transmitted signal $r_{elec}(t)$ and the delay is proportional to its frequency component relative to central frequency (zero in the base band equivalent case). The EEPN, thus in this perspective, can be seen to be caused due to interference of multiple delayed versions of the original signal with itself. The EEPN spectrum, as confirmed by eq. (3.2), is almost identical to the signal spectrum as the broadening due to the laser linewidth is negligible compared to the signal baudrate. Thus, linear filtering cannot mitigate EEPN [50] and [108]. Further, in case of systems employing ideal optical dispersion compensation, the accumulated dispersion *k* is then zero and eq. (3.4) reduces to the equation for back to back transmission without EEPN. In case of digital QAM modulations, the received signal is given as

$$r'(t)=\sum_{n=-\infty}^{\infty}c_n\int_{-\infty}^{\infty}X_{LO}(f_1)\cdot h_{ps}\left(t-nT_s-\frac{kf_1}{\pi}\right)\cdot e^{-jkf_1^2}\cdot e^{j\varphi_{Tx}\left(t-\frac{kf_1}{\pi}\right)}\cdot e^{j\varphi_{Tx+LO}^{CPR}(t)}\cdot e^{j2\pi f_1 t}df_1. \quad (3.5)$$

The statistical analysis of the received signal impaired by EEPN is then performed by following the steps detailed in [108]. The statistical analysis reveals that the signal impaired by EEPN is zero mean and the variance is given by,

$$\sigma_{r'(t)}^2=\int_{-\infty}^{\infty}E\left[\left|r_{elec}\left(t-\frac{kf}{\pi}\right)\right|^2\right]\cdot E\left[\left|X_{LO}(f)\right|^2\right]\cdot df. \quad (3.6)$$

For LO laser with Lorentzian line shape eq. (26) can be rewritten as,

$$\sigma_{r'(t)}^2=\int_{-\infty}^{\infty}E\left[\left|r_{elec}\left(t-\frac{kf}{\pi}\right)\right|^2\right]\cdot\frac{r_{sp}}{f^2+\left(\frac{LW}{2}\right)^2}\cdot df. \quad (3.7)$$

It is interesting to note that there is a one to one correspondence between the multipath influenced signal in wireless communication [113] and the terms in eq. (3.7). The term r_{sp}

corresponds to the path gain due to reflection from the surface in wireless communication, the denominator in the integral corresponds to the free space path loss and the term $E\left[\left|r_{elec}\left(t-\frac{kf}{\pi}\right)\right|^2\right]$ corresponds to the delayed version of the signal. This correspondence assist us to adopt the approximations used to analyze multipath influenced signal in wireless, for instance, due to central theorem, the probability density function (PDF) can be approximated to Gaussian distributed. Hence mean and variance becomes sufficient to characterize EEPN in coherent optical systems. For digital QAM modulations the variance and EVM which is defined as the ratio of noise variance to average ideal constellation power is given by

$$\sigma^2_{r'(t)} = E\left[\left|c_n\right|^2\right]\sum_{n=-\infty}^{\infty}\int_{-\infty}^{\infty}\left|h_{ps}\left(t-nT_s-\frac{kf}{\pi}\right)\right|^2\cdot S_{LO}(f)\cdot df. \tag{3.8}$$

$$EVM^2 = \left\{\sum_{n=-\infty}^{\infty}\int_{-\infty}^{\infty}\left|h_{ps}\left(t-nT_s-\frac{kf}{\pi}\right)\right|^2\cdot S_{LO}(f)\cdot df\right\}-1. \tag{3.9}$$

Eq. (3.8) contains contributions both from EEPN and ISI originating due to a general band-limited pulse shaping. However, in case of family of pulse shaping filter which provide zero ISI at optimal sampling point EVM^2 in eq. (3.9) is due to EEPN only. The corresponding analyses for all the rest possible system configurations are performed in Paper VII. Paper VII reveals that there exist in principle three configurations, which do not result in EEPN phenomena. Furthermore, it is shown the equivalence of the EEPN statistical properties to that derived in this section.

Table 3.2: Look-up Table Useful for System Design For All Practicable Schemes of Coherent Optical Systems with EDC

Scheme (see Table 3.1)	**Source of EEPN**	**Required Design Parameter**
Scheme 1	LO	Tolerable Linewidth
Scheme 2	Tx	Tolerable Linewidth
Scheme 3	N/A	Mitigation Bandwidth
Scheme 4	LO	Tolerable Linewidth
Scheme 5	N/A	Mitigation Bandwidth
Scheme 6	Tx	Tolerable Linewidth
Scheme 7	N/A	Mitigation Bandwidth
Scheme 8	Tx	Tolerable Linewidth

Note: N/A stands for Not Applicable

3.2.1 System Design Aspects

Now the parameters essential for system design, with and without EEPN mitigation, can be derived from the analysis performed in the previous section. In the design of a system not involving any EEPN mitigation technique, it is essential to know the tolerable linewidth or the penalty due to lasers with certain linewidth. While for systems employing mitigation technique, the required mitigation bandwidth to limit system penalty below a certain limit is of essence.

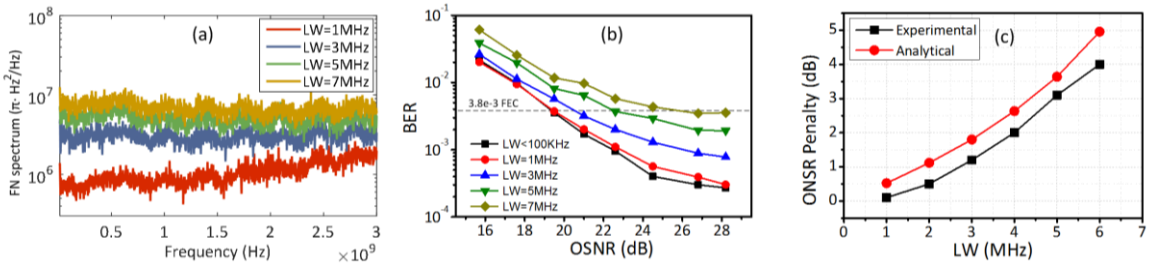

Figure 3.3: (a) FN-PSD of the LO laser after phase modulation for different linewidths, (b) BER vs. OSNR for 28 Gbd 16-QAM after 520 km of fiber and different LO linewidths (c) OSNR penalty (@ FEC limit=3.8e-3) vs. LO linewidth both experimental and analytical given by eq. (28).

As was shown in [108], for systems with Nyquist pulse shaping and Lorentzian lineshape laser and any modulation format, the square of the error vector magnitude for the configurations resulting in EEPN, is given by

$$EVM_{EEPN}^2 = \pi^2 \cdot |\beta_2| \cdot L \cdot Baudrate \cdot LW \tag{3.10}$$

in this equation, LW corresponds to the linewidth of the laser resulting in EEPN in a given scheme, *Baudrate* is the symbol rate, L is the equivalent of fiber for which the accumulated dispersion is compensated. Thus the baudrate-length product is limited by EEPN and makes it dependent of laser linewidth and accumulated dispersion. The tolerable linewidth for a given system specification as derived in [108] is given by

$$Tolerable\ Linewidth = \frac{1-10^{\frac{-p}{10}}}{\pi^2 \cdot |\beta_2| \cdot L \cdot Baudrate \cdot OSNR_{ref\_inband}} \tag{3.11}$$

where, p is the tolerable system penalty and $OSNR_{ref\_inband}$ is the in-band reference OSNR to achieve a certain BER for a given modulation format and system configuration. Similarly, the mitigation bandwidth (cutoff frequency f_{cutoff}, discussed in previous section) as derived in [108] is given by

$$Mitigation\ Bandwidth = LW \cdot \tan\left(\frac{\pi}{2}\left[1-\frac{1-10^{-\frac{p}{10}}}{OSNR_{ref\_inband}}\right]\right) \tag{3.12}$$

relating to EEPN that is essential for the system designer to make an informed choice regarding practicable configuration and its design is summarized as a simple look up table in Table 3.2. The identification code of a given scheme is provided in the first column of Table 3.2. The source of EEPN in a given configuration, if any, is provided in the second column. Column three provides the variance of the received signal influenced by EEPN. Finally, the required parameter in order to design the system with given digital impairment processing configuration is stated in the last column. The validation of the system design parameters using numerical simulations was reported in **Paper III** [108]**.** While the experimental validation of these system design parameters along with the detailed description of experimental setup was reported in **Paper IV** [114]. Fig 3.3 provides the experimental validation of eq. (3.11) with a transmission of a 28 Gbaud 16-QAM signal transmission over ~520 km of SSMF. The FN-PSD of the LO laser after phase modulation for different linewidths is shown in Fig. 3.3 a). The BER versus OSNR performance after reception with this LO for different linewidths is shown in Fig. 3.3 b) and finally the validation of analytical estimation using eq. (3.11) with the experimentally obtained penalty is illustrated in Fig. 3.3 c). The slight offset of about 0.5 dB is observed which is attributed to two reasons, first the experimental results employ rectangular pulse shaping while the analytical estimation assumes Nyquist pulse shaping. Secondly, due to hardware limitations of the AWG to generate frequency noise less than 15 MHz. Similarly, the experimental validation of eq. (3.12) is provided in Fig. 3.4. Fig. 3.4 a) depicts the high pass filtered FN-PSD of LO laser with 8 MHz white frequency noise level for different cut-off frequency f_{cutoff} Fig. 3.4 b) shows the impact of high-pass filtering with different cut-off frequencies on BER versus OSNR performance. Finally,

the analytical estimation of the penalty as function of cut-off frequency, using eq. (3.12) compared to experimentally achieved results is shown in Fig. 3.4 c).

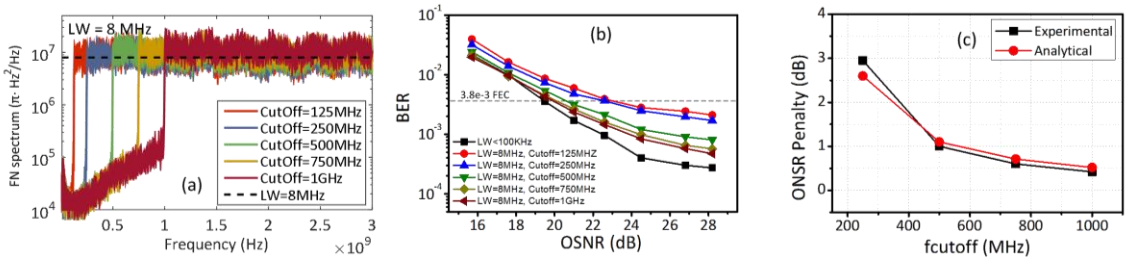

Figure 3.4: (a) High Pass filtered FN-PSD of the 8 MHz LO laser for different cut-offs, (b) BER vs. OSNR for 28 Gbd 16-QAM after 520 km of fiber and 8 MHz LO laser with different cut-off frequencies (c) OSNR penalty (@ FEC limit=3.8e-3) vs. cut-off frequency experimental versus analytical given by eq. (29).

3.3 Theory for Coherent Optical Systems utilizing laser with general non-white frequency noise spectrum

In the previous section, we have analyzed coherent fiber optical systems assuming that the employed lasers have only white frequency noise. However, lasers in general have a non-white frequency noise spectrum due to the presence of 1/f noise and carrier induced noise, as discussed in Chapter 2. The analysis for the lasers with a realistic non-white frequency noise spectrum remains elusive and a statistical analysis is no longer sufficient. Even for the case of white frequency after performing the statistical analysis, many questions remain unanswered. For instance, why the Nyquist pulse shaping is more sensitive to EEPN as compared to rectangular pulse shaping which has higher bandwidth compared to Nyquist. Thus, a more in-depth analysis compared to the previously provided statistical analysis is needed to understand the EEPN origin and provide the criteria relevant for efficient system/laser design in presence of realistic non-white frequency noise spectrum. In this section, we provide the experimentally validated theory of coherent fiber optical systems utilizing a general laser with non-white frequency noise spectrum as discussed in **Paper V** [115].

The temporal phase evolution of a laser output and hence its instantaneous frequency is given by $\phi(t)$ and $f(t)=(1/2\pi)\cdot d\phi/dt$ respectively. Then the phase evolution and instantaneous frequency evolution function over the observation period τ around the time instant t_0 can be written as

$$\phi_\tau(t') = \phi(t') \text{ and } f_\tau(t') = f(t') \;\; t' \in \left[t_0 - \frac{\tau}{2}, t_0 + \frac{\tau}{2} \right] \tag{3.13}$$

The phase evolution over observation period τ in eq. (3.13) can rewritten in terms of mean frequency over this observation period $f_{\tau,mean}(t_0) = E_\tau\left[f_\tau(t') \right]$ as

$$\phi_\tau(t') = 2\pi f_{\tau,mean}(t_0) t' + \phi_\tau^{res}(t') \;\; t' \in \left[t_0 - \frac{\tau}{2}, t_0 + \frac{\tau}{2} \right] \tag{3.14}$$

where, $E_\tau[]$ is the mean operator over the observation period and the residual phase around the phase given by mean frequency is $\phi_\tau^{res}(t')$. All fluctuations slower than $1/\tau$ are contained in $f_{\tau,mean}(t_0)$ and the residual phase contains all fluctuations faster than $1/\tau$ and is zero mean, during the observation period. The laser output, assuming no amplitude fluctuation noise, over the observation period around time instant t_0 is given by

$$x_\tau(t') = Ae^{j\phi_\tau(t')} = Ae^{j\left\{2\pi f_{\tau,mean}(t_0)t' + \phi_\tau^{res}(t')\right\}} \;\; t' \in \left[t_0 - \frac{\tau}{2}, t_0 + \frac{\tau}{2} \right] \tag{3.15}$$

The frequency response over the observation period can then be written as

$$X_\tau(f, t_0) = A\delta\left(f - f_{\tau,mean}(t_0) \right) \otimes X_\tau^{res}(f, t_0) = AX_\tau^{res}\left(f - f_{\tau,mean}(t_0), t_0 \right) \tag{3.16}$$

where, the Fourier transform of the laser output due to fluctuations faster than *1/τ* is given by $X_{\tau}^{res}(f,t_0)$.

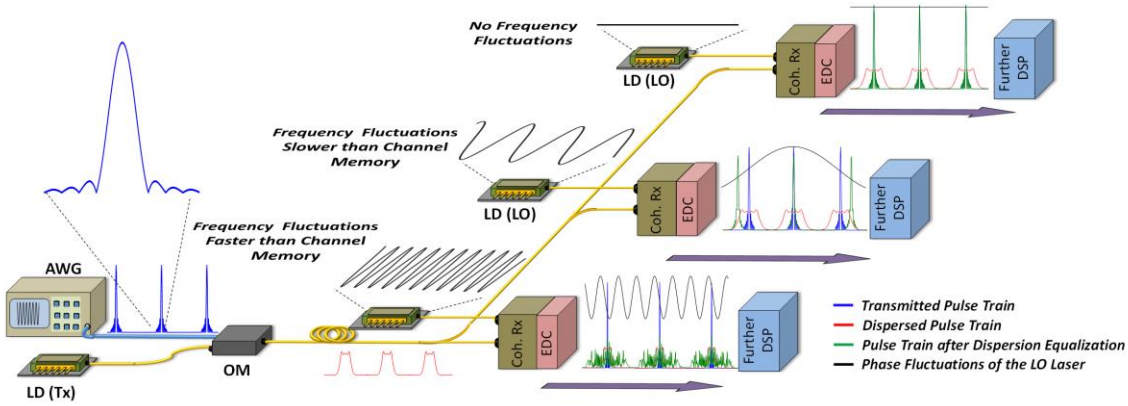

Figure 3.5: Qualitative representation of the phenomenon. The envelop of On-Off keying encoded pulse train of Nyquist pulses after the electrical transmitter is shown in blue. The dispersed pulse train after optical modulation and transmission over fiber is shown in red. The phase of the LO laser is shown in black. The received pulse train envelope after EDC is shown in green superimposed with the transmitted and dispersed pulse train neglecting the latency of the fiber. AWG: Arbitrary Waveform Generator, LD (Tx): Laser Diode (Transmitter), OM: Optical Modulator, LD (LO): Laser Diode (Local Oscillator), Coh. Rx.: Coherent Receiver, EDC: Electronic Dispersion Compensation, DSP: Digital Signal Processing.

In the context of coherent fiber optical communication links with EDC the above discussion and the representation of laser output becomes important. At first, the most common configuration given by Scheme 1 in Table 3.1 will be considered for the developing the general theory. The results from this exercise will then be utilized to draw conclusions for other schemes.

For the system model described in Fig. 3.5 with impairment processing in the order given by Scheme 1, the time domain response utilizing eq.(3.16) and steps detailed in [108] for the band limited electrical signal $r_{elec}(t)=\sum_n r_{pulse}^n(t)$ composed of pulses $r_{pulse}^n(t)$, after the EDC is then given by

$$r'(t)=\sum_n \int_{-\infty}^{\infty} r_{pulse}^n\left(t-\frac{kf'}{\pi}-\frac{kf_{\tau,mean}[n]}{\pi}\right) X_{\tau,LO}^{res,n}(f')\cdot e^{j\phi_{Tx}\left(t-\frac{kf'}{\pi}-\frac{kf_{\tau,mean}[n]}{\pi}\right)}\cdot e^{jk\left\{f'^2+f_{\tau,mean}^2[n]+2f'f_{\tau,mean}[n]\right\}}\cdot e^{j2\pi\left(f't+f_{\tau,mean}[n]t\right)}df' \tag{3.17}$$

where, $X_{\tau,LO}^{res}(f)$ is the LO laser frequency response due to the residual fluctuations around the mean $f_{\tau,\text{mean}}$ over the observation period. The observation period in context of such systems is the broadening of the signal, seen by the LO laser, after the dispersive fiber, commonly known as the channel memory. In this system configuration, no dispersion induced pulse broadening is

seen by the Tx laser, and therefore the frequency noise of the Tx laser only causes phase noise impairment. Similarly, in the special case of ideal optical dispersion compensation where the accumulated dispersion factor k=0, the LO phase noise observed by the symbols is equal to the symbol period- Thus, the LO frequency noise also appears only as phase noise impairment. Consider the case of systems utilizing digital QAM modulation, eq. (61) can be rewritten as

$$r'(t)=\sum_{n}\int_{-\infty}^{\infty}c_n\cdot h_{ps}\left(t-nT_s-\frac{kf'}{\pi}-\frac{kf_{\tau,mean}[n]}{\pi}\right)X_{\tau,LO}^{res,n}(f')\cdot e^{j\phi_{Tx}\left(t-\frac{kf'}{\pi}-\frac{kf_{\tau,mean}[n]}{\pi}\right)}\cdot e^{jk\left\{f'^2+f_{\tau,mean}^2[n]+2f'f_{\tau,mean}[n]\right\}}\cdot e^{j2\pi\left(f't+f_{\tau,mean}[n]t\right)}df' \tag{3.18}$$

by plugging in $r_{elec}(t)=\sum_n c_n h_{ps}(t-nT_s)$. For Nyquist pulse shaped signal with a given *Rolloff* can approximately be written as $\tau_{CM}\approx\left(k\cdot Baudrate\cdot\{1+Rolloff\}\right)/\pi$ [89]. Fig. 3.5 qualitatively depicts the implications of eq. (3.17) and (3.18) and the accompanying discussion using envelop evolution of an on-off encoded train of Nyquist pulses with Rolloff=0.15. The Tx laser is modulated with a train of Nyquist pulse generated (shown in blue) by the electrical transmitter. The pulses suffer dispersion induced broadening depicted in red after transmission over dispersive fiber. The impact of the frequency noise of the LO is then illustrated by considering the coherent detection of the dispersed signal (shown in red) with three different LO lasers having different sinusoidal frequency fluctuations (for depiction purpose). In the first case, the pulse train (shown in green) is completely recovered overlapping the transmitted pulse train (the latency due to fiber transmission is neglected) after coherent detection, of the transmitted pulse train, with a laser with no frequency fluctuations (depicted by zero phase evolution in black). In the second case, each pulse in the train is delayed by the observed delay given by $\Delta\tau_{mean}=\frac{kf_{\tau,mean}}{\pi}$ in eq. (3.17-3.18) after coherent detection with a LO laser having frequency fluctuations slower than channel memory. Positive or negative delay proportional to the slope of the phase modulation (and hence the mean frequency over the observation time) is seen by the side pulses while the central pulse suffers almost no delay. In the last case, multiple delayed versions of the pulse are demodulated by fluctuations faster than τ_{CM}^{-1} as could be seen from eq (3.17-3.18). These delayed versions interfere to cause inter and intra symbol interference.

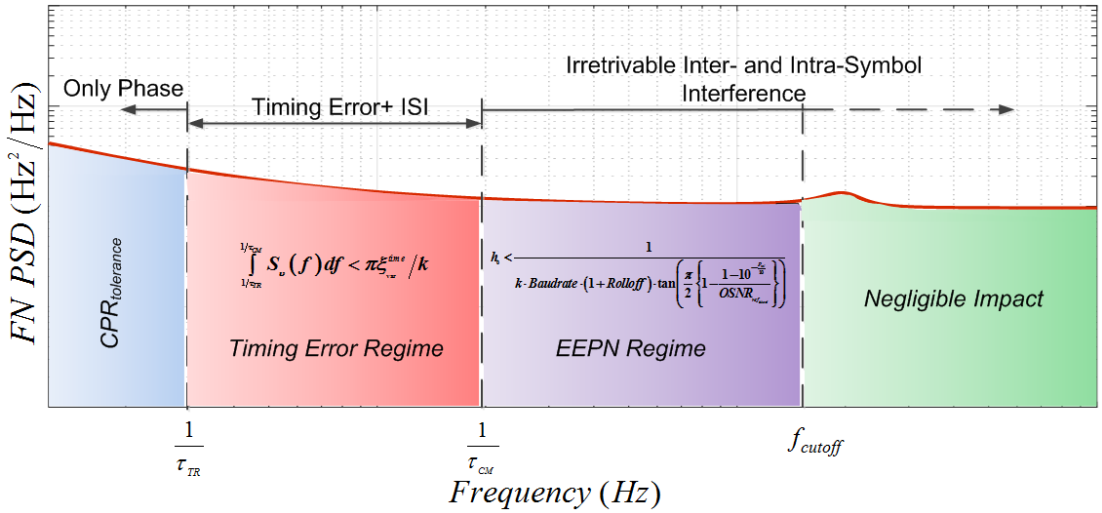

Figure 3.6: Regime segmentation of frequency noise spectrum. $\mathrm{CPR}_{\mathrm{tolerance}}$*: Carrier Phase Recovery tolerance,* $1/\tau_{\mathrm{TR}}$ *: Timing Recovery Bandwidth,* τ_{CM}*: Dispersion Channel Memory,* $\mathrm{f}_{\mathrm{cutoff}}$*: Cut off frequency.*

All symbols thus statistically observe the same amount of modulation. In reality both timing drift, timing jitter and inter and intra symbol interference will be present as the frequency fluctuations faster and slower than CM co-exist. The maximum timing fluctuation $\Delta\tau_{mean}[n]-\Delta\tau_{mean}[0]$ between the present (0^{th}) and the n^{th} symbol will be caused by a FN spectral component at $1/(\tau_{CM}+nT_s/2)$. This phenomenon also results in inter-symbol interference as the timing drift is not due to the sampling clock but due to movement of symbol. This timing drift converts into timing jitter and finally into irretrievable intra and inter symbol interference with the increase in speed of fluctuation of the carrier frequency above the channel memory. Fig. 3.6 illustrates various regimes of the frequency noise spectrum. In each regime, either optimization of corresponding DSP algorithms can improve the performance or the relevant criteria in terms of single sided frequency noise spectrum $S_\upsilon(f)$ .needs to be fulfilled, for optimal system design.

For the frequency noise regime $f<1/\tau_{TR}$ where $1/\tau_{TR}$ is the timing recovery bandwidth, the dominant impairment is the phase impairment, as ideally, the timing recovery algorithms tracks and compensates for any timing fluctuation slower than the timing recovery bandwidth. The frequency noise spectrum should meet the following criteria for a given CPR algorithm phase tolerance $CPR_{tolerance}$

$$\int_{0}^{1/\tau_{TR}} S_{\upsilon}(f)\,df < CPR_{Tolerance} \tag{3.19}$$

For the frequency noise regime $1/\tau_{TR} < f < 1/\tau_{CM}$, along with the carrier phase recovery algorithm the adaptive filter design and the bandwidth of the timing recovery algorithm can be optimized to minimize the impairment. Alternatively, the following criteria in terms of tolerable timing error variance $\varepsilon_{\text{variance}}$ is satisfied while designing the system

$$\int_{1/\tau_{TR}}^{1/\tau_{CM}} S_{\upsilon}(f)\,df < \pi\varepsilon_{\text{variance}}/k \tag{3.20}$$

No DSP optimization exists to minimize the impact of the frequency noise in the regime $f > 1/\tau_{CM}$., as irretrievable inter and intra-symbol interference is caused by the frequency noise in this regime. In order to improve the performance one either needs to choose a laser meeting the criteria below,

$$h_0 < \frac{1}{k \cdot Baudrate \cdot (1+Rolloff) \cdot \tan\left(\frac{\pi}{2}\left\{1-\frac{1-10^{-\frac{P_{tol}}{10}}}{OSNR_{ref_{inband}}}\right\}\right)} \tag{3.21}$$

or mitigate the frequency noise using hardware based techniques. In this equation the maximum tolerable white frequency noise level above the channel memory is given by h_0 in order to limit the system penalty below P_{tol} (dB) as was derived and experimentally validated in [108] and [114]. The weighting factor $X_{\tau,LO}^{res}(f)$ in equation (3.17-3.18) falls off inversely proportional to frequency f as was shown in eq. (3.7). Thus, the impact of frequency noise above the upper cut-off frequency f_{cutoff} can be neglected. Based on the understanding developed in this section, the dispersion induced broadening seen by each laser before broadening compensation decides the regimes and the corresponding design criteria. In the previous section, laser source which causes the noise enhancement in any given scheme and equivalence of these scheme in terms of design requirements was ascertained. Thus, results obtained here are generic and applicable to other schemes as well.

Timing jitter tolerance is defined in terms of sinusoidal jitter whose amplitude, when applied to an equipment input, causes a designated degradation in error performance [116] [117]. Numerical simulation to validate the above analysis was reported in **Paper V** [115].

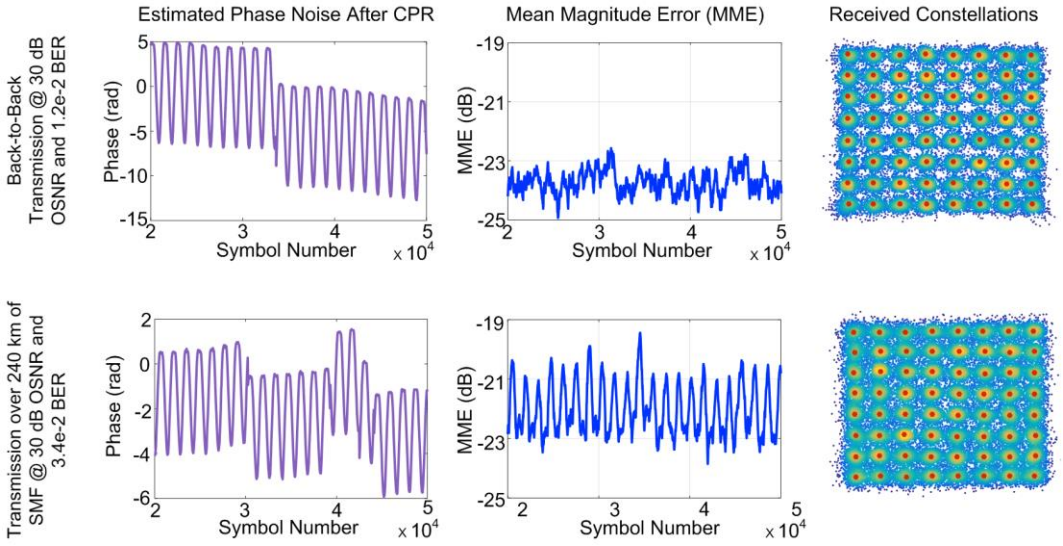

Figure 3.7: (a) Estimated phase noise in violet, mean magnitude error in blue and the received constellation (from left to right) for 28 Gbaud 64-QAM signal for back to back and after transmission over ~250 km of SMF fiber.

Experimental validation of the above analysis was carried out using the experimental set-up described in [115] and [118]. 28 Gbaud 16 and 64-QAM signals transmission over ~520 km and ~250 km respectively were utilized for the analysis. Fig. 3.7 depicts the qualitative analysis in terms of recovered phase after CPR, MME and the received constellation.

The analysis compares the impact of fiber transmission to the back-to-back transmission case. Conforming to the simulations, it could be seen that while the sinusoidal phase modulation have no impact on MME, it causes periodic variations after fiber transmission due to timing error.

The period of variation in MME is same as that of phase modulation due to asymmetry in the modulated phase. An experimental validation of the analytically derived regimes and the peak relative delay parameter is depicted in Fig. 3.8. Fig. 3.8(a) depicts BER versus Peak Relative Delay at 20 MHz modulation frequency for LO frequency modulation amplitude as well as equivalent artificially induced sinusoidal timing error.

The results validates the theoretical results that the LO phase modulation results in a timing error in coherent optical links utilizing EDC with a relative peak delay i.e. $\Delta\tau_{mean}^{peak} = kf_{\tau,mean}^{peak} / \pi T_s$. Fig. 3.8 b) depicts the impact of LO phase modulation frequency on system MME for 16 and 64-QAM transmission links. The analysis is performed for the relative peak delay of 0.11 and 0.06 respectively at 30 dB of OSNR. In the case of 28 Gbaud 16-QAM signal transmission over ~520 km link, the MME increases with the increase in modulation frequency until the frequency defined by the inverse CM (τ_{CM}^{-1}) of ~470 MHz. Then fall in the MME is seen, as expected. Also in the case of 28 Gbaud 64-QAM signal transmission over ~250 km link, the MME increases until the frequency τ_{CM}^{-1} of ~970 MHz corresponding to ~250 km transmission and falls off thereafter as expected. Detailed discussions on experimental results are provided in [115].

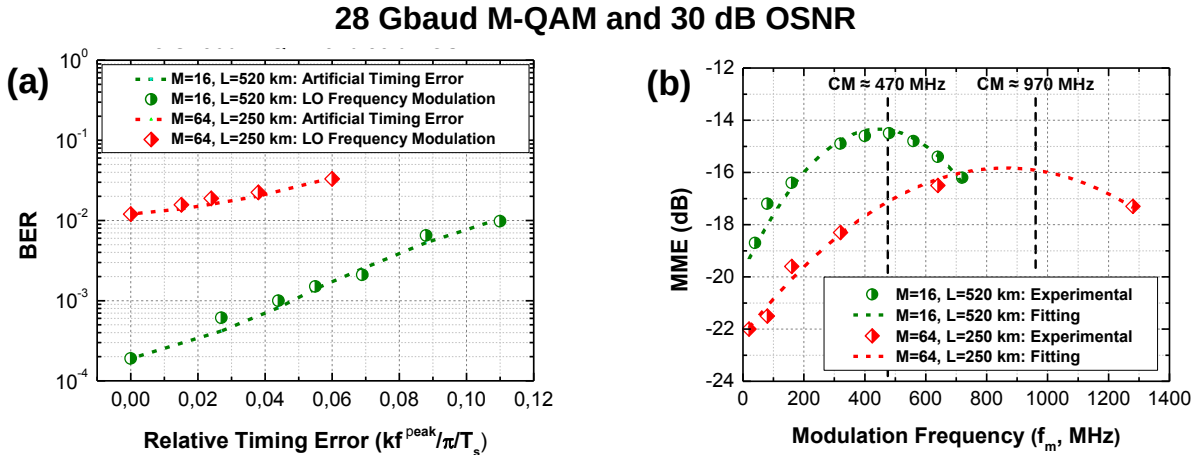

Figure 3.8: (a) BER vs. Relative Timing Error for 28 Gbaud M-QAM transmission (M=16 and 64) over 520 km and 250 km SMF fiber respectively compared to artificially induced timing at 30 dB OSNR and 20 MHz modulation frequency, (b) MME vs. Modulation Frequency for peak relative timing error of 0.11 and 0.06 respectively at 30 dB OSNR for same specification. CM shows the theoretical channel memory for different configurations.

Chapter 4

Mitigation of Laser Frequency Noise Induced Impairments in Coherent Optical Systems

In the previous chapter, we have discussed the general theory of coherent optical links with EDC employing lasers with a generic frequency noise spectrum. It was concluded that depending on the scheme of DSP processing each laser (Tx and LO) causes different set of impairments. The frequency noise of both the lasers at least cause phase related impairment. Whether a particular laser in a given configuration causes amplitude impairments as well depends on the laser phase noise seen by the dispersion broadened pulse. In this chapter we will discuss mitigation methods for different laser frequency noise induced impairments in coherent optical systems proposed in **Paper VIII** to **Paper XVI**. In Section 4.1, we discuss the low bandwidth hardware assisted EEPN mitigation technique and its implementations proposed in **Paper VIII to Paper IX**. We then, in Section 4.2, discuss the high performance and low complexity schemes for carrier phase recovery proposed and experimentally validated in **Paper X to Paper XVI** for QAM.

4.1 Low Bandwidth Hardware assisted EEPN Mitigation

In Chapter 3, it was shown that the impact of EEPN increases as we opt for higher order modulation format, baud rate-distance product and/or lasers with large frequency noise in coherent optical links. In such links, it might become imperative to mitigate for EEPN. It was discussed that there are three all electronic impairment mitigation schemes which do not ideally results in EEPN. In these schemes, the symmetry of the link was maintained by ensuring that the impairments were mitigated in the order of their occurrence. However, in these schemes, it is

difficult to perform phase estimation process for more that reason. For instance, in Scheme 3, it is difficult to estimate the phase from the received signal before the EDC as it dominant impairment is dispersion. Further, after reception, it is difficult to isolate the phase noise estimate of the Tx and LO lasers. Similarly, in Scheme 5 and 7, a-priori information of the Tx laser phase noise impacting the system is required, before it actually impairs the signal. Even utilization of pilot tones as shown in [54] are not efficient in mitigating EEPN. In this we discuss low bandwidth hardware assisted EEPN mitigation technique and its two possible implementations as proposed in [110] and [111]. This method utilizes low bandwidth implementation of Digital Coherence Enhancement (DCE) interferometric hardware and simple DSP processing to perform interpolation and integration. The bandwidth requirements of the DCE optical to electrical conversion (O/E) front end, is drastically relaxed owing to the need to track only low frequency noise [108] and [112]. However, this results in the requirement of in-between differential phase samples to match the signal sampling rate. Therefore, requiring an interpolator, that is inherently a non-causal process. The number of required future samples for the interpolation increases with the spline order. Also it requires a large digital buffer to store the incoming signal sampled at much higher rate while waiting for future samples from the low speed hardware. This in turn would significantly increase the cost and complexity of the system.

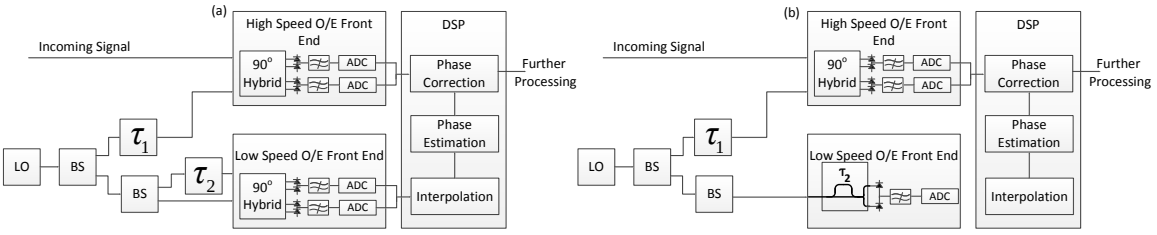

Figure 4.1: (a) Dual Arm Architecture of causal low speed DCE, (b) Single Arm Architecture of causal low speed DCE.

Fig. 4.1 depicts the two proposed architecture of the simple and real time processing compatible implementation of low speed DCE, without the need of large digital buffers. Fig. 4.1 (a) depicts dual arm implementation which requires a 90^o hybrid followed by balanced detection. The single arm implementation requiring just an interferometer and balanced detector is shown in Fig. 4.1 (b). The advantage of the first scheme is the utilization of the phase diversity scheme making it possible to track even very slow frequency fluctuations at the cost of increased complexity.

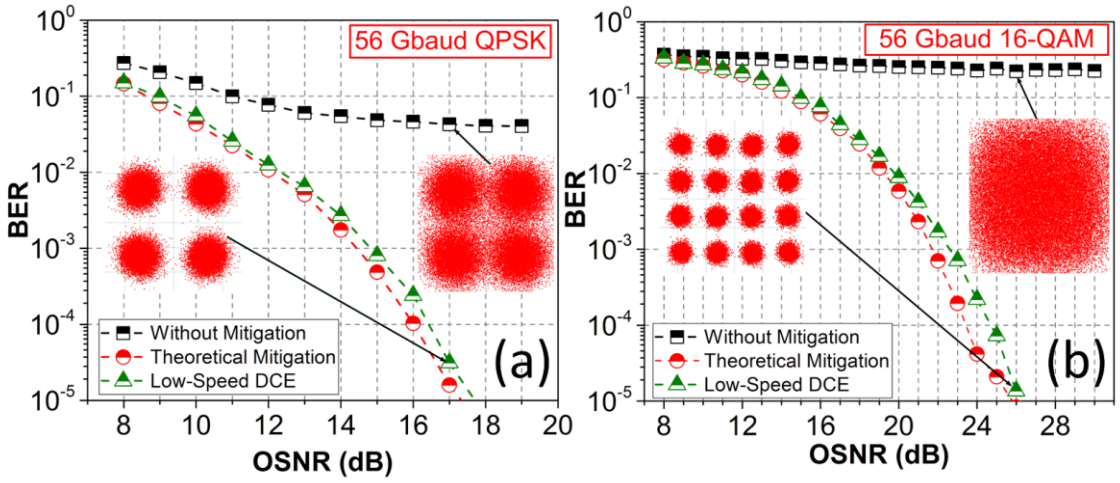

Figure 4.2: (a) BER versus OSNR for QPSK with and without mitigation (received signal constellation with and without mitigation are shown in inset), (b) BER versus OSNR for 16QAM with and without mitigation (received signal constellation with and without mitigation are shown in inset).

The increase in complexity due to the requirement of 90° hybrid and multiple ADCs and photodiodes. The second implementation reduces the required number of components, but as a tradeoff requires a mechanism to stabilize for the very slow central frequency fluctuations. In order to understand the operation and evaluate the performance of the two implementations, we assume, without the loss of generality, Scheme 3, where the LO causes EEPN. Depending on the dual arm or single arm implementation, the DCE generate an output signals

$$I_{DCE}(t) \propto e^{j\left[2\pi f_{LO}\tau_2 + \theta_{Rx}(t) - \theta_{Rx}(t-\tau_2)\right]} \tag{4.1}$$

$$I_{DCE}(t) \propto \mathrm{Re}\left[E_{LO}(t)\cdot E_{LO}^{*}(t-\tau_2)\right] \propto \cos\left[2\pi f_{LO}\tau_2 + \theta_{Rx}(t) - \theta_{Rx}(t-\tau_2)\right] \tag{4.2}$$

respectively. In the single arm case, represented by eq. (4.2), the interferometer needs to biased such that $2\pi f_{LO}\tau_2 = \pi/2$. This ensures that in the case differential phase noise fluctuation at the output of the interferometric hardware << 1 then the output of the interferometer is $\propto \sin\left[\theta_{Rx}(t) - \theta_{Rx}(t-\tau_2)\right] \propto \theta_{Rx}(t) - \theta_{Rx}(t-\tau_2)$. Interpolation followed by standard phase estimation processing in DCE and finally phase correction is performed on the received sampled signal before EDC in the DSP.

In order to ensure real time implementation, the amount of the necessary look ahead time, τ_1, is given by,

$$\tau_1 = \frac{n}{f_{DCE}} + \tau_{\text{int}} \tag{4.3}$$

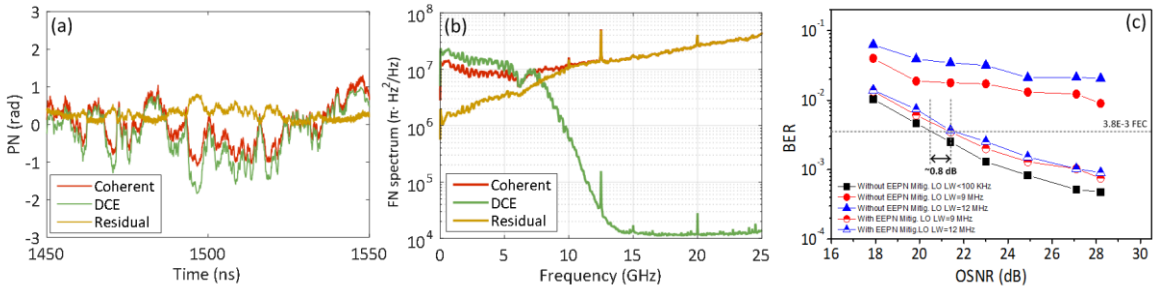

Figure 4.3: a) Temporal depiction of low frequency noise tracking, b) Frequency noise spectrum after low frequency noise mitigation, c) BER vs. OSNR of 28 Gbd 16-QAM transmission over 520 km of fiber with and without EEPN mitigation for LO linewidths of 9 and 12 MHz.

As could be seen from eq. (4.3), the required look ahead time depends on the number of future samples *n* required by the interpolation technique, sampling rate f_{DCE} of the low speed O/E front end ADC and τ_{int} is the constant intrinsic delay of the phase estimation method. The requirements on the interpolation technique, electrical signal to noise ratio (ESNR) at the DCE front end and the performance was evaluated through simulations and discussed in **Paper VIII** [110], considering the dual arm architecture. The simulation set-up used in the analysis is also described in detail in [110]. The performance evaluation of the method with ESNR= 15 dB, Linear interpolation, Nyquist rate sampling and DCE bandwidth of 300 MHz and 60 MHz for 56Gbaud QPSK and 16-QAM transmission links, respectively, with LO linewidth of 5 MHz and 160000 ps/nm accumulated dispersion, is shown in Fig. 4.2. The results show that the causal low bandwidth DCE for realistic system specification achieves performance close to the theoretical mitigation. In the results, theoretical mitigation corresponds to an ideal case of utilizing a local oscillator laser having zero frequency noise below the cut-off frequency, which is equal to the bandwidth of the DCE technique.

The experimental validation of EEPN mitigation in coherent transmission systems using the simple single arm technique was shown in **Paper IX** [111]. The details for the experimental set-up could be found in [111]. Fig. 4.3 shows the performance of the proposed EEPN mitigation technique. Fig. 4.3 a) and b) depict the low frequency noise tracking using the single arm DCE in temporal and frequency domain respectively. The temporal evolution of the phase noise in the

coherent signal branch is shown by the red curve; the temporal tracking of the low frequency noise of the LO by the single arm DCE branch is shown in green; and the residual phase (after low frequency noise mitigation) in mustard. Finally, the BER vs. OSNR performance of a 28 Gbaud 16-QAM signal after transmission with and without the proposed mitigation is shown Fig. 4.3 c). It can be seen that LO having linewidth of 9 MHz and 12 MHz, even over relatively moderate fiber link length, results in an irretrievable error floor. The OSNR penalty from an error floor to <0.8 dB compared to the reference BER curve, at 7% overhead FEC limit, is achieved after tracking and suppressing the low frequency noise.

4.2 Carrier Phase Recovery for High Order QAM

Phase impairment due to laser frequency noise is a critical impairment in coherent optical links requiring a CPR module for its compensation. Decrease in Euclidean distance as we opt for high order QAM put strict requirements on CPR performance while trying to maintain low implementation complexity. As discussed earlier, different CPR schemes basically based on two approaches that are the M-th power operation [36] and the conventional blind phase search (C-BPS) algorithm [41] have been proposed. The BPS algorithm is directly applicable to any general QAM constellation and provides high phase noise tolerance but is computational intensive. The computation complexity increases with modulation order as the required number of test phases to attain certain performance level increases. On the other hand, algorithms based on the M-th power operation are less computationally intensive, but require constellations points to have constant phase offsets, such as in PSK constellations. In sq.-QAM the number of points having this property decreases with increase in modulation order resulting in a poor phase noise tolerance of these type of algorithms. Additionally, for low optical to signal noise ratios (OSNRs) the accuracy of symbol amplitude discrimination required for symbol classification or partitioning decreases [38], [40] and [42]. Many two-stage schemes, in order to relax the computational complexity while achieving performance similar to single-stage BPS (C-BPS), utilizing both approaches have been proposed [39], [42], [44] and many more. Alternatively, C-QAMs which intrinsically provide higher phase noise tolerance compared to Sq-QAMs and are compliant to M- th power operation are also interesting alternatives [48].

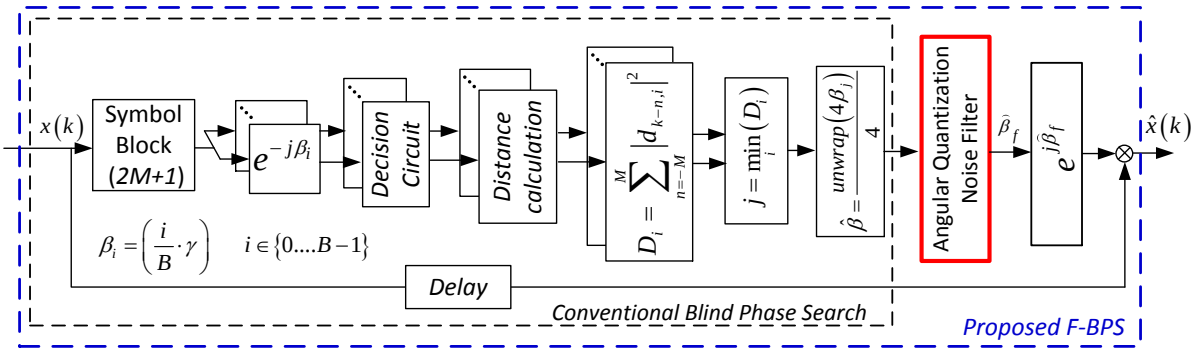

Figure 4.4: Operation Principle of the Filtered-BPS Scheme.

In this section, firstly, single and multi-stage architectures applicable to any general QAM as proposed in **Paper X** to **Paper XII** are discussed. This is followed by the discussion of CPR schemes applicable to C-QAM systems as proposed in **Paper XIII** to **Paper XVI**.

4.2.1 CPR Schemes for any general QAM

The blind phase search algorithm is seen as potential CPR contender for high capacity coherent optical links as it provides high phase noise tolerance and is applicable to any general QAM constellation. In this subsection, we discuss the intrinsic limitation of the BPS algorithm that adversely affects both, its achievable performance and reduction in computational complexity. Single stage and multistage schemes incorporating the techniques to overcome this limitation are discussed.

4.2.1.1 Single Stage Scheme

The operation principle of the proposed single-stage filtered BPS (F-BPS) scheme is illustrated in Fig. 4.4. The initial part of the scheme represents the conventional BPS scheme. The phase estimator after the phase unwrap module provides the final C-BPS phase estimator. The FN-PSD and the temporal evolution of the C-BPS phase estimator after unwrapping for different number of test phase angles in a sliding window CPR approach are depicted in Fig. 4.5 a) and b) respectively. As could be seen from Fig. 4.5 a) the decrease in the number of employed test phase results in increase in frequency noise. This is attributed to the angular quantization noise in the phase estimator due to the discrete phase search nature of the C-BPS algorithm. This can be appreciated by observing the temporal evolution of the estimated phase shown in Fig. 4.5 b).

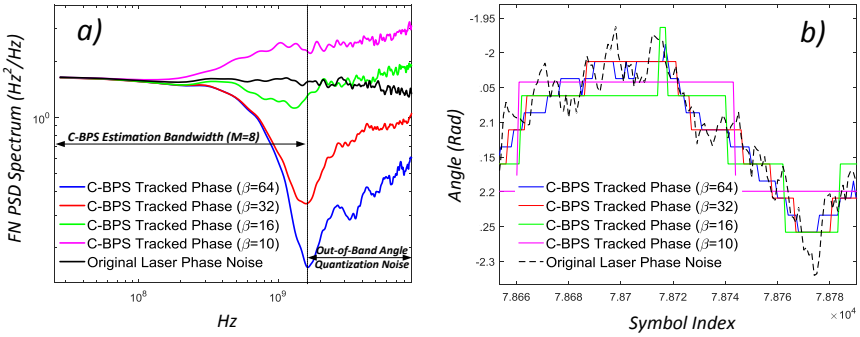

Figure 4.5: a) FN-PSD and b) Temporal evolution of estimated phase estimator after C-BPS for different test phases compared to original laser phase noise.

The angular jumps due to angular quantization are bigger for lower values of test phases translating into larger quantization noise and hence frequency noise enhancement. In order to reduce this out-of-band quantization in the C-BPS algorithm, an angular quantization noise filter consisting of a low pass filter operation on the C-BPS phase noise estimator is proposed in the F-BPS scheme as shown in Fig. 4.4. The post-BPS filter should be designed such that the out-of-band noise is reduced while ideally not distorting the in-band information of the C-BPS phase estimator. Design considerations would also include the trade-off between achievable performance and the filter implementation complexity.

In practice, a sliding averaging filter without weighting coefficient is sufficient to achieve a significant improvement in the CPR performance while drastically reducing its required implementation complexity. The validation of the F-BPS scheme was carried out both in simulations and experiments using the set-ups and details described in [119]. Results prove a significant increase in phase noise tolerance and a potential reduction of its implementation complexity compared to that of the C-BPS scheme.

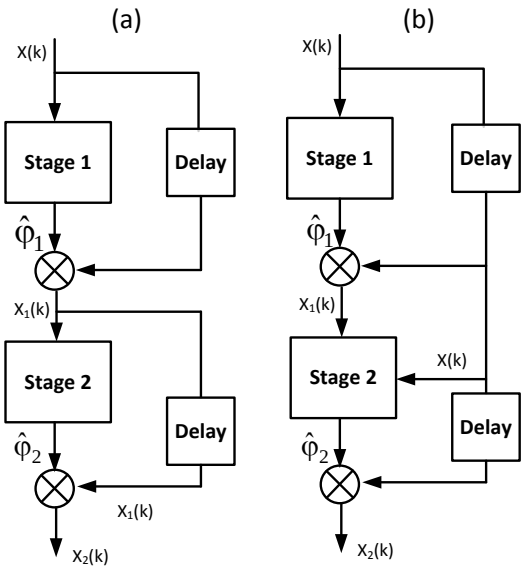

Figure 4.6: Multi-stage CPR architecture.

4.2.2 Multi-Stage Stage Schemes

Another alternative to achieve high phase noise tolerant yet low implementation complexity is to opt for multi-stage algorithms. In our proposed schemes, we try to exploit the advantages from both, the BPS and the N-th power approaches. In our proposed schemes, we employ the F-BPS with less number of test phases as the first stage so as to employ all constellation points for phase noise estimation. We consider three different options for a low complex second stage: the maximum likelihood estimator (MLE) [46], the Viterbi and Viterbi (V&V) CPR or repeating the BPS algorithm in a cascaded BPS-BPS scheme for a narrower phase search **Paper XII** [120].

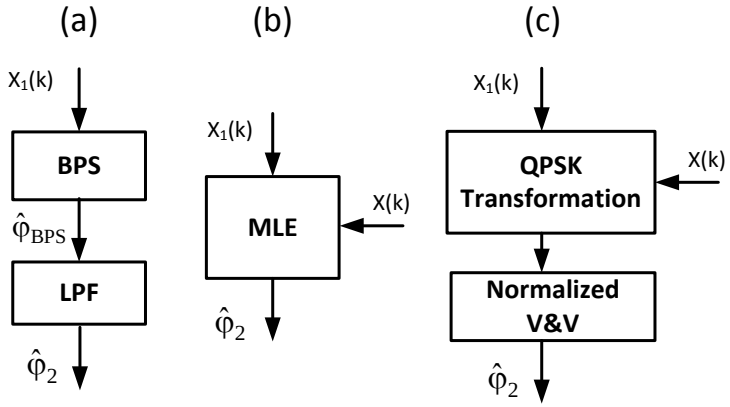

Figure 4.7: Different schemes for the stage 2 of the multi-stage CPR with BPS+LPF as the first stage.

Two different multi-stage CPR architectures are depicted in Fig. 4.6. In implementation a) the second stage compensates the residual phase noise of the output symbols from the first stage. However, in implementation b) the second stage compensates for the phase noise of the initial/input symbols to the first stage.

Further in implementation a) the phase noise characteristic of the input signal to the second stage are altered by the first BPS stage due to angular quantization noise. This will hinder the performance of the second stage. This is avoided in the implementation b).where the phase noise

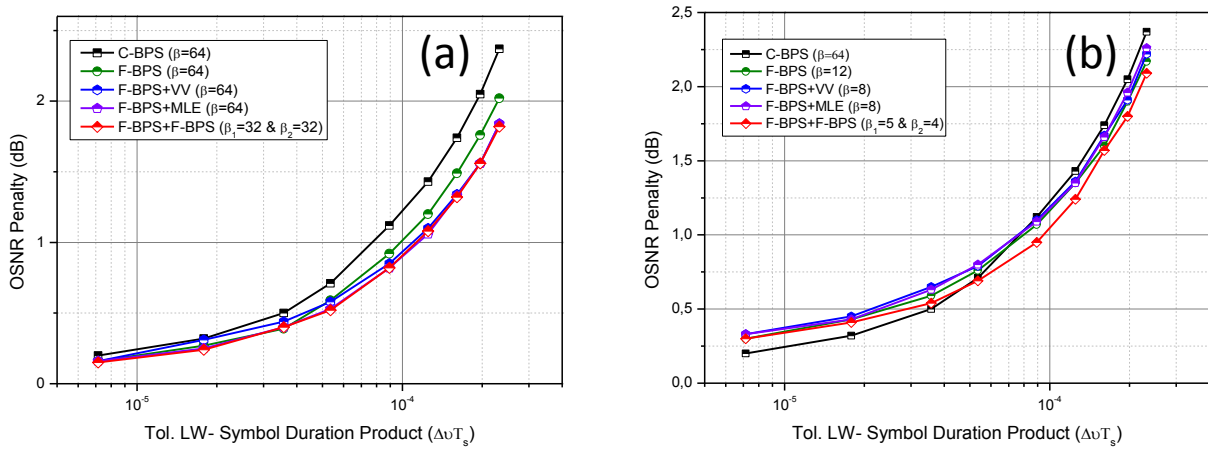

Figure 4.8: (a) OSNR Penalty versus Tolerable linewidth-symbol duration product (ΔvTs) at BER=2e-2 in case of 28 Gbaud 64 QAM signal for different CPR schemes and 64 effective number of test phases. (b) OSNR Penalty versus Tolerable linewidth-symbol duration product (ΔvTs) at BER=2e-2 in case of 28 Gbaud 64 QAM signal for different CPR schemes with different number of effective test phases.

characteristics of the input signal are preserved and compensated for during the second stage. As shown in previous section, lowering the number of test phases in the first stage in order to maintain a low overall computational complexity impacts the performance of the overall scheme (considering implementation a) due to angular quantization noise.

The impact of the quantization noise is reduced in implementation b) as it employs the original CPR input symbols (X(k)) for CPR in the second stage. In the schemes employing MLE or V&V in the second stage, the output of the first stage (F-BPS stage with low β) corresponds to a rough estimation of the transmitted constellation, which is considered as "a priori" information for the second stage to perform CPR on initial input symbols.

In the F-BPS+F-BPS case, a finer estimation of the remaining phase noise is performed on the received signal after coarse phase recovery from the first stage as described in **Paper XII** [120]**.** More details related to these multistage schemes with the second stages as depicted in

Figure 4.7 can be found in [120]. The performance of these multi-stage schemes compared to the C-BPS and F-BPS was carried out with the simulation set-up described in **Paper XII** [120].

The OSNR sensitivity penalty versus ΔνTs in the case of 64-QAM for 64 total phases is depicted in Fig. 4.8 a) for the different proposed multistage CPR schemes. Figure 4.8 b) shows the performance of these algorithms when employing low values of test phases representing a low implementation complexity of the algorithms. In the first case, when employing 64 total test phases, the achievable performance increases as we opt for F-BPS based multi-stage schemes. While Fig. 4.8 b) shows that performance similar to C-BPS with β=64 is achieved by the proposed algorithms with as less as 8~9 total number of test phases. The F-BPS+F-BPS scheme outperforms the other algorithms in this regime by a factor of 1.35. The computational complexity reduction factors of the proposed multistage algorithms with respect to the C-BPS and F-BPS can be found in [120].

Experimental performance validation of the F-BPS and F-BPS+VV was carried out using the

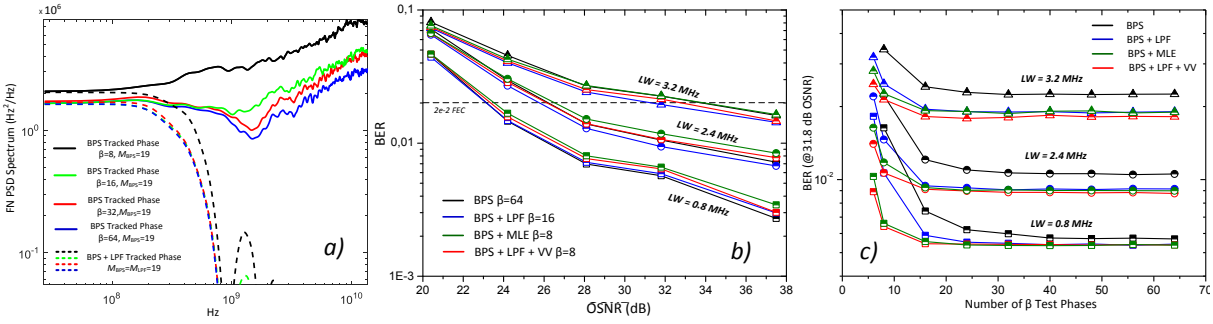

Figure 4.9: a) Frequency noise spectrum of different BPS phase noise tracked sequences with different β with and without LPF at 37.5 dB of OSNR and 2.2 MHz of linewidth. b) BER vs OSNR for three different linewidths and four CPR algorithms. c) BER vs number of test phases for three different linewidths at 31.8 dB OSNR.

experimental set-up described in **Paper XI** [121]. The performance was compared to C-BPS and C-BPS+MLE. The results of the analysis are shown in Fig. 4.9. Fig. 4.9 a) shows the FN-PSD of estimated phase noise by C-BPS with and without filtering as proposed in F-BPS for different test phases.

Fig. 4.9 b) shows the BER versus OSNR performance of the proposed algorithms for different linewidths in a 28 Gbaud 64-QAM system. Fig. 4.9 c) BER (@ 31.8 dB OSNR) versus test phases for the different schemes at different linewidth levels. The proposed BPS+LPF+VV (F-BPS+VV) scheme (β=8) outperforms BPS+MLE (β=8) for all three linewidths. Thus, the

algorithms with the proposed angular quantization noise filtering outperform state of art algorithms.

4.2.3 CPR Schemes specifically for Circular QAM

In the previous subsection, we have focused on CPR schemes for general QAM constellation. As discussed earlier the C-mQAM constellations, owing to their constellation shape, have higher phase noise tolerance and the widely known M-th power V&V method could be directly applied to these constellations. But applying the V&V method directly to these constellations have certain drawbacks such as asymmetric cycle slips as discussed in **Paper XV**. In this subsection, we discuss the V&V based schemes to overcome these problems to attain low complexity and high performance CPR for C-QAM as proposed in **Paper XIII** to **Paper XVI**.

4.2.3.1 Single Stage Schemes

High phase noise variance can cause cycle slips in the VV algorithm in the phase unwrap stage leading to degradation of phase noise tolerance [122]. Differential decoding is generally used to overcome this problem. However, in C-QAM constellations, differential decoding itself is not sufficient due to asymmetrical rotations of the constellation caused by cycle slips. This leads to a decrease in phase noise tolerance of the VV CPR for C-QAM constellations. The use of pilot-symbol aided CPR is one of the proposed methods to overcome this problem [123].

We proposed blind cycle slip mitigation based on adaptive boundary scheme. In this scheme, the distance of the received block of symbol is compared to the ideal constellation and to its $2\pi/N$ rotated version. Based on the minimum distance metric, a decision on the reference constellation is made for the symbol under study.

The optimum block size for the decision depends on the OSNR and the cycle-slip probability. Fig. 4.10 depicts the block diagram of the proposed scheme and the details of this algorithm could be found in **Paper XV** [68]. The adaptive boundaries assist to overcome asymmetrical constellation rotations due to cycle slips. However, differential decoding still needs to be performed and a valid differential decoding scheme for this constellation is shown in [68].

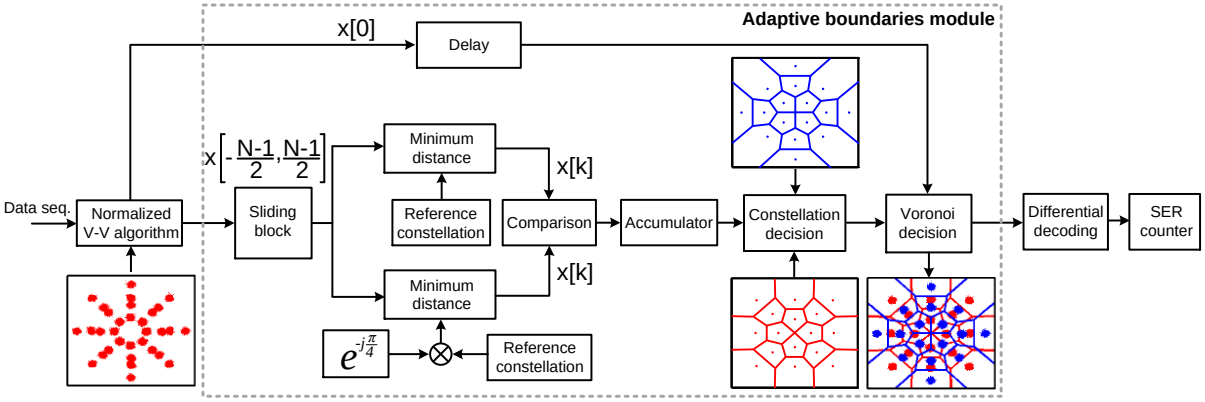

Figure 4.10: Block diagram for the proposed adaptive boundaries module. Particular case of C-16QAM is shown.

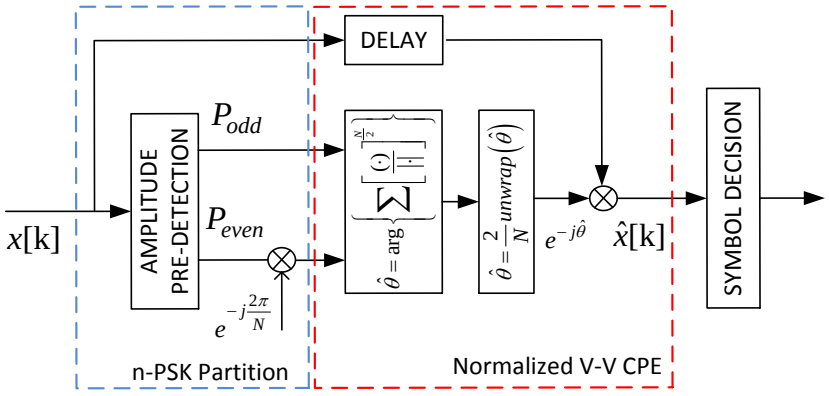

Figure 4.11: Block diagram of the proposed n-PSK partitioning CPR scheme. N represents the total number of different phases in a C-QAM constellation.

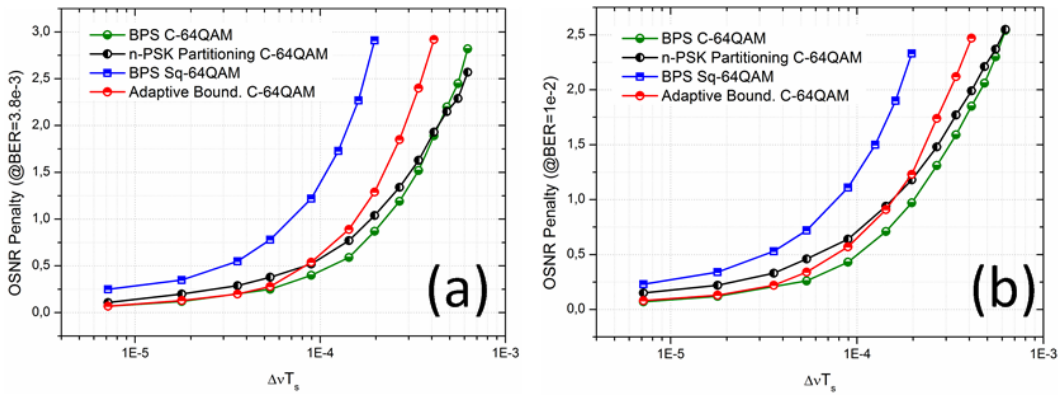

Figure 4.12: OSNR sensitivity penalty versus combined linewidth symbol duration product comparative for C-64QAM and Sq-64QAM using different CPR schemes (a) at a BER of 3.8e-3 and (b) at a BER of 1e-2.

The adaptive boundary scheme requires an additional module for estimation of the reference constellation, which increases the computational complexity of the overall algorithm. Thus, an alternative scheme will lower complexity than that of directly applying V&V was proposed in [67]. The proposed n-PSK partitioning scheme is shown in Fig. 4.11, the amplitude pre detection is performed to segregate the received symbols into even and odd levels as shown in [67]. A rotation on the even symbols of $2\pi/N$ is applied followed by normalized V&V CPR with the N/2th power. The utilization of N/2th power removes the asymmetric constellation rotations due to cycle slips and results in a reduction in complexity of the V&V algorithm. A differential sector based encoding and bit mapping schemes was also proposed as discussed in [67].

The performance validation of adaptive boundary scheme and n-PSK partitioning scheme was performed using the simulation setup given in [67]. OSNR penalty versus $\Delta\nu Ts$ at two different BER levels of 3.8e-3 and 1e-2 for C-64QAM is shown in Fig. 4.12 (a, b). As could be seen for the circular QAM outperforms square QAM in linewidth tolerance. In addition, the n-PSK performs better than the adaptive boundary scheme and slightly worse than the performance of the BPS for C-QAM. The reduction computational complexity factors in terms of real multiplier and real adders, compared to n-PSK partitioning scheme can be found in [67].

4.2.3.2 Multi Stage Scheme

Although the n-PSK partitioning algorithm for C-QAM achieves high phase noise tolerance with low computation complexity, its performance is undermined at low OSNRs due to the required amplitude discrimination for symbol classifications. This problem could be reduced by using a two stage n-PSK partitioning scheme. The architecture of the two-stage n-PSK partitioning is shown in Fig. 4.13.

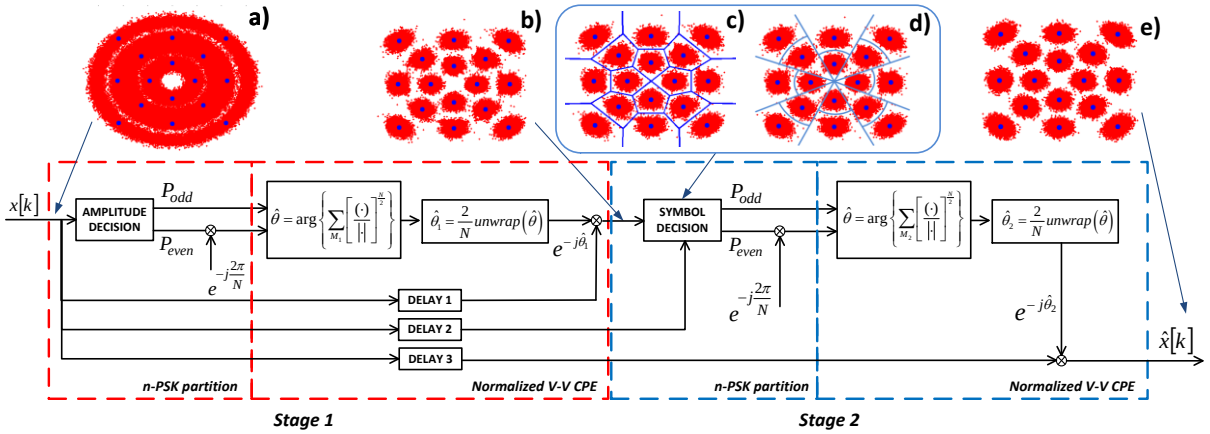

Figure 4.13: Block diagram of the proposed two stage n-PSK partitioning CPR scheme. (a) Input symbols. (b) Estimated constellation after first stage. (c) Detection of symbols with optimal decision boundaries. (d) Detection of symbols using sub-optimal decision boundaries (an alternative option to (c) for complexity reduction). (e) Final corrected symbols.

In this algorithm, the n-PSK partitioning algorithm is applied twice. The first stage is used to provide an estimate of the constellation for the second stage. The second stage uses this estimate to classify the input received symbols by employing optimal decision boundaries in the complex plane. In this way, the less efficient symbol amplitude discrimination for the n-PSK partitioning scheme can be avoided. Since most of the calculations required for the second stage have been previously calculated during the first stage, they can be reutilized to limit the complexity implementation of the scheme. Further details on the performance of this scheme together with a discussion of its implementation complexity can be found in [123].

The performance validation of two n-PSK partitioning scheme was performed using the simulation setup given in [124]. OSNR penalty versus ΔvTs for C-64QAM at two different BER levels of 3.8e-3 and 1e-2 with sub-optimal boundaries is shown in Fig. 4.14 (a, b). The two stage n-PSK performs better than the single stage scheme outperforming BPS for C-QAM. It is interesting to note that the use of the proposed sub-optimal boundaries do not degrade the performance compared to the optimal decision boundaries. The reduction factors of the computation complexity in terms of real multiplier and real adders, compared to two stage n-PSK partitioning scheme with sub optimal boundaries and optimal boundary are reported in [124].

The experimental validation of the performance of the single and two stage n-PSK partitioning schemes was carried out using the experimental set-up detailed in [125]. The BER vs. OSNR performance analysis was performed using 28 Gbaud C-16QAM signals for different laser

linewidth and performance is compared to the BPS algorithm. It could be observed from Fig. 4.15 that the n-PSK partitioning have slightly worse phase noise tolerance compared to BPS while the two-stage n-PSK partitioning outperforms BPS with much lesser computational complexity.

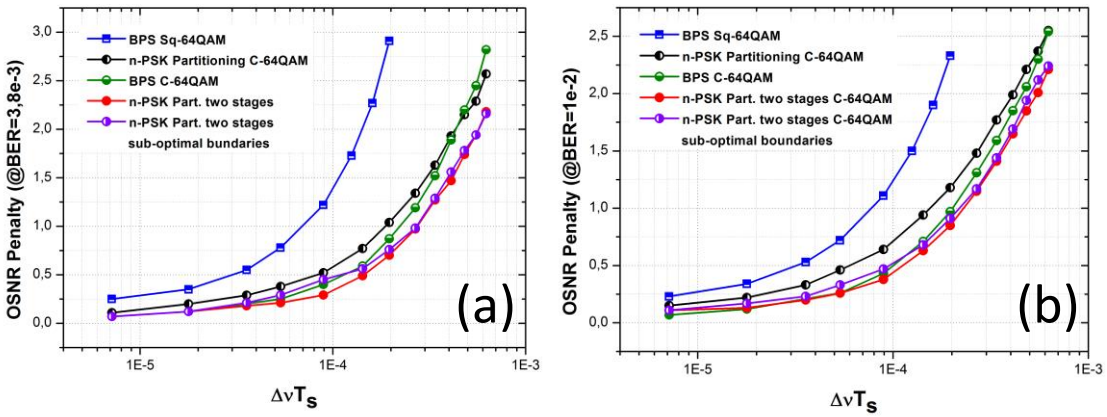

*Figure 4.14: OSNR sensitivity penalty versus $\Delta\nu T_s$ for C-16QAM and Sq-16QAM utilizing different CPR schemes at a BER of 1e-2 (**a**) and 3.8e-3 (**b**).*

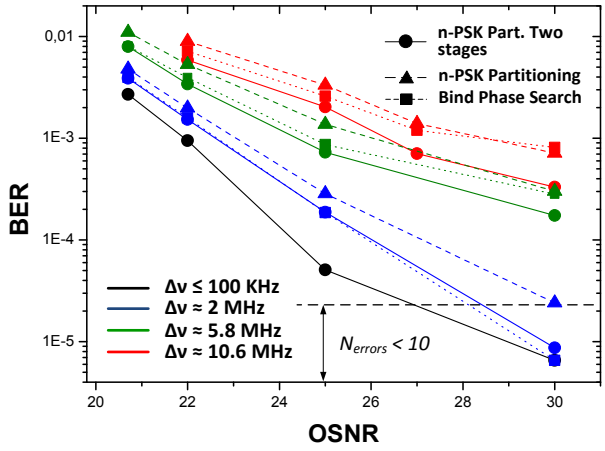

Figure 4.15: BER versus OSNR curves of a 28 Gbaud C-16QAM back-to-back transmission employing different CPR algorithms for different laser linewidths. Nerrors: Number of errors.

Chapter 5

Conclusions and Future Works

5.1 Conclusions

In this thesis, we have systematically analyzed the impact of laser frequency noise induced impairments on coherent optical link and DSP design. The statistical analysis of all eight categories of practicable all-electronic mitigation configurations assuming lasers with white frequency noise is provided. It is shown that five out of eight configurations result in EEPN while the remaining three do not ideally result in EEPN. All the five configurations resulting in EEPN are statistically equivalent. In three of these five configurations, Tx laser causes EEPN while in the remaining two LO laser cause EEPN. The system design parameters are validated through simulations and experiments. Statistical properties such as mean, variance, error vector magnitude (EVM) of the received signal are derived. Closed form expressions for the system design parameters such as necessary linewidth and/or mitigation bandwidth of the laser causing EEPN for a given system configuration and specified OSNR penalty, are given. The analysis elucidates that as we opt for higher order constellations and/or higher baud rate, EEPN impact becomes important, even for metro links utilizing low linewidth lasers. A general theory for coherent optical links with lasers having a generic non-white spectrum and EDC is then propounded. FN-induced symbol displacement that causes timing jitter and/or inter/intra-symbol interference is elucidated as the cause of EEPN related impairments. It is shown that, even in the case of ideal white frequency noise, different regimes of FN-spectrum of the laser cause different set of impairments. The frequency noise above the channel memory results in irretrievable even theoretically. While the impact of the impairments below the channel memory are not

theoretically irretrievable. For all schemes, regimes depend on the laser phase noise seen by dispersion broadened pulse before compensation of this broadening. Theoretical boundaries of these regimes and corresponding criteria applicable to system/laser design are provided. The simulation and experiments validate the findings of the general theory.

Low bandwidth hardware assisted EEPN mitigation technique is then proposed. The method uses low speed digital coherent enhancement (DCE) front end with DSP based interpolation and phase estimation. The method could be implemented with dual arm architecture or single arm architecture. It is shown through simulations that a realistic DCE based EEPN mitigation, with low hardware bandwidth along with Nyquist sampling rate and a linear interpolator, is sufficient for impairment mitigation. It is also experimentally validated that the proposed method with single arm architecture achieves from above FEC to <1 dB penalty for 28 Gbaud 16-QAM over 520 km with high LO linewidth.

Further, single stage and multi-stage CPR schemes applicable to any general QAM are proposed and discussed. It is shown that the conventional BPS (C-BPS) introduces angular quantization noise in its phase estimator which limits its achievable performance. This quantization noise is due to the discrete phase search nature of the C-BPS algorithm. A novel filtered BPS (F-BPS) scheme is proposed to mitigate the quantization noise by low pass filtering the C-BPS phase estimator. The evaluation of the method through experiments and simulations for 16-QAM and 64-QAM is carried out. The results confirm that improved performance of the F-BPS scheme makes it possible to drastically reduce the number of necessary test phases and hence implementation complexity. It is further shown that this quantization noise hinders the performance of the subsequent stage and hence overall performance and achievable reduction in computational complexity. Guidelines for design of low complexity and high performance multi-stage schemes are provided. It is shown that employing F-BPS instead of C-BPS in multistage schemes drastically improves both performance and achievable implementation complexity reduction. Further performance can be improved by utilizing the initial input symbols for the phase noise estimation in second and subsequent stages. Performance is evaluated for three multi-stage schemes with F-BPS as first stage with MLE, VV or F-BPS for the second stage. It is shown that two stage F-BPS scheme outperforms all the other scheme in both achievable performance and complexity reduction.

Finally, three CPR schemes specific to C-QAM fully based on VV CPR scheme are proposed and discussed. It is shown that direct application of VV to the C-QAM results in asymmetric rotation of the constellation due to cycle slips. Adaptive boundary scheme to overcome this asymmetric rotations due to cycle slips is proposed and evaluated. Since this method although improves the performance but also increases the implementation complexity, thus a new n-PSK partitioning scheme is proposed. This scheme overcomes both the asymmetric cycle slip problem and reduces the computational complexity compared to direct application of VV algorithm. It is shown that further increase in performance while maintaining low implementation complexity can be achieved by using two stage n-PSK partitioning scheme. The two stage n-PSK partitioning scheme outperforms C-BPS both in performance and implementation complexity.

5.2 Future work

High capacity coherent optical communication has been a hot topic in the recent years. However, as the transceiver requirements in the network moves towards high capacity and pluggable coherent optical transceivers cost-efficiency and energy-efficiency become very important considerations. Thus leading to many new research along with existing questions to be addressed. Some of them are listed below:

- Study of impact of impairments due to EEPN on FEC design in high capacity optical transceivers.
- How to optimize the semiconductor laser design to meet the EEPN criteria in different FN spectral regimes?
- Design of an efficient DSP based fiber nonlinearity mitigation technique.
- Design and optimization of DSP algorithms and FEC for cost and energy efficient coherent transceivers especially for space division multiplexed systems.
- Design of intelligent transceivers for dynamic elastic optical networking.

Chapter 6

Summary of the Original Works

In this chapter, a summary of original work and the author's contribution for the publications included in the thesis is presented.

Paper I:	**A. Kakkar**, R. Schatz, X. Pang, J. Rodrigo Navarro, H. Louchet, O. Ozolins, G. Jacobsen, S. Popov, "Impact of local oscillator frequency noise on coherent optical systems with electronic dispersion compensation," *Opt. Express* 23(9), 11221-11226 (2015).

In this paper, we carried out the frequency domain analysis of equalization enhanced phase noise (EEPN) and its mitigation. The analysis showed that the transmission penalty in coherent optical communication links with electronic dispersion compensation is mainly due to slow optical frequency fluctuations of the local oscillator (LO). It was validated with system simulations that elimination of frequency noise below certain cutoff frequency results in significant reduction in transmission penalty. The required cut-off frequency increases linearly with the linewidth of the Lorentzian line shape LO, while it is virtually independent of the symbol rate and accumulated dispersion.

Contributions: Original idea, mathematical analyses, design and execution of the simulation, and writing of the manuscript.

Paper II:	**A. Kakkar**, X. Pang, O. Ozolins, R. Schatz, J. Rodrigo Navarro, H. Louchet, G. Jacobsen, S. Popov, "A Path to Use Large Linewidth LO in 28 Gbd 16-QAM Metro Links", in *Proc. of ECOC 2015 (OSA/IEEE, 2015)*, paper Tu.3.4.6.

In this paper, we experimentally validated the findings from the frequency domain analysis of equalization enhanced phase noise (EEPN) presented in Paper I. Low frequency noise of the local oscillator laser as the main source of EEPN penalty is experimentally confirmed.
Contributions: Original idea, design and execution of the experiment, and preparation of the manuscript.

Paper III: **A. Kakkar**, J. Rodrigo Navarro, R. Schatz, H. Louchet, X. Pang, O. Ozolins, G. Jacobsen, S. Popov, "Comprehensive Study of Equalization-Enhanced Phase Noise in Coherent Optical Systems," *IEEE/OSA J. Lightwave Technol.* 33(23), 4834-4841 (2015).

A rigorous non-linear time variant analysis of equalization enhanced phase in coherent optical links utilizing local oscillator (LO) with white frequency noise, is presented. Statistical properties, of the received signal influenced by EEPN, such as mean, variance and error vector magnitude are derived, for complex multilevel modulation formants. The correspondence between EEPN in coherent optical systems utilizing electronic dispersion compensation and multipath fading in wireless communication systems in shown. Finally, we provide closed form expressions of necessary LO linewidths and/or theoretical mitigation bandwidth for a general system configuration utilizing white frequency noise lasers and a specific OSNR penalty.
Contributions: Original idea, basic theory and analytical derivations, design and execution of the simulation, and preparation of the manuscript.

Paper IV: **A. Kakkar**, O. Ozolins, J. Rodrigo Navarro, X. Pang, M. I. Olmedo, R. Schatz, H. Louchet, G. Jacobsen, S. Popov, “Design of Coherent Optical Systems Impaired by EEPN”, in *Proc. Of OFC2016 (OSA, 2016)*, paper Tu2A.2.

As an extension of Paper III, experimental validation of the novel and closed form expressions essential for design of coherent optical system impaired by EEPN was performed. We demonstrate that the formulae are useful for estimating and/or mitigating the impact of EEPN for any general system configuration.

Contributions: Original idea, design and execution of the experiments and preparation of the manuscript.

Paper V: **A. Kakkar**, J. Rodrigo Navarro, R. Schatz, X. Pang, O. Ozolins, A. Udalcovs, H. Louchet, S. Popov, G. Jacobsen, "Laser Frequency Noise in Coherent Optical Systems: Spectral Regimes and Impairments," *Scientific Reports 7, 844 (2017), doi:10.1038/s41598-017-00868-4*

In the previous papers, mathematical analysis was carried out for the specific case of lasers with white frequency noise. However, in general, lasers have a non-white frequency noise spectrum due to e.g., the presence of 1/f flicker noise and carrier induced noise for which the previous analysis becomes insufficient. In this paper, an experimentally validated theory of the influence of lasers having a general non-white frequency noise spectrum on coherent optical links with EDC was presented. The origin of the noise enhancement commonly known as EEPN was shown to be frequency noise induced symbol displacement that causes time jitter and/or inter/intra-symbol interference. It is demonstrated that different regimes of the frequency noise spectrum results in different set of impairments. Some regimes cause irretrievable impairment while for the impact of the impairments due to other regimes can be reduced by optimizing the corresponding mitigation algorithms. Finally we provide theoretical boundaries of these regimes along with criteria applicable to system/laser design.
Contributions: Original idea, basic theory and analytical derivations, design and execution of simulation and experiments.

Paper VI: **A. Kakkar**, J. Rodrigo Navarro, R. Schatz, X. Pang, O. Ozolins, F. Nordwall, D. Zibar, G. Jacobsen, S. Popov, "Influence of Lasers with Non-White Frequency Noise on the Design of Coherent Optical Links," in *Proc. Of OFC2017 (OSA, 2017)*, paper Th2A.55.

In this paper we provide the experimental validation of the theoretical boundaries and criteria applicable for system/laser design derived in Paper 5. It is shown that in 16/64-QAM metro links, the LO frequency noise mainly cause timing impairment apart from phase impairment.
Contributions: Original idea, design and execution of experiments, preparation of the manuscript.

Paper VII: **A. Kakkar**, J. Rodrigo Navarro, R. Schatz, X. Pang, O. Ozolins, H. Louchet, G. Jacobsen, S. Popov, "Equalization Enhanced Phase Noise in Coherent Optical Systems with Digital Pre- and Post-Processing," *MDPI Photonics* 3(2), 12 (2016).

An exhaustive analysis of equalization enhanced phase noise (EEPN) for all practical dispersion compensation configurations was presented in this paper. The analysis demonstrates that for all eight practicable configurations, the existence and origin, i.e. whether EEPN is caused by transmitting or local oscillator laser, depends on the order of digital signal processing. The analysis finally provides a simple look-up table for the system designer to make an informative choice.

Contributions: Original idea, mathematical analyses and preparation of the manuscript.

Paper VIII: **A. Kakkar**, J. Rodrigo Navarro, R. Schatz, X. Pang, O. Ozolins, H. Louchet, G. Jacobsen, S. Popov, "Mitigation of EEPN in Coherent Optical Systems With Low-Speed Digital Coherence Enhancement," *IEEE Photonics Technology Letters*, 27(18), 1942-1945 (2015)..

In this paper, a low bandwidth dual arm digital coherent enhancement (DCE) method for equalization enhanced phase noise (EEPN) mitigation in coherent optical systems is proposed. It is shown that the method can be implemented with a low-speed DCE front end and a linear digital interpolator with a small implementation penalty.

Contributions: Original idea, design and execution of simulations, preparation of the manuscript.

Paper IX: **A. Kakkar**, M. Iglesias Olmedo, O. Ozolins, J. Rodrigo Navarro, X. Pang, R. Schatz, H. Louchet, G. Jacobsen, S. Popov, "Overcoming EEPN in Coherent Transmission Systems", in *Proc. of CLEO2016 (OSA, 2016)*, paper SM4F.3.

In this paper, we propose and experimentally demonstrate a single arm implementation of digital coherence enhancement method for equalization enhanced phase noise mitigation. We show with a 28 Gbaud 16-QAM transmission over 520 km that performance can be recovered from above FEC to <1 dB while utilizing high linewidth local oscillators.

Contributions: Original idea, design and execution of the experiment, preparation of the manuscript.

Paper X: J. Rodrigo Navarro, **A. Kakkar**, R. Schatz, X. Pang, O. Ozolins, A. Udalcovs, S. Popov, G. Jacobsen, "Blind phase search with angular quantization noise mitigation for efficient carrier phase recovery," MDPI Photonics, to appear.

In this paper, we show that the high frequency noise enhancement due to the inherent properties of blind phase search (BPS) limits the achievable performance and implementation complexity of the method. We demonstrate that a substantial increase in performance can be achieved with lower implementation complexity by low pass filtering the BPS phase estimator.

Contributions: Original idea, design and of simulation and experiment set-up, execution of the experiments, preparation of the manuscript.

Paper XI: J. Rodrigo Navarro, **A. Kakkar**, R. Schatz, X. Pang, O. Ozolins, F. Nordwall, H. Louchet, S. Popov, G. Jacobsen, "High Performance and Low Complexity Carrier Phase Recovery Schemes for 64-QAM Coherent Optical Systems," in *Proc. Of OFC2017 (OSA, 2017)*, paper W2A.53

In this paper, we experimentally validate the performance of filtered phase estimator for BPS and its multi-stage variant utilizing Viterbi & Viterbi as the second stage. The performance of the two algorithms is compared with the state of art carrier phase recovery algorithms.

Contributions: Original idea, design and execution of the experiments, preparation of the manuscript.

Paper XII: J. Rodrigo Navarro, **A. Kakkar**, X. Pang, O. Ozolins, A. Udalcovs, R. Schatz, S. Popov, G. Jacobsen, "Design of Multi-stage carrier phase recovery schemes for high order coherent optical mQAM Systems," *IEEE/OSA J. Lightwave Technol.*, under preparation.

In this paper, we provide the design guidelines for multi-stage carrier phase recovery schemes for high order constellations utilizing blind phase search (BPS) at any stage.

Different multi-stage schemes based on the proposed guidelines are presented and their performance and implementation complexity is compared with state of art BPS algorithm.
Contributions: Original idea, design of simulation and experimental setup, execution of experiments, preparation of the manuscript.

Paper XIII: J. Rodrigo Navarro, **A. Kakkar**, X. Pang, O. Ozolins, R. Schatz, M. Iglesias Olmedo, G Jacobsen, S. Popov, "Carrier Phase Recovery Algorithms for Coherent Optical Circular mQAM Systems," *IEEE/OSA J. Lightwave Technol.* 34(11), 2717-2723 (2016).

In this paper, a novel low complexity and high performance carrier phase recovery scheme based on normalized Viterbi & Viterbi is proposed for circular-mQAM constellations. We also provide a differential decoding and a bit mapping scheme for circular-mQAM constellations. It is shown through simulations that a performance comparable to state of the art BPS algorithm is achieved with a drastic reduction in computational complexity.
Contributions: Original idea, design of simulation setup, preparation of the manuscript.

Paper XIV: J. Rodrigo Navarro, **A. Kakkar**, X. Pang, M. Iglesias Olmedo, O. Ozolins, F. Da Ros, M. Piels, R. Schatz, D. Zibar, G. Jacobsen, S. Popov, "Two-Stage n-PSK Partitioning Carrier Phase Recovery Scheme for Circular mQAM Coherent Optical Systems," *MDPI Photonics*. 3(2), 37 (2016).

In this paper, a novel two stage n-PSK partitioning based carrier phase recovery scheme for circular-mQAM constellation, is proposed. It is demonstrated with a 28 Gbaud circular-16QAM system that the proposed method outperforms the state of the art Blind phase search algorithm for circular-mQAM constellations.
Contributions: Original idea, design of simulations and experiment, execution of experiments, preparation of the manuscript.

Paper XV: J. Rodrigo Navarro, X. Pang, **A. Kakkar**, O. Ozolins, R. Schatz, G. Jacobsen, S. Popov, "Adaptive Boundaries Scheme for Cycle-Slip Mitigation in C-mQAM Coherent Systems," *IEEE Photonics Technology Letters*, 27(20), 2154-2157 (2015).

The limitation of the normalized Viterbi & Viterbi CPR in circular-mQAM systems due to cycle slips is shown in this paper. A method for cycle slip mitigation is proposed and its performance is evaluated with a 28 Gbaud C-16QAM and C-64QAM systems for different laser linewidths.

Contributions: Original idea, design of simulations, preparation of the manuscript.

Paper XVI: J. Rodrigo Navarro, M. I. Olmedo, **A. Kakkar**, X. Pang, O. Ozolins, R. Schatz, G. Jacobsen, S. Popov, D. Zibar, "Phase Noise Tolerant Carrier Recovery Scheme for 28 Gbaud Circular 16QAM", in *Proc. of ECOC 2015 (OSA/IEEE, 2015)*, paper Mo.4.3.5.

In this paper, we experimentally validate the performance of the n-PSK partioning based carrier phase recovery scheme with a 28 Gbaud C-16QAM system for different laser linewidths.

Contributions: Original idea, design and execution of experiment, preparation of the manuscript.

References

[1] Cisco, ”Cisco Visual Networking Index: Forecast and Methodology, 2015-2020 White Paper,” Cisco, 2016.

[2] Y. Yamamoto, ”Receiver performance evaluation of various digital optical modulation–demodulation systems in the 0.5–10 μm wavelength region,,” *IEEE J. Quantum Electrons.,* vol QE-16, nr 11, pp. 1251-1259, Nov, 1980.

[3] T. Okoshi, K. Emura, K. Kikuchi och R. T. Kersten, ”Computation of bit error rate of various heterodyne and coherent-type optical communication schemes,” *J. Opt. Commun.,* vol. 2, nr 4, pp. 134-141, Sep. 1981.

[4] O. E. DeLange, ”Wide-band optical communication systems—Part II: Frequency-division multiplexing,” *Proc. IEEE,* vol. 58, nr 10, pp. 1683-1690, Oct. 1970.

[5] K. Kikuchi och T. Okoshi, ”Frequency stabilization of semiconductor lasers for heterodyne-type optical communication systems,” *Electron. Lett.,* vol. 16, nr 5, pp. 179-181, Feb. 1980.

[6] D. LeGuen och F. Favre, ”High frequency stability of laser diode for heterodyne communication systems,” *Electron. Lett.,* vol. 16, nr 18, pp. 709-710, Aug. 1980.

[7] T. Okoshi, S. Ryu och K. Kikuchi, ”Polarization-diversity receiver for heterodyne/coherent optical fiber communications,” *International Conf. on Integrated Optics and Optical Fiber Communication*, Tokyo, Japan, Jun. 27-30, 1983.

[8] B. Glance, ”Polarization independent coherent optical receiver,” *J. Lightw. Technol.,* vol. 2LT-5, nr 2, pp. 274-276, Feb., 1987.

[9] N. Shibata, Y. Sasaki, K. Okamoto och T. Hosaka, ”Fabrication of polarization-maintaining and absorption-reducing fibers,” *J. Lightw. Technol.,* vol. LT-1, nr 1, pp. 38-43, Mar. 1983.

[10] N. Monerie och L. Jeunhomme, ”Polarization-maintaining single-mode fiber cable design,” *Electron. Lett.,* vol. 16, nr 24, pp. 921-922, Nov. 1980.

[11] T. Okoshi, K. Kikuchi och A. Nakayama, ”Novel method for high resolution measurement of laser output spectrum,” *Electron. Lett.,* vol. 16, nr 16, pp. 630-631, Jul. 1980.

[12] C. H. Henry, ”Theory of the linewidth of semiconductor lasers,” *IEEE J. Quantum Electron.,* vol. QE-18, nr 2, pp. 259-264, Feb. 1982.

[13] K. Vahala och A. Yariv, ”Semiclassical theory of noise in semiconductor lasers—Part I,” *IEEE J. Quantum Electron.,* vol. QE-19, nr 6, pp. 1096-1101, Jun. 1983.

[14] ”Measurement of FM noise, AM noise, and field spectra of 1.3 μm InGaAsP DFB lasers and determination of the linewidth enhancement factor,” *IEEE J. Quantum Electron.,* vol. QE-21, nr 11, pp. 1814-1818, Nov. 1985.

[15] T. Imai, Y. Hayashi, N. Ohkawa, T. Sugie, Y. Ichihashi och T. Ito, ”Field demonstration of 2.5 Gbit/s coherent optical transmission through installed submarine fibre cables,” *Electron. Lett.,* vol. 26, nr 17, pp. 1407-1409, Aug. 1990.

[16] S. Norimatsu, K. Iwashita och K. Sato, ”PSK optical homodyne detection using external cavity laser diodes in Costas loop,” *IEEE Photon. Technol. Lett.,* vol. 2, nr 5, pp. 374-376, May 1990.

[17] R. J. Mears, L. Reekie, I. M. Jauncey och D. N. Payne, ”Low-noise Erbium-doped fibre amplifier at 1.54 μm,” *Electron. Lett.,* vol. 23, nr 19, pp. 1026-1028, Sep. 1987.

[18] J. M. Kahn och K. -P. Ho, ”Spectral efficiency limits and modulation/detection techniques for DWDM systems,” *IEEE J. Sel. Topics Quantum Electron.,* vol. 10, nr 2, pp. 259-272, Mar.Apr. 2004.

[19] R. Griffin och A. Carter, ”Optical differential quadrature phase-shift key (oDQPSK) for high capacity optical transmission,” *Optical Fiber Communication Conf.*, Anaheim, CA, USA, Mar. 17–22, 2002.

[20] S. Tsukamoto, D.-S. Ly-Gagnon, K. Katoh och K. Kikuchi, ”Coherent demodulation of 40-Gbit/s polarization-multiplexed QPSK signals with 16-GHz spacing after 200-km transmission,” *Optical Fiber Communication Conf.*, Anaheim, CA, USA, Mar. 6–11, 2005.

[21] D. MacGhan, C. Laperle, A. Savchenko, C. Li, G. Mak och M. O'Sullivan, ”5120 km RZ-DPSK transmission over G652 fiber at 10 Gb/s with no optical dispersion compensation,” *Optical Fiber Communication Conf.*, Anaheim, CA, USA, Mar. 6–11, 2005.

[22] D.-S. Ly-Gagnon, S. Tsukamoto, K. Katoh och K. Kikuchi, ”Coherent detection of optical quadrature phase-shift keying signals with carrier phase estimation,” *J. Lightw. Technol.,* vol. 24, nr 1, pp. 12-21, Jan. 2006.

[23] K. Kikuch, ”Phase-diversity homodyne detection of multi-level optical modulation with digital carrier phase estimation,” *IEEE J. Sel. Topic Quantum Electron.,* vol. 12, nr 4, pp. 563-570, Jul./Aug. 2006.

[24] S. Tsukamoto, K. Katoh och K. Kikuchi, ”Coherent demodulation of optical multilevel phase shift-keying signals using homodyne detection and digital signal processing,” *IEEE Photon. Technol. Lett.,* vol. 18, nr 10, pp. 1131-1133, May 2006.

[25] Y. Mori, C. Zhang, K. Igarashi, K. Katoh och K. Kikuchi, ”Unrepeated 200-km transmission of 40-Gbit/s 16-QAM signals using digital coherent receiver,” *Opt. Exp.,* vol. 17, nr 32, pp. 1435-1441, Feb. 2009.

[26] M. Taylor, ”Coherent detection method using DSP for demodulation of signal and subsequent equalization of propagation impairments,” *IEEE Photon. Technol. lett.,* vol. 16, nr 2, pp. 674-676, Feb. 2004.

[27] S. Tsukamoto, K. Katoh och K. Kikuchi, ”Unrepeated transmission of 20-Gbit/s optical quadrature phase-shift keying signal over 200-km standard single-mode fiber based on digital processing of homodyne-detected signal for group-velocity dispersion compensation,” *IEEE Photon. Technol. Lett.,* vol. 18, nr 9, pp. 1016-1018, May 2006.

[28] S. J. Savory, G. Gavioli, R. I. Killey och P. Bayvel, ”Electronic compensation of chromatic dispersion using a digital coherent receiver,” *Opt. Exp.,* vol. 15, nr 5, pp. 2120-2126, 2007.

[29] T. Xu, G. Jacobsen, S. Popov, M. Forzati, J. Martensson, M. Mussolin, J. Li, K. Wang, Y. Zhang och A. T. Friberg, ”Frequency-Domain Chromatic Dispersion Equalization Using Overlap-Add Methods in Coherent Optical System,” *Journal of Optical Communications,* vol. 32, nr 2, pp. 131-135, 2011.

[30] S. Tsukamoto, Y. Ishikawa och K. Kikuchi, ”Optical homodyne receiver comprising phase and polarization diversities with digital signal processing,” *European Conf. onOptical Communication*, Cannes, France, Sep. 24–28, 2006.

[31] K. Kikuchi och S. Tsukamoto, ”Evaluation of sensitivity of the digital coherent receiver,” *J. Lightw. Technol.,* vol. 20, nr 13, pp. 1817-1822, Jul. 2008.

[32] S. J. Savory, ”Digital filters for coherent optical receivers,” *Opt. Exp.,* vol. 16, nr 2, pp. 804-817, Jan. 2008.

[33] H. Sun, K.-T. Wu och K. Roberts, ”Real-time measurements of a 40-Gb/s coherent system,” *Opt. Exp.,* vol. 16, nr 2, pp. 873-879, Jan. 2008.

[34] L. E. Nelson, S. L. Woodward, M. D. Feuer, X. Zhou, P. D. Magill, S. Foo, D. Hanson, D. McGhan, H. Sun, M. Moyer och M. O'Sullivan, ”Performance of a 46-Gb/s dual-polarization QPSK transceiver in a high-PMD fiber transmission experiment,” *Optical Fiber Communication Conf.*, San Diego, CA, USA, Feb. 24–28, 2008.

[35] E. Yamazaki, S. Yamanaka, Y. Kisaka, T. Nakagawa, K. Murata, E. Yoshida, T. Sakano, M. Tomizawa, Y. Miyamoto, S. Matsuoka, J. Matsui, A. Shibayama, Abe, J., Y. Nakamura, H. Noguchi, K. Fukuchi, H. Onsaka, K. Fukumitsu, K. Komaki, O. Takeuchi, Y. Sakamoto, H. Nakashima, T. Mizuochi, K. Kubo, Y. Miyata, H. Nishimoto, S. Hirano och K. Onohara, ”Fast optical channel recovery in field demonstration of 100-Gbit/s Ethernet over OTN using real-time DSP,” *Opt. Exp.,* vol. 19, nr 14, pp. 13139-13184, Jul. 2011.

[36] A. J. Viterbi och A. M. Viterbi, ”Nonlinear Estimation of PSK Modulated Carrier Phase with Application to Burst Digital Transmission,” *IEEE Trans. Inf. Theory.,* vol. 29, nr 4, pp. 543-551, July, 1983.

[37] I. Fatadin, D. Ives och S. J. Savory, ”Laser linewidth tolerance for 16-QAM coherent optical systems using QPSK partitioning,” *IEEE Photon. Technol. Lett.,* vol. 22, nr 9, pp. 631-633, May, 2010.

[38] S. M. Bilal, G. Bosco, J. Cheng, A. P. T. Lau och C. Lu, ”Carrier phase estimation through the rotation algorithm for 64-QAM optical systems,” *J. Lightwave. Technol.,* vol. 27, nr 8, pp. 1766-1773, 2015.

[39] F. Zhang, J. Wu, Y. Li, K. Xu och J. Lin, ”Multi stage feed-fordward optical carrier phase estimation based on QPSK partitioning for 64 QAM signals,” *Optik International journal for Light and Electron Optics.,* vol. 124, nr 16, pp. 2557-2560, 2013.

[40] S. M. Bilal, C. R. S. Fludger, V. Curri och G. Bosco, ”Multistage carrier phase estimation algorithms for phase noise mitigation in 64-quadrature amplitude modulation optical systems,” *J. Lightwave. Technol.,* vol. 32, nr 17, pp. 2973-2980, 2014.

[41] T. Pfau, S. Hoffmann, Noe och R. Noe, ”Hardware-Efficient coherent digital receiver concept with feed forward carrier recovery for m-QAM constellations,” *J. Lightwave. Technol.,* vol. 27, nr 8, pp. 989-999, 2009.

[42] X. Su, L. Xi, X. Tang, Z. Zhang och X. Zhang, ”A multistage CPE scheme based on crossed constellation transformation for M-QAM,” *IEEE Photon. Technol. Lett.,* vol. 27, nr 1, pp. 77-80, 2015.

[43] M. Xiang, S. Fu, L. Deng, M. Tang, P. Shum och D. Liu, ”Low-complexity feed-fordward carrier phase estimation for M-ary QAM based on phase search acceleration by quadratic approximation,” *Opt. Express.,* vol. 23, nr 15, pp. 50-57, 2015.

[44] K. P. Zhong, J. H. Ke, Y. Gao och J. C. Cartledge, ”Linewidth-tolerant and low-complexity two-stage carrier phase estimation based on modified QPSK partitioning for dual polarization 16-QAM systems,” *J. Lightwave. Technol.,* vol. 31, nr 1, pp. 50-57, 2013.

[45] J. Li, L. Li, Z. Tao, T. Hoshida och J. C. Rasmussen, ”Laser-linewidth-tolerant feed-fordward carrier phase estimator with reduced complexity for QAM,” *J. Lightwave. Technol.,* vol. 29, nr 16, pp. 2358-2364, 2011.

[46] X. Zhou, ”An improved feed-forward carrier recovery algorithm for coherent receivers with m-QAM modulation format,” *IEEE Photon. Technol. Lett.,* vol. 22, nr 14, pp. 1051-1053, 2010.

[47] X. Zhou, C. Lu, A. P. T. Lau och K. Lonh, ”Low-complexity carrier phase recovery for square m-QAM based on S-BPS algorithm,” *IEEE Photon. Technol. Lett.,* vol. 26, nr 18, pp. 1863-1866, 2014.

[48] S. O. Zafra, X. Pang, G. Jacobsen och G. Popov, ”Phase noise tolerance study in coherent optical circular QAM transmissions with Viterbi-Viterbi carrier phase estimation,” *Opt. Exp.,* vol. 22, nr 25, pp. 30579-30585, 2014.

[49] W. Shieh och K. P. Ho, ”Equalization-enhanced phase noise for coherent detection systems using electronic digital signal processing,” *Opt. Exp,* vol. 16, nr 20, pp. 15718-15727, Sep. 2008.

[50] A. P. T. Lau, T. S. R. Shen, W. Shieh och K. P. Ho, ”Equalization enhanced phase noise for 100 Gb/s transmission and beyond with coherent detection,” *Opt. Exp.,* vol. 18, nr 16, pp. 17239-17251, Jul. 2010.

[51] T. Xu, G. Jacobsen, S. Popov, J. Li, A. T. Friberg och Y. Zhang, ”Analytical estimation of phase noise influence in coherent transmission system with digital dispersion equalization,” *Opt. Exp.,* vol. 19, nr 8, pp. 7756-7768, Apr. 2011.

[52] G. Jacobsen, M. S. Lidon, T. Xu, S. Popov, A. T. Friberg och Y. Zhang, ”Influence of pre- and post compensation of chromatic dispersion on equalization enhanced phase noise in coherent multilevel systems,” *J. Opt. Commun.,* vol. 32, pp. 257-261, May 2012.

[53] G. Jacobsen, T. Xu, S. Popov och S. Sergeyev, ”Study of EEPN mitigation using modified RF pilot and Viterbi-Viterbi based phase noise compensation,” *Opt. Exp.,* vol. 21, nr 10, pp. 12351-12362, may 2013.

[54] G. Jacobsen, T. Xu, S. Popov, J. Li, A. T. Friberg och Y. Zhang, ”EEPN and CD study for coherent optical nPSK and nQAMsystems with RF pilot based phase noise compensation,” *Opt. Exp.,* vol. 20, nr 8, pp. 8862-8870, Apr. 2012.

[55] S. Oda, C. Ohshima, T. Tanaka, T. Tanimura , H. Nakashima, N. Koizumi, T. Hoshida, H. Zhang, Z. Tao och J. Rasmussen, ”Interplay between local oscillator phase noise and electrical chromatic dispersion compensation in digital coherent transmission system,” *Eur. Conf. Optical Communication*, Torino, Italy, 2010.

[56] C. Xie, ”Local oscillator phase noise induced penalties in optical coherent detection systems using electronic chromatic dispersion compensation,” *Optical Fiber Communication Conf.*, San Diego, CA, USA, 2010.

[57] I. Fatadin och S. J. Savory, ”Impact of phase to amplitude noise conversion in coherent optical systems with digital dispersion compensation,” *Opt. Express.,* vol. 18, nr 15, pp. 16273-16278, Jul. 2010.

[58] W. Shieh och I. Djordjevic, OFDM for Optical Communications, Academic Press, Oct, 2009.

[59] J. Armstrong, ”OFDM for optical communications,” *J. Lightw. Technol.,* vol. 27, nr 3, pp. 189-204, Feb. 2009.

[60] R. Van Nee och R. Prasad, OFDM for Wireless Multimedia Communications, Artech House Publishers, Dec. 1999.

[61] J. G. Proakis, Digital Communications, 4th Ed., McGraw-Hill, Aug. 2000.

[62] F. Buchali, L. Schmalen, A. Klekamp, K. Schuh och A. Leven, ”5 x 50 Gb/s WDM transmission of 32 Gbaud DP-3-PSK over 36000 km fiber with spatially coupled LDPC coding,” *Optical Fiber Communication Conf.* , Mar. 2014.

[63] G. J. Foschini, R. D. Gitlin och S. B. Weinstein, ”Optimization of Two-Dimensional Signal Constellation in the Presence of Gaussian Noise,” *IEEE Trans. of Comm.,* vol. COM-22, nr 1, pp. 28-37, Jan. 1974.

[64] T. Pfau, X. Liu och S. Chandrasekhar, ”Optimization of 16-ary quadrature amplitude modulation constellations for phase impaired channels,” *Proc. of European Conf. on Opt. Comm. (ECOC)*, Sep. 2011.

[65] R. Krishnan, A. Graell i Amat, T. Eriksson och G. Colavolpe, ”Constellation optimization in the presence of strong phase noise,” *IEEE Trans. Commun.,* vol. 61, nr 12, pp. 5056-5066, Dec. 2013.

[66] E. Agrell, J. Lassing, E. G. Ström och T. Ottosson, ”Gray Coding for Multilevel Constellations in Gaussian Noise,” *IEEE Trans. on. Inf. Theory.,* vol. 53, nr 1, pp. 224-235, Jan. 2007.

[67] J. R. Navarro, A. Kakkar, X. Pang, O. Ozolins, R. Schatz, M. I. Olmedo, G. Jacobsen och S. Popov, ”Carrier Phase Recovery Algorithms for Coherent Optical mQAM Systems,” *J. Lightw. Technol.,* vol. 33, nr 9, pp. 1766-1773, 2015.

[68] J. R. Navarro, X. Pang, A. Kakkar, O. Ozolins, R. Schatz, G. Jacobsen och S. Popov, ”Adaptive boundaries scheme for cycle-slip mitigation in C-mQAM coherent systems,” *IEEE Photon. Technol. Lett.,* vol. 27, nr 20, pp. 631-633, Jul. 2015.

[69] K. Kasai, J. Hongo, H. Goto, M. Yoshida och M. Nakazawa, ”The use of a Nyquist filter for reducing an optical signal bandwidth in a coherent QAM optical transmission,” *IEICE Electronics Express,* vol. 5, nr 1, pp. 6-10, 2008.

[70] S. Gringeri, E. Basch och T. Xia, ”Technical considerations for supporting data rates beyond 100 Gb/s,” *IEEE Commun. mag.,* vol. 50, nr 2, pp. s21-s30, Feb. 2012.

[71] M. I. Olmedo, X. Pang, R. Schatz, O. Ozolins, H. Louchet, D. Zibar, G. Jacobsen, I. T. Monroy och S. Popov, ”Effective Linewidth of Semiconductor Lasers for Coherent Optical Data Links,” *MDPI Photonics,* vol. 3, nr 2, 2016.

[72] M. Lax, ”Classical Noise v. noise in self-sustained oscillators,” *Phys. Rev.,* vol. 160, pp. 290-307, Aug. 1967.

[73] G. Foschini och G. Vannucci, ”Characterizing filtered light waves corrupted by phase noise,” *IEEE Trans. Inf. Theory,* vol. 34, nr 6, pp. 1437-1448, Nov. 1988.

[74] M. I. Olmedo, X. Pang, M. Piels, R. Schatz, G. Jacobsen, S. Popov, I. T. Monroy och D. Zibar, ”Carrier Recovery Techniques for Semiconductor Laser Frequency Noise for 28 Gbd DP- 16 QAM,” *Optical Fiber Communication Conference*, Los Angeles, CA, USA, 2015.

[75] Y. Matsui, T. Pham, W. A. Ling, R. Schatz, G. Carey, H. Daghighian, T. Sudo och C. Roxlo, ”55-GHz bandwidth short-cavity distributed reflector laser and its application to 112-Gb/s PAM-4,” *Optical Fiber Commun. Conf.*, Anaheim, CA, USA, 2016.

[76] O. Ozolins, M. I. Olmedo, X. Pang, S. Gaiarin, A. Kakkar, A. Udalcovs, K. M. Engenhardt, T. Asyngier, R. Schatz, J. Li, F. Nordwall, U. Westergren, D. Zibar, S. Popov och G. Jacobsen, ”100 GHz EML for High Speed Optical Interconnect Applications,” *European Conf. on Optical Commun.*, Dusseldorf, Germany, 2016.

[77] G. P. Agrawal, Fiber-Optic Communication Systems 3rd ed., Wiley Interscience, 2002.

[78] G. P. Agrawal, Nonlinear Fiber Optics, 3rd ed., Academic Press, Jan. 2001.

[79] H. Hodgikinson, R. A. Harmon och D. W. Smith, ”Demodulation of optical DPSK using in-phase and quadrature detection,” *Electron. Lett.,* vol. 21, nr 19, pp. 867-868, Sep. 1985.

[80] A. W. Davis, M. J. Pettit, P. J. King och S. Wright, ”Phase diversity techniques for coherent optical receivers,” *J. Lightw. Technol.,* vol. 5, nr 4, pp. 561-572, Apr. 1987.

[81] F. Derr, ”Optical QPSK transmission system with novel digital receiver concept,” *Electron. Lett.,* vol. 27, nr 23, pp. 2177-2179, Nov. 1991.

[82] K. Kikuchi, ”Fundamentals fo Coherent Fiber Communications,” *J. Lightw. Technol.,* vol. 34, nr 1, pp. 157-179, Jan, 2016.

[83] S. J. Savory, ”Digital coherent optical receiver: Algorithms and subsystems,” *IEEE J. Sel. Topics Quantum Electron.,* vol. 16, nr 5, pp. 1164-1179, Sep. 2010.

[84] A. Kakkar, J. R. Navarro, R. Schatz, X. Pang, O. Ozolins, H. Louchet, G. Jacobsen och S. Popov, ”Equalization Enhanced Phase Noise in Coherent Optical Systems with Digital Pre- and Post-Processing,” *MDPI Photonics,* vol. 3(2), 2016.

[85] T. Tanimura, S. Oda, T. Tanaka, T. Hoshida, Z. Tao och J. Rasmussen, ”A simple digital skew compensator for coherent receiver,” *Proc. Eur. Conf. Opt. Commun.*, Sep. 2009.

[86] S. Haykin, Adaptive Filter Theory, Englewood Cliffs, NJ: Prentice-Hall, 2001.

[87] I. Mayer, ”On Lowdin's method of symmetric orthogonalization,” *Int. J. Quantum Chem.,* vol. 90, nr 1, pp. 63-65, Oct. 2002.

[88] D. Scofield, ”Note on Lowdin orthogonalization and square root of a postive self-adjoint matrix,” *Int. J. Quantum Chem. ,* vol. 7, nr 3, pp. 561-568, 1973.

[89] E. Forestieri och G. Prati, ”Novel Optical Line Codes Tolerant to Fiber Chromatic Dispersion,” *IEEE J. Lightw. Technol.,* vol. 19, nr 11, pp. 1675-1684, 2001.

[90] G. Goldfarb och G. Li, ”Chromatic dispersion compensation using digital IIR filtering with coherent detection,” *IEEE Photon. Technol. Lett.,* vol. 19, nr 13, pp. 969-971, Jul. 2007.

[91] R. Raheli och G. Picchi, ”Synchronous and fractionally-spaced blind equalization in dually-polarized digital radio links,” *Proc. IEEE Int. Conf. Commun. (ICC), Conf. Record., Jun., vol. 1, pp. 156–161*, 1991.

[92] D. Godard, ”Self-recovering equalization and carrier tracking in two-dimensional data communication systems,” *IEEE Trans. Commun.,* vol. 20, nr 10, pp. 776-778, 1980.

[93] P. Winzer, A. Gnauck, C. Doerr, M. Magarini och L. Buhl, ”Spectrally efficient long-haul optical networking using 112-Gb/s polarization-multiplexed 16-QAM,” *J. Lightw. Technol.,* vol. 28, nr 4, pp. 547-556, Feb. 2010.

[94] M. J. D. Powell, Approximation Theory and Methods, Cambridge, U. K.: Cambridge Univ. Press, 1982.

[95] P. Prandoni och M. Vetterli, ”From Lagrange to Shannon. and back: Another look at sampling [DSP Education],” *IEEE Signal Process. Mag.,* vol. 26, nr 5, pp. 138-144, Sep. 2009.

[96] J. R. Higgins, Sampling Theory in Fourier and Signal Analysis: Foundations, Oxford, U.K.: Oxford Science, 1996.

[97] M. Unser, A. Aldroubi och M. Eden, ”Polynomial spline signal approximations: Filter design and asymptotic equivalence with Shannon’s sampling theorem,” *IEEE Trans. Inf. Theory,* vol. 38, nr 1, pp. 95-103, Jan. 1992.

[98] G. Oetken, T. W. Parks och H. W. Schussler, ”New results in the design of digital interpolators,” *IEEE Trans. Acoust., Speech, Signal Process.,* vol. 23, nr 3, pp. 301-309, Jun. 1975.

[99] F. Gardner, ”A BPSK/QPSK timing-error detector for sampled receivers,” *IEEE Trans. Commun.,* vol. COM-34, nr 5, pp. 423-429, May 1986.

[100] K. Mueller och M. Mueller, ”Timing recovery in digital synchronous data receivers,” *IEEE Trans. Commun.,* vol. COM-24, nr 5, pp. 516-531, May 1976.

[101] H. Meyr, M. Moeneclaey och S. A. Fechtel, Digital Communication Receivers: Synchronization, Channel Estimation, and Signal Processing, New York: Wiley, 1997.

[102] M. Oerder och H. Meyr, ”Digital Filter and square timing recovery,” *IEEE Trans. on Commun.,* vol. 36, nr 5, pp. 605-612, 1988.

[103] D. Godard, ”Passband timing recovery in an all-digital modem receiver,” *IEEE Trans. on Commun.,* vol. 26, nr 5, pp. 517-523, 1978.

[104] S. Lee, ”A new non--data aided feedforward symbol timing estimator usinig two samples per symbol,” *IEEE Commun. Lett.,* vol. 6, nr 5, pp. 205-207, 2002.

[105] L. Huang, D. Wang, A. P. T. Lau, C. Lu och S. He, ”Performance analysis of blind timing phase estimators for digital coherent receivers,” *Opt. Express.,* vol. 22, nr 6, pp. 6749-6763, 2014.

[106] X. Zhou, J. Yu, M. -F. Huang, Y. Shao, T. Wang, L. E. Nelson, P. D. Magill, M. Birk, P. I. Borel, D. W. Peckham och R. Lingle, ”64-Tb/s, 8 b/s/Hz, PDM-36QAM transmission over 320 km using both pre- and post-transmission digital signal processing,” *J. Lightwave Technol.,* vol. 29, nr 4, pp. 571-577, Feb. 2011.

[107] X. Zhou, L. E. Nelson, P. Magill, R. Isaac, B. Zhu, D. W. Peckham, P. Borel och K. Carlson, ”High spectral efficiency 400 Gb/s transmission using PDM time-domain hybrid 32-64QAM and training-asssisted carrier recovery,” *J. Lightwave Technol.,* vol. 31, nr 7, pp. 999-1005, Apr. 2013.

[108] A. Kakkar, J. R. Navarro, R. Schatz, H. Louchet, X. Pang, O. Ozolins, G. Jacobsen och S. Popov, ”Comprehensive Study of Equalization-Enhanced Phase Noise in Coherent Optical Systems,” *IEEE J. Lightw. Technol.,* vol. 33, nr 23, pp. 4834-4841, 2015.

[109] G. Colavolpe, T. Foggi, E. Forestieri och M. Secondini, ”Phase Noise Sensitivity and Compensation Techniques in Long-Haul Coherent Optical Links,” *IEEE Global Telecommun. Conf. (GLOBECOM)*, Miami, FL, USA, Dec. 2010.

[110] A. Kakkar, J. R. Navarro, R. Schatz, X. Pang, H. Louchet, O. Ozolins, G. Jacobsen och S. Popov, ”Mitigation of EEPN in Coherent Optical Systems with Low Speed Digital Coherence Enhancement,” *IEEE Photon. Technol. Lett.,* vol. 27, pp. 1942-1945, 2015.

[111] A. Kakkar, M. I. Olmedo, O. Ozolins, J. R. Navarro, X. Pang, R. Schatz, H. Louchet, G. Jacobsen och S. Popov, ”Overcoming EEPN in Coherent Transmission Systems,” i *Proc. of CLEO*, San Jose, CA, USA, 2016.

[112] A. Kakkar, X. Pang, R. Schatz, J. R. Navarro, H. Louchet, O. Ozolins, G. Jacobsen och S. Popov, ”Impact of local oscillator frequency noise on coherent optical systems with electronic dispersion compensation,” *Opt. Express,* vol. 23, nr 9, pp. 11221-11226, 2015.

[113] R. E. Ziemer och W. H. Tranter, Principles of Communications, 5th ed., Hoboken, NJ, USA: Wiley, 2002.

[114] A. Kakkar, O. Ozolins, J. R. Navarro, X. Pang , M. I. Olmedo, R. Schatz, H. Louchet, G. Jacobsen och S. Popov, ”Design of Coherent Optical Systems Impaired by EEPN,” *Proc. of Optical Fiber Commun. Conf.*, Anaheim, CA, USA, 2016.

[115] A. Kakkar, J. R. Navarro, R. Schatz, X. Pang, X. Ozolins, A. Udalcovs, H. Louchet, S. Popov och G. Jacobsen, ”Laser Frequency Noise in Coherent Optical Systems: Spectral Regimes and Impairments,” *Nature Scientific Reports,* 2017.

[116] C. M. Miller och D. J. McQuate, ”Jitter Analysis of High-Speed Digital Systems,” *Hewlett-Packard Journal,* 1995.

[117] R. Neil, ”Understanding Jitter and Wander Measurement and Standards Second Edition,” *Agilent Technologies.*

[118] A. Kakkar, J. R. Navarro, R. Schatz, X. Pang, O. Ozolins, F. Nordwall, D. Zibar, G. Jacobsen och S. Popov, ”Influence fo Lasers with Non-White Frequency Noise on the Design of Coherent Optical Links,” *Proc. of Optical Fiber Commun. Conf.*, Los Angeles, CA, USA, 2017.

[119] J. R. Navarro, A. Kakkar, R. Schatz, X. Pang, O. Ozolins, A. Udalcovs, S. Popov och G. Jacobsen, ”Blind phase search with angular quantization noise mitigation for efficient carrier phase recovery,” *MDPI Photonics (submitted),* 2017.

[120] J. R. Navarro, A. Kakkar, X. Pang, O. Ozolins, A. Udalcovs, R. Schatz, S. Popov och G. Jacobsen, ”Design of Multi-stage carrier phase recovery schemes for high order coherent optical mQAM systems,” *IEEE J. Lightw. Technol. (under preparation),* 2017.

[121] J. R. Navarro, A. Kakkar, R. Schatz, X. Pang, O. Ozolins, F. Nordwall, H. Louchet, S. Popov och G. Jacobsen, ”High Performance and Low Complexity Carrier Phase Recovery Schemes for 64-QAM Coherent Optical Systems,” *Proc. of Optical Fiber Commun. Conf.*, Los Angeles, CA, USA, 2017.

[122] E. Ip och J. M. Kahn, ”Feedforward Carrier Recovery for Coherent Optical Communication,” *IEEE J. Lightw. Technol.,* vol. 25, nr 9, pp. 2675-2692, Sep. 2007.

[123] H. Cheng, Y. Li, F. Zhang, J. Wu, G. Zhang, J. Xu och J. Lin, ”Pilot-symbol aided cycle slip mitigation for DP-16QAM optical communication systems,” *Opt. Express.,* vol. 21, nr 19, pp. 22166-22172, Sep. 2013.

[124] J. R. Navarro, A. Kakkar, X. Pang, M. I. Olmedo, O. Ozolins , F. Da Ros, M. Piels, R. Schatz, D. Zibar, G. Jacobsen och S. Popov, ”Two-Stage n-PSK Partitioning Carrier Phase Recovery Scheme for Circular mQAM Coherent Optical Systems,” *MDPI Photonics,* vol. 23(2), 37, 2016.

[125] J. R. Navarro, M. I. Olmedo, A. Kakkar, X. Pang, O. Ozolins, R. Schatz, G. Jacobsen, S. Popov och D. Zibar, ”Phase Noise Tolerant Carrier Recovery Scheme for 28 Gbaud Circular 16QAM,” *Proc. of Eur. Conf. on Optical Commun.*, Valencia, Spain, 2015.

[126] I. Fatadin, D. Ives och S. J. Savory, ”Compensation of frequency offset for differentially encoded 16- and 64-QAM in the presence of laser phase noise,” *IEEE Photon. Technol. Lett.,* vol. 22, nr 32, pp. 176-179, Feb. 2010.

[127] J. R. Navarro, A. Kakkar, X. Pang, M. I. Olmedo, O. Ozolins, F. Da Ros, M. Piels, R. Schatz, D. Zibar, G. Jacobsen och S. Popov, ”Carrier Phase Recovery Algorithms for Coherent Optical Circular mQAM systems,” *IEEE/OSA J. Lightw. Technol.,* pp. 2717-2723, 2016.